A Study of the Developing Melanoblast and Telencephalon Lineages in the Mouse Embryo by *in vitro* Manipulation and Retrospective Clonal Analysis

Alison Louise Wilkie

Thesis presented for the Degree of

Doctor of Philosophy at The University of Edinburgh

2001

Declaration

I declare

a) that this thesis is composed by myself, and

b) that this work is my own, except where otherwise stated.

Alison L Wilkie

September 2001

Abstract

Neural crest-derived melanoblasts are the progenitors of melanocytes, the pigment cells of the skin, hair, and eyes. Melanoblast development is affected by many gene products acting in a variety of pathways, from those affecting melanoblast specification in the neural crest to the production of pigment in mature melanocytes. A primary neural crest culture assay was used to study the early stages of melanoblast specification, proliferation, and migration. The roles of cell signalling pathways known to affect melanoblast development were studied. KITL increased the proportion of crest cells that were melanoblasts and the distance they migrated, while EDN3 only affected the proportions of cells that were melanoblasts. HGF promoted migration, while MSH affected neither melanoblast migration nor numbers.

Studies of adult chimaeras derived from embryos carrying different coat colour markers have suggested melanoblasts are derived from a small number of progenitors, each generating a discrete unilateral transverse band of colour with minimal mixing between clones. In this study, two complementary approaches were used to assess the behaviour of labelled clones. Firstly, aggregation chimaeras were made between *Dct-LacZ* and non-transgenic embryos. The *Dct* promoter drives expression from E10 in melanoblasts and the telencephalon. Resultant patterns of labelled melanoblasts were studied during mid-gestation. Secondly, transgenic mice were generated that carry a modified *LacZ* reporter construct containing a 300bp duplication (*LaacZ*), driven by the *Dct* promoter. *LaacZ* is normally inactive, but it reverts to wild type *LacZ* at low frequency, labelling a cell and all its progeny at random. Chimaeric and mosaic embryos suggested melanoblasts are derived from a large number of progenitors, a pool of melanoblasts may reside in the cervical region, and melanoblasts undergo considerable longitudinal migration, illustrating significant axial mixing between clones.

Interestingly, radially arrayed, labelled clones were also generated in the telencephalon in *Dct-LaacZ* embryos. By analysing the distribution of labelled columns in reconstructed embryos, it was possible to record the migratory path of neurogenic stem cells which are proposed to disperse tangentially in the ventricular zone during corticogenesis. In addition, monitoring variations in the clone labelling frequency between E10.5 and E14.5 revealed that a dramatic period of cell death removes a large proportion of progenitor cells from the telencephalon at around E14.0.

Acknowledgements

Firstly, I would like to thank my supervisors, Ian Jackson and Siobhán Jordan. I am grateful for their continual guidance, encouragement, and teaching. I am grateful, especially, for their encouragement and support of my efforts to persue a field of research that was outside of our own laboratory's direct interest. Peter Budd and Ruth Suffolk provided technical assistance and advice. In addition to this, I thank them and the entire lab for providing a happy environment in which to work.

I thank Brendan Doe, who patiently taught me to microinject eggs and transfer embryos, Scott Rhodes, and all of the staff in the transgenic facility for their constant entertainment, support, and endless plug checking. Paul Perry worked tirelessly for what must have felt like an age to devise the neural crest analysis script. I thank him for this and for his friendly support. I thank Andrew Carothers for essential statistical analyses and advice. I am grateful to James Sharpe for his invaluable contribution of reconstructing telencephalon clones and for his interest in the project. I thank Douglas Stewart for his excellent photographic service and friendly support.

I am grateful to John West, in whose lab I learned to make chimaeras, for this and for helpful discussions. I also thank Jean Flockhart, who kindly taught me to make chimaeras.
I am grateful to David Price for many stimulating discussions on the telencephalon clones generated in *Dct-LaacZ* embryos, and for encouraging me to dive into an area about which I knew nothing. I thank Grace Grant for kindly improving my histology techniques.

I would like to thank my mum, Eileen, brothers, Calum and David, and fiancé, Benjamin, for their constant encouragement and support (often financial and always kind).

Despite screening over 3000 embryos, I never tired of looking at them or failed to be amazed that they form perfectly almost every time. So, lastly, I acknowledge the literally thousands of embryos and their hundreds of mothers who generated the data for this thesis. While I firmly believe it right to have used them, it remains a unique liberty that I hope I did not take for granted.

I dedicate this thesis to my parents, Eileen and Robert Wilkie.

Table of Contents

List of Tables

List of Figures

List of Photographic Plates

List of Abbreviations

A_{600}	absorbance at 600nm
A12	line containing the *Dct-LacZ* transgene
A195	line containing the *Dct-LaacZ* transgene
α-MSH	α–Melanocyte stimulating hormone
AP	alkaline phosphatase
BDNF	Brain-derived nerve growth factor
bFGF	basic Fibroblast growth factor
BMP	Bone morphogenic protein
BSA	Bovine serum albumin
β-gal	β-galactosidase
CLF	clone labelling frequency
CNS	central nervous system
DAG	1,2-diacylglycerol
DAPI	4',6-Diamidino-2-phenylindole dihydrochloride
Dct	Dopachrome tautomerase
DEPC	diethyl pyrocarbonate
dH_2O	distilled water
DIC	differential interference contrast
DMF	dimethyl formamide
DNA	deoxyribonucleic acid
dNTP	dinucleotide triphosphate
DREZ	dorsal root entry zone
DRG	dorsal root ganglia
E	embryonic day
ECE-1	Endothelin converting enzyme-1
ECM	extracellular matrix
E.coli	*Escherischia coli*
EDN1	Endothelin-1
EDN3	Endothelin-3
EDNRA	Endothelin A receptor
EDNRB	Endothelin B receptor
EDTA	ethyldiaminetetra-acetic acid di-sodium salt

FCS	foetal calf serum
g	gramme
GFP	green fluorescent protein
GM	glial and melanoblast progenitor cell
hCG	human chorionic gonadotrophin
HCl	hydrogen chloride
HG	high grade (chimaera)
HGF	hepatocyte growth factor
HGU	Human Genetics Unit
HISS	heat-inactivated sheep serum
ISEL	*In Situ* End Labelling
Kit^{W}	*white-spotting* mutation
$Kit^{W\text{-}sh}$	*white-spotting, sash* mutation
$Kit^{W\text{-}v}$	*white spotting, viable* mutation
KITL	KIT ligand
$Kitl^{Sl}$	*Steel* mutation
$Kitl^{Sl\text{-}D}$	*Steel-dickie* mutation
LHS	left hand side
LNGFR	Low affinity nerve growth factor receptor
LG	low grade (chimaera)
LRD	lysinated rhodamine dextran
M	molar
m	prefix *milli*
μ	prefix *micro*
MAPK	Mitogen-activated protein kinase
Mc1r	Melanocortin-1 receptor
MITF	Micropthalmia transcription factor
MSA	migration staging area
n	prefix *nano*
NG	neurone and glial progenitor cell
NGF	Nerve growth factor
NGM	neurone, glial, and melanoblast progenitor cell
NT-3	Neurotrophin-3
OPT	optical projection tomography
P	postnatal day

PBS	phosphate buffered saline
PCD	programmed cell death
PCR	polymerase chain reaction
PFA	paraformaldehyde
PI-3'-kinase	Phosphatidylinositol-3'-kinase
PKC	Protein kinase C
PNS	peripheral nervous system
RHS	right hand side
SDS	sodium dodecyl sulphate
Sl	*Steel* class of mutations
sl	*lethal-spotting* mutation
s^l	*piebald-lethal*
SPF	specific pathogen free
SAPK	stress-activated protein kinase
SVZ	subventricular zone
TAE	Tris, acetic acid, EDTA
TBE	Tris, boric acid, EDTA
TdT	terminal deoxynucleotidal-transferase
TE	Tris, EDTA
TESPA	3-aminopropyl-triethyloxysaline
TYRP1	Tyrosinase-related protein 1
TYRP2	Tyrosinase-related protein 2
TUNEL	terminal dUTP nick end labelling
UV	Ultraviolet
VZ	ventricular zone
W	*White-spotting* class of mutations
Xgal	5-bromo-4-chloro-3-indolyl-β-D-galactoside

Aims

Manipulating melanoblast development in vitro

The aim of this project is to develop a primary tissue culture system to manipulate melanoblast development *in vitro* with the addition of growth factors, blocking antibodies, and modulators of signal transduction pathways. Such manipulations will allow the roles of the different signalling pathways in the specification, proliferation, survival, and migration of melanoblasts to be determined using a novel method of analysis.

Clonal analysis of melanoblast development

The aim of this project is to try to assess the number of melanoblast progenitors in the mouse embryo and to study how their progeny are distributed during their migration from the neural crest in the mid-gestation embryo. To do this, two independent approaches will be used: 1. Generate a *Dct-LaacZ* transgenic line that can be used to label melanoblasts and their progeny at low frequency and randomly during development, and 2. Make aggregation chimaeras between wild type embryos and embryos carrying the *Dct-LacZ* transgene.

Chapter 1

Introduction

Gavin... can somehow metabolize at will one of his amino acids, tyrosine. This will produce melanin, which is the brown-black pigment responsible for human skin color. Gavin can... inhibit this metabolizing by... varying the level of his blood phenylalanine. So he can change his color from most ghastly albino up through a smooth spectrum to very deep, purplish, black. ...he can keep this up,... for weeks. ... he... gradually drifts back to his rest state, a pale freckled redhead's complexion. ... we do know that the dermal cells which produce melanin- the melanocytes- were once,... at an early stage of embryonic growth, part of the central nervous system. But as the embryo grows, as tissues go on differentiating, some of these nerve cells move away from what will be the CNS, and migrate out to the skin, to become melanocytes. They keep their original tree-branch shapes, the axon and dendrites of the typical nerve cell. But the dendrites are used now to carry not electric signals but skin pigment.

Thomas Pynchon (1973).[1]

[1] Quoted from Pynchon, T. (1973). *Beyond the Zero* in **Gravity's Rainbow**. The Viking Press, Inc.New York, U.S.A.

The Neural crest

The neural crest is a heterogeneous population of migratory cells originating between the dorsal neural tube and the overlying ectoderm. These cells are highly proliferative and give rise to a diverse range of cell types that populate many different regions of the vertebrate embryo. Neural crest cells provide a model for studying many aspects of developmental genetics. In particular, questions relating to how an initially apparently homogeneous group of cells can adopt unique and diverse fates, how these cells interact with their dynamic extracellular environment, and how they migrate to specific destinations have been a focus of research for many decades.

One of the neural crest lineages, the melanoblast lineage, is particularly amenable to study. Melanoblasts give rise to mature melanocytes which are the pigment producing cells of the skin, hair, and eyes. In the mouse, neural crest-derived melanoblasts migrate from a region lateral to the neural tube at around embryonic day nine (E9). They migrate over the somites and through the dermal mesenchyme towards the ventrum between E10 and E12, and they move from the dermis to the epidermis, colonising the developing hair follicles by E15 (1). Mature melanocytes begin to synthesise pigment at around postnatal day four (P4). Pigment is stored in specialised melanosomes which are related to the lysosomes found in other cell types (2). Melanosomes are transported from melanocytes via their dendrites into keratinocytes and hair bulbs, where they pigment the skin and hair. Since pigmentation is not essential for viability in laboratory mouse strains, many mutations have been isolated that affect melanocyte biology at all stages of development. By characterising these mouse mutations, and from *in vivo* and *in vitro* manipulations of neural crest cells using other model organisms, notably from the use of chick/quail chimaeras, but also from *Xenopus*, and more recently, zebrafish, it has been possible to address the interactions between gene products and the embryonic environment during the development of neural crest-derived melanoblasts.

In addition to the availability of mouse mutants, mice can be manipulated genetically to follow gene expression patterns using reporter constructs and to determine the effects of eliminating gene activity. Recently, *in vitro* neural crest culture systems have been developed in the mouse providing opportunities to manipulate neural crest cells from both mutant and wild type embryos. Using a combination of these approaches, it is possible to study the early events of lineage specification through to the cell biology of fully

differentiated melanocytes and their unique metabolic pathways. In this introduction, I will discuss how the neural crest lineage is thought to be specified within the ectoderm, how the diverse range of sublineages may be established and maintained, with particular reference to the melanoblast lineage, and how the dynamic extracellular matrix (ECM) provides migratory pathways. Finally, I will briefly introduce some mutations that affect melanoblast development and pigment synthesis. Several of these mutations will be described in greater detail in some of the results chapters.

Specification of the neural crest lineage

In the late gastrula and early neurula stages of urodeles, presumptive neural crest tissue has been fate-mapped to a narrow band of ectoderm at the border between prospective epidermis and prospective neural plate. Similarly, in the chick, grafting experiments fate-mapped prospective neural crest to the epiblast cells between the neural and epidermal fields (3;4). At this early stage, the prospective neural crest has been specified, but cells are not committed; they are still competent to form epidermal and neural derivatives. These three ectodermal derivatives do not segregate until neural tube closure (3;5), however, the neural crest and neural tube lineages do not segregate until very late, probably not until crest cells delaminate from the neural tube. Individually labelled cells in both the chick (6) and mouse (7) dorsal neural tube can give rise to both neural crest and neural tube derivatives. Also, individually labelled chick neural crest cells that have already left the neural tube can contribute to ventral neural tube derivatives (floor plate cells and motoneurones) if they are transplanted back into ventral neural plate (8). These experiments suggest that specification of neural crest fate is reversible until late stages.

Classical grafting and co-culture experiments have shown that mesodermal tissue can induce neuronal differentiation in overlying ectoderm. *Xenopus* dorsal mesoderm can induce central nervous system (CNS) tissue in adjacent ectoderm and neural crest tissue in distant ectoderm. Lateral mesoderm induces both CNS and neural crest, while ventral mesoderm can only induce neural crest fates (3;9). This induction is believed to occur by inhibition of BMP4 activity in the ectoderm. High levels of BMP4 signalling in the ectoderm generate epidermal derivatives, while low levels generate CNS derivatives (9). The dorsal mesoderm (organiser) produces the neural inducing molecules chordin, follistatin, and noggin. These molecules inhibit BMP signalling by binding to BMPs and preventing them from binding to their receptors. Thus, dorsal ectodermal cells adopt neural fates by being exposed to BMP

inhibitors. Addition of BMPs to chick neural plate induces expression of the neural crest marker, *slug*, and over expression of noggin in *Xenopus* results in ectopic neural crest development (9).

Marchant, *et al* (9) proposed a model in which the BMP concentration specifies the neural crest fate. A BMP gradient is established as a result of the high BMP expression in ventral ectoderm (prospective epidermis) being neutralised dorsally by neural inducers produced in the mesoderm. High levels of neural inducer produced by the organiser may diffuse away to inhibit BMPs strongly in presumptive CNS but only weakly in presumptive neural crest. Alternatively, dorsolateral mesoderm may produce a low level of neural inducer that acts in the overlying ectoderm (presumptive neural crest).

Using another model, LaBonne (10) argues that the BMP concentration may not be critical and that as long as neural plate tissue is adjacent to epidermis, neural crest will form. Over-expression of BMP4 mRNA in *Xenopus* prospective ectoderm produced ventralised embryos with microcephaly, but the neural crest was largely unaffected. As long as there was ectoderm next to neural plate, a normal amount of neural crest was specified. Over-expression of chordin only induced low levels of the neural crest markers *Xslug* and its close relative *Xsnail*. However, co-culturing chordin-expressing explants with mesoderm induced high levels of neural crest markers and melanocyte differentiation. In addition, eFGF and Xwnt-8 could substitute mesoderm in this assay. *Slug* expression was not sufficient to induce neural crest. However, *slug* expressing ectoderm could give rise to neural crest in the presence of eFGF or Xwnt-8. This effect was lost when a dominant negative Xwnt-8 was over-expressed (10). These experiments suggested that BMP activity specified neural crest cell fate at the neural plate/ prospective epidermis border, but that a second signal, probably from the mesoderm, was required to maintain that fate.

The *slug* gene has been used extensively as a neural crest cell marker in *Xenopus*, zebrafish, and avian embryos. *slug* encodes a 269 amino acid zinc finger protein. It is expressed in presumptive neural crest from the late gastrula stage in *Xenopus* and then in premigratory and migratory neural crest cells. In addition to the neural crest lineage, *Xslug* is expressed later in the lateral plate mesoderm from the mid-neurula stage. The injection of *Xslug* antisense RNA inhibited neural crest emigration by downregulating expression of *Xslug* and *Xsnail* (11). In the chick, *slug* is expressed during gastrulation in the primitive streak and later in the neural folds (3;12). The use of *slug* antisense oligonucleotides in the chick

suggested it may have a role in epithelial to mesenchymal transitions during the delamination of mesodermal cells from the primitive streak and of neural crest cells from the dorsal neural tube (13). Expression of a fusion protein containing the *Xslug* DNA-binding domain and *Drosophila engrailed* transcriptional repressor domain in *Xenopus* had the same effect as wild type *Xslug* expression, indicating that *slug* functions as a transcriptional repressor (14).

Although *slug* appeared to be important for neural crest development in the chick and *Xenopus*, it does not appear to be essential for neural crest development in the mouse (12). Jiang, *et al* produced mice carrying a null allele of *Slugh*, the mouse *slug* homologue, in which the zinc finger coding region was replaced with the *LacZ* coding region. They showed *Slugh* is first expressed in the extraembryonic mesoderm, and later in several mesodermal derivatives, but not in the primitive streak. *Slugh* is expressed in migratory neural crest cells, but not in premigratory crest cells. Mice homozygous for the null allele showed no defects of neural crest or mesoderm development, however, there may be a degree of redundancy between *slug* and related genes such as *snail*.

A novel protein involved in neural crest development was identified after screening a quail neural tube cDNA library (15). Over expression of Noelin-1 upregulates *slug* expression and prolongs neural crest cell emigration from the neural tube in a non-cell autonomous manner. Prior to the onset of *slug* expression, Noelin-1 is found in a graded manner in the neural plate, wth the highest expression level in the neural folds. Its expression is subsequently restricted to the dorsal neural tube and then to a subset of migrating neural crest cells. Although the method of action of Noelin-1 is not completely understood, it appears that this protein confers neural crest competence to neural tube cells (15).

Delamination of neural crest cells from the dorsal neural tube

As suggested earlier, neural crest and CNS lineages probably do not segregate until the neural crest becomes morphologically distinct as a mesenchymal population. While mechanisms regulating epithelial to mesenchymal transitions are not fully understood, they must be accompanied by reduced cell-cell adhesion, increased cell-matrix adhesion, and increased cell motility. Cell-cell adhesion in epithelia is mediated by homophilic interactions between members of the cadherin protein family at the apical surfaces of epithelial cells, and the coordinated expression patterns of different family members may

regulate neural crest cell movements. For example, N-cadherin has been implicated in neural crest cell delamination from the dorsal neural tube.

Although several models have been proposed to explain the delamination of neural crest cells, little evidence supports one particular model. Cells may delaminate following asymmetric divisions in the dorsal neuroepithelium, and in the chick, 70% of mitotic spindles are oriented to give an asymmetric cell division. Alternatively, cells may generate a tractional force which pulls them free of cadherins junctions. Indeed, newly emigrated cells look bottle-shaped and remnants of adherens junctions remain on the neural tube (4). During delamination, the dorsal neural tube does not have a basal lamina. The formation of the basal lamina may lead to the cessation of neural crest cell delamination. It has been shown that *rhoB*, a member of the *rho* family of GTP binding proteins, is required for delamination of neural crest cells in the chick. *rhoB* is expressed in the dorsal neural tube and in early migrating crest cells (16). Its expression is selectively upregualted by BMP4 activity, and ablation of *rhoB* activity prevents delamination of neural crest cells.

BMP4 signalling is thought to coordinate neural crest cell delamination as well as its specification. In avian embryos, BMP4 is expressed dorsally along the length of the neural tube, and its specific inhibitor, noggin, is expressed in a graded manner, with higher concentrations caudally, and low concentrations rostrally. Addition of ectopic noggin rostrally inhibited neural crest delamination, with an accompanying reduction in *rhoB* and *cadherin-6B* expression. Conversely, over expression of BMP4 accelerated neural crest cell emigration (17).

There are similarities between mechanisms of neural crest induction in different species. The BMP4 signalling pathway is common to different species and it probably acts in each to pattern the ectoderm. Morphological variations between vertebrates may result from modified domains of gene expression and variations in gene targets, but many aspects of the genetic pathways are conserved.

Neural crest cell diversity

Derivatives of the neural crest

Neural crest cell derivatives vary along the rostrocaudal axis. This axis is normally divided into the cranial, vagal, trunk, and lumbosacral neural crest. The developmental potential of a

neural crest cell at a given axial level is greater than its fate (5;18;19). For example, melanocytes can develop *in vitro* from all axial levels of neural crest in the chick, but most melanocytes are derived from trunk and lumbosacral crest (19), although quail-chick chimaera experiments show that cranial neural crest does generate melanocytes (20).

In addition, in the chick and mouse, cranial neural crest cells give rise to Schwann cells and the ciliary and sensory ganglia of the peripheral nervous system (PNS), and mesectodermal cells which generate the bone, cartilage, and smooth muscle of the face (5;19;21). The vagal crest gives rise to sympathetic and parasympathetic neurones, enteric neurones, glial cells, and neuroendocrine cells, as well as some mesectodermal derivatives (5;18;22). The trunk crest gives rise to neurones of the sympathetic and dorsal root ganglia (DRG), Schwann cells, adrenomedullary cells, and melanocytes. Finally, the sacral crest generates melanocytes, glial cells, and neurones of the sympathetic, dorsal root, and posterior enteric ganglia. If trunk neural tube is grafted to vagal regions, grafted cells contribute to the enteric nervous system, indicating that they can change their fate in response to a new environment (22). If cranial neural tube is grafted to the trunk, some grafted cells form cartilage, while others contribute to the sympathetic and dorsal root ganglia. All axial levels have the potential to form sympathetic, parasympathetic, and sensory neurones, while mesenchymal derivatives can only form from cranial and vagal neural crest (22).

Zebrafish neural crest produces derivatives similar to those of amniotes, generating sensory and autonomic neurones, glial cells, and pigment cells. As in the chick and mouse, zebrafish cranial neural crest generates mesectodermal cells ('ectomesenchyme') which give rise to the head and gills (23). However, unlike amniotes, in zebrafish, the ectomesenchyme forms from trunk crest as well as cranial neural crest (23).

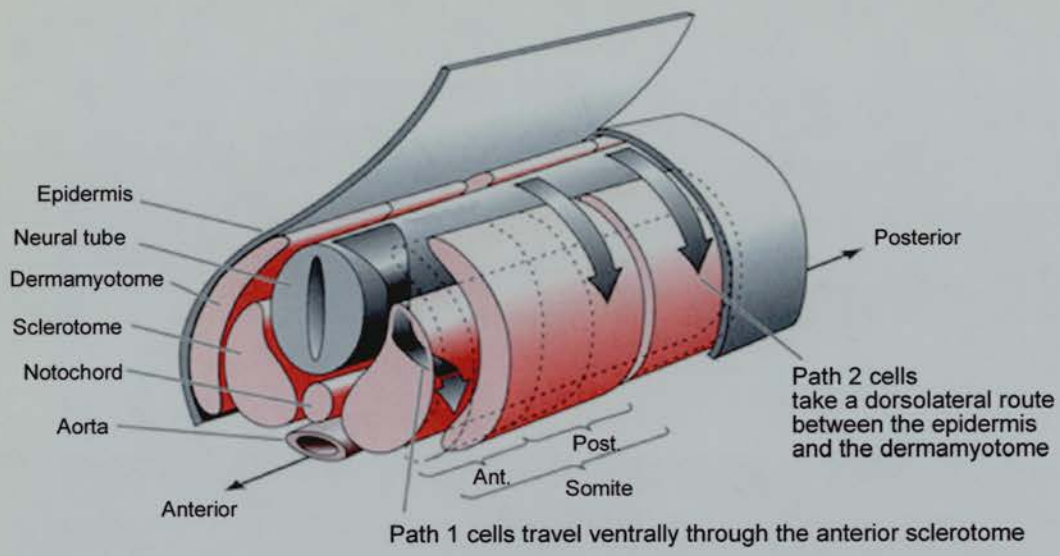

Figure 1. Migration pathways of neural crest cells.[2]

[2]*Figure adapted from Gilbert, S. (1994). Developmental Biology (fourth edition). Sinauer Associates Inc. Massachusetts, U.S.A. (page 274).*

Migratory pathways of trunk neural crest cells

Neural crest cells at all axial levels migrate along unique and defined pathways in the embryo. I will describe the migration pathways of the trunk neural crest only. In the chick, cells emigrate from the neural tube at the level of the most recently formed somite (4), and migration is initiated in a rostrocaudal manner (as is somite development). When crest cells first detach from the neuroepithelium, they enter a cell-free area filled with extracellular matrix molecules immediately lateral to the dorsal neural tube. This region has been termed the dorsal wedge (24) or 'migration staging area' (MSA) (25). The MSA is bordered medially by the neural tube, dorsally by the overlying ectoderm, and laterally by the somites. From this region, cells migrate along one of two distinct pathways: the ventral pathway or the dorsolateral pathway.

Migration in the ventral pathway

Cells that give rise to neurones and glia of the sympathetic and sensory (dorsal root) ganglia migrate ventrally at E2.5 in the chick at the level of the wingbud (26) and at around E9 in the mouse at the level of the forelimb (24). Cells invade the anterior dorsal somite between the myotome and sclerotome, and migrate laterally and ventrally, forming sympathetic and sensory ganglia, or they continue to migrate along the ventral motor nerve roots, where they differentiate into glial cells (see Figure 1). Cells migrating along the ventral pathway always avoid the region around the notochord and the posterior half of a somite. Chick/quail chimaera studies have shown that crest cells adjacent to the posterior somite either migrate rostrally through the anterior half of the same somite or caudally through the anterior half of the next somite down. Also, chick neural crest cells cultured with blocks of anterior or posterior somite tissue withdraw cellular processes on contacting posterior somite and migrate in another direction (4). These observations suggest that there are distinct regions in the pathway that are inhibitory to neural crest cell migration. In zebrafish embryos, this pathway corresponds to the medial migration pathway (23).

Melanoblasts migrate along the dorsolateral pathway

Neural crest cells in the chick and mouse specified as melanoblasts only migrate along the dorsolateral pathway between the dermatome and the overlying ectoderm (see Figure 1). In zebrafish, this pathway is called the lateral pathway. Cells migrate evenly over the surface of the dermatome and are not restricted to the anterior somite (26). At least in the chick, cells must be specified as melanoblasts to migrate along this pathway (27;28). These cells

move dorsally and migrate in the dorsolateral pathway even if they are placed in the ventral pathway. Also, neural crest cells that are not specified as melanoblasts undergo apoptosis if they enter the dorsolateral pathway (29). In zebrafish, however, melanoblasts can migrate along both pathways (23). In the mouse, melanoblasts then migrate towards the ventrum through the developing dermis (dermal mesenchyme), where they move as individual cells rather than in groups. They invade the basement membrane between the epidermis and the dermis between E11 and E12. By E13 and E14, they have colonised the epidermis. By E15, melanoblasts migrate from the epidermis into the developing hair follicles where they continue to proliferate until postnatal day 4 (P4), when they begin to synthesise pigment (30).

Differences in migration patterns among vertebrates

In avian and zebrafish embryos, migration along the trunk dorsolateral pathway is delayed compared to ventral migration (19;23;26). Dorsolateral migration begins as ventral migration is finishing and sympathetic and sensory ganglia are already beginning to form. In avian embryos at least, this delay is due to late emigration of melanoblast precursors from the neural tube, rather than from migratory arrest lateral to the neural tube (28;31). Although this delay in the trunk crest has been considered a universal feature of dorsolateral migration, there is no such delay from avian cranial or vagal neural crest where both early and late migrating crest cells have equivalent developmental potential (20;26). Also, this delay is not seen at all in the mouse. By labelling neuroepithelial cells with the lipophilic dye, DiI, Serbedzija *et al* (24) showed that dorsolateral and ventral migration occur simultaneously in the mouse.

There are other important differences in neural crest development among vertebrates. Indeed, there are several differences between *Xenopus* neural crest development and that of the mouse and chick. *Xenopus* crest cells migrate along one of five distinct pathways in the trunk, rather than in one of the two pathways seen in the mouse and chick. Rostral and mid-trunk crest cells migrate dorsally into the fin and dorsal pigment stripe, ventrally past the neural tube and notochord to prospective spinal ganglia, and laterally under the epidermis. Caudal crest cells migrate along two additional pathways: the 'tail tip'pathway along the dorsal neural tube or dorsal fin, around the tail, and into the ventral fin, and the 'enteric' pathway, directly towards the anus and ventral fin (32). In addition, although in the mouse and chick, there seem to be many crest cells per segment, there are only a few in *Xenopus* (33). This is also true for zebrafish, where there are only 12 large crest cells per segment

(23). Also, while crest cells avoid the caudal sclerotome in the chick and mouse, *Xenopus* crest cells do not (33). It must always be borne in mind that observations made in one system may not apply to all vertebrates.

Extracellular matrix molecules in migratory pathways

A fundamental issue of neural crest development is whether cell fate is determined by extrinsic or intrinsic factors. Do cells differentiate according to their migratory microenvironment, or do they first adopt a particular fate with associated changes in gene expression, and then select an appropriate migratory pathway? It is clear that environmental cues greatly influence neural crest cell migration, since for example, posterior somite tissue is not permissive to crest cell invasion. However, a degree of fate restriction seems essential since only melanoblasts are capable of migrating along the dorsolateral path and they never migrate ventrally. In this section, I will describe some permissive and non-permissive molecules present in the extracellular environment and the roles they may play in directing cell migration.

Permissive molecules

Extracellular matrix (ECM) molecules permissive to neural crest migration include fibronectin, laminin, tenascin, and the collagens. These glycoproteins are distributed uniformly above the neural tube, in the sclerotome, and along the migration pathways (34). Neural crest cells themselves express laminin $\alpha 1$ and $\beta 1$ cDNAs, illustrating how they can influence their own migratory environment (35). $\alpha 1$ laminin is also expressed strongly in the dermamyotome through which melanoblasts migrate, but not by the sclerotome, neural tube, or notochord (35). Neural crest cells express integrin receptors for permissive molecules. These interactions facilitate communication between the actin cytoskeleton and the ECM, resulting in changes in cell behavior such as cell attachment, spreading, and migration (21).

Fibronectin, the most well-studied of all the permissive molecules, is a large homodimer of 500kDa and each subunit contains independently folding domains (FN repeats I, II, and III). Soluble fibronectin dimers are loosely folded and cells wrap the fibronectin around themselves, extending it into a matrix of fibrils. The fibrils are elastic and cells can pull on the matrix to generate tension (36). Other ECM molecules having similar repeats, such as tenascin, are thought to be extended by cells in a similar fashion. Avian trunk neural crest

cells preferentially migrate on fibronectin rather than laminin when given a choice of the two, and they migrate more quickly over fibronectin, at a speed of 50μm/hour (37). Crest cells migrating on fibronectin have a shorter cell cycle time compared to those on collagen or plastic (38). The increased cell density caused by increased proliferation is thought to favour cell dispersion onto the migratory pathways. Crest cells are most likely to migrate in a directional manner rather than randomly if there is a high cell density and their motility is not reduced following cell-cell contact or cell overlapping (37).

Migrating cells communicate with the ECM via integrin receptors. Integrins are heterodimers of an α and β subunit. There are 15 α chains and eight β chains. Integrin receptors bind multiple ligands and some ligands can be recognised by several integrins. Analyses of targeted mouse mutations in genes encoding various integrin subunits have revealed a degree of redundancy (39), however, α4β1 and α5β1 integrins recognise fibronectin cell binding domains. Beauvais *et al* (40) demonstrated that S180 cells expressing α5 and low levels of α4 subunits migrate along the ventral and dorsolateral migration pathways simultaneously when transplanted into chick embryos, while parental and host neural crest cells remain delayed in their invasion of the dorsolateral path (40). They suggest that melanoblasts can only migrate along this pathway once they have begun expressing these integrins. By inhibiting the α4 integrin subunit in a neural crest explant system, Kil *et al* (41) showed that the α4 integrin is also required for neural crest cell migration away from the neural tube in the mouse.

When cells migrate, they extend a leading edge forwards and adhere to the substrate via these receptors. The receptors diffuse freely in the cell membrane and upon cellular attachment to the substrate, they localise to focal adhesions. Receptor cross-linking and ligand binding localises actin filaments to the adhesion site and recruits other proteins which stabilise the complex. Depending on the rigidity of the interaction, the complexes remain stationary as the cell moves forward. The cell can exert a stronger force on a rigid or stressed ECM. The cell can move forward because the forces exerted at the leading dege are strong and transient, while at the rear, where the complexes are recycled, they are weak but stable (42;43).

The presence of cells in the ECM affects the properties of the extracellular environment. Migrating cells may bind to and extend permissive molecules and expose otherwise concealed binding sites (36). The dynamic nature of the ECM is illustrated by the fact that

some molecules distributed uniformly early in neural crest cell migration, such as collagens type I and III, and keratin sulphate proteoglycan, become localised to the posterior sclerotome later when many neural crest cells are in the extracellular space (21). In addition, migrating crest cells reorganise the ECM *in vitro*, re-aligning thin fibronectin filaments into thick bundles along which cells migrate more efficiently (37).

Non-permissive molecules

The main non-permissive molecules found in the ECM are the peanut agglutinin (lectins) binding molecules and chondroitin sulphate proteoglycans such as aggrecan and versican. T cadherin and the ephrin ligands also inhibit migration. These molecules are found in the posterior sclerotome, perinotochordal mesenchyme, dorsolateral space, and, during the initial stages in chick crest cell migration, on the surface of the dermatome (21;34). Aggrecan binds collagen type I and versican binds fibronectin. These non-permissive molecules may act by concealing cell binding sites on the permissive molecules. In the quail, novel chondroitin sulphate proteoglycans have been isolated that bind collagen type I. These molecules inhibited neural crest cell spreading *in vitro* (44). In the mouse, chondroitin sulphate distribution negatively correlates with patterns of neural crest migration on the ventral pathway (45). When the synthesis of these molecules was inhibited, neural crest cells invaded both the posterior and anterior sclerotome.

Mutations in the paired box gene, *Pax3*, result in the *Splotch* phenotype. Heterozygous animals have white spots on the belly, tail, and feet, while homozygotes have almost no coat pigmentation and exhibit reduced or absent DRGs with failure of neural tube closure (46;47). Neural crest cells from *Splotch* mutant mice migrate normally *in vitro*, suggesting that environmental influences retard their migration *in vivo*. Versican is overexpressed in *Splotch* embryos (46) and this over-expression correlates with reduced neural crest cell migration, suggesting PAX3 negatively regulates versican expression.

Another family of ECM molecules restricting neural crest cell migration are the ligands for the Eph-related family of receptor tyrosine kinases. Lerk2/Ephrin-B1 is present in the posterior sclerotome. Neural crest cells express EphB3, the receptor for Ephrin-B1. Crest cells cultured *in vitro* on alternating lanes of Ephrin-B1 and control lanes preferentially migrate on control lanes, however, cells can migrate on a surface uniformly coated with Ephrin-B1 (4).

Members of the semaphorin family affect growth cone movement. One member, collapsin-1 is expressed in the chick caudal somite and it induces growth cone collapse. Neural crest cells cultured on alternating strips of collapsin-I/ fibronectin or fibronectin alone avoid collapsin-1-coated regions and preferentially migrate on fibronectin (48). They express neurophilin-1 in response to collapsin-1, and the authors suggest neurophilin-1 is the receptor for collapsin-1. This inhibitory molecule is also present in the chick dermatome and overlying ectoderm.

The role of non-permissive molecules in the trunk neural crest migration pathways, particular in the posterior somite, may simply be to establish the metameric pattern of the PNS and axial musculature. They may not function to specify neural crest cell fate. Non-permissive molecules might only act to guide fully or partially specified neural crest cells, and fate may be specified by paracrine interactions or by inherent differences among cells. However, temporal changes in ECM composition may control the migration of subsets of neural crest cells. For example, although the delayed dorsolateral migration of crest cells in the chick is primarily due to delayed emigration from the neural tube, removal of the dermamyotome results in premature invasion by cells on the dorsolateral pathway (although migration is still delayed compared to ventral migration) (49). Peanut agglutinin binding proteins and chondroitin-6-sulphate proteoglycan are initially present in the dermamyotome, and their disappearance precedes dorsolateral migration of crest cells (49).

Specification of the neural crest sublineages and the clonal nature of the neural crest

The restriction of developmental potential and the specification of cell fate are such central issues in neural crest development that several approaches, both *in vivo* and *in vitro* have been developed to investigate their mechanism and time course. *In vivo* studies primarily involve labelling individual or groups of cells before or shortly after their emigration from the neural tube (6-8;50). *In vitro* approaches are based on plating neural crest cells at clonal dilutions and assessing the cell types that differentiate in culture (31;51;52). These two approaches are complementary; *in vivo* analyses give an indication of cell fate, while *in vitro* analyses assess the developmental potential of a cell or a population of cells.

In vivo studies and the analysis of cell fate

In one study (6), chick neural tube cells were labelled with the vital dye, lysinated rhodamine dextran (LRD), grown for two days, and the number and distribution of their progeny was assessed. In some of the clones, progeny were observed in the neural tube only. Of those that generated neural crest cells, clone size varied greatly, with the smallest clone comprising only four cells, and the largest, 70. In half of the clones, the distribution of progeny was bilaterally symmetrical. Sixty per cent of clones that generated neural crest cells also gave rise to neural tube derivatives, illustrating the late segregation of these lineages. Some labelled cells generated progeny of only one cell type, while one cell generated progeny in the neural tube, DRG, ventral root, adrenal medulla, and dorsolateral pathway (melanoblast progenitor). More than half of the marked cells whose progeny left the neural tube generated multiple cell types.

When the equivalent experiment was done in the mouse (7), many labelled cells also gave rise to progeny in the neural tube and in the neural crest, and many clones also generated multiple crest derivatives. Neural tube cells labelled early generated dorsal and ventral crest derivatives (e.g., sympathetic and sensory derivatives), while those labelled later generated only dorsal derivatives (dorsal root neurones and presumptive melanoblasts). In another study, individual chick migratory crest cells in the somite were labelled with LRD and grown for two days (50). There was a great variation in the proliferative capacity of labelled cells, with clones ranging in size from two to 67 cells. Even at this later stage, many cells gave rise to multiple cell types. The progeny of most cells was confined to a single segment, but some clones contributed to two adjacent segments.

Surprisingly, chick neural tube cells labelled with DiI when neural crest cell migration is complete revealed a second wave of migration from the neuroepithelium (53). These cells leave the neural tube through the dorsal root entry zone (DREZ) and they give rise to sensory neurones, satellite cells, and melanocytes. The DREZ is the only region of the neural tube that cells can penetrate because, by this stage, a basal lamina has formed around the rest of the neural tube. The authors suggested these migratory cells may be clonally related to the earlier migrating crest cells. This result further demonstrates the late specification of cell fate in the neuroepithelium, and suggests that "neural crest" specification may be an ongoing process (18).

In vitro studies and the analysis of developmental potential

In early culturing experiments, cells were plated at a low cell density to determine whether non-crest cells were required for differentiation (52). Quail trunk neural crest cells cultured individually in medium containing horse serum and embryo extract generated three types of clones: pigmented, unpigmented, and mixed. Similar experiments using quail cephalic neural crest (51) demonstrated that single cells can be multipotent, giving rise to neurones, glia, cartilage (a mesectodermal derivative), and melanocytes. Other cells generated only neurones, glia, and cartilage. They also identified unipotent crest cells. Similar experiments in the mouse also produced pigmented, unpigmented, and mixed clones, suggesting that at the time of emigration, neural crest cells comprise a heterogeneous population of cells with developmental potentials varying from unipotent to multipotent (54). Interestingly, a further difference between species was highlighted by the finding that clones containing exclusively pigmented cells accounted for only eight percent of islolated clones in mouse neural crest cultures, compared to 40 to 60% in the quail (52;54).

To correlate these observations with the timing of neural crest cell emigration, Henion and Weston (31) explanted quail neural tubes, allowed cells to migrate out on to the substrate, and transferred the neural tubes to a new dish. They repeated this twice and isolated populations of neural crest cells that had emigrated during the first six hours, six-16 hours, and 30-36 hours. Nearly half of the cells emigrating in the first six hours were already fate restricted, with 30% giving rise to only glial cells, 11% to neurones, and just 2% to melanoblasts. Most of the pluripotent clones generated neuronal and glial progenitors (NG cells), some generated glial and melanoblast progenitors (GM cells), and only a very small proportion (less than 2%) gave rise to cells of all three lineages (NGM). Subsequent culturing periods revealed that melanoblasts begin to emerge in large numbers later (13-16 hours). The largest clones were formed by GM cells. Neural and glial lineages segregated before glial and melanocyte lineages. By 30-36 hours, nearly all marked cells generated fate-restricted precursors. This highly informative study illustrated several points. Almost half of the early migrating cells are already fate restricted. The neural and melanoblast lineages segregate almost immediately, followed by glial and neural lineages, and finally glial and melanoblast lineages.

The combined results of *in vivo* and *in vitro* studies suggest that the neural crest is a truly heterogeneous population of cells, consisting of clones with varying proliferative and developmental potentials. These developmental potentials are asynchronously restricted.

Also, at least in avian embryos, melanoblast progenitors are delayed in their emigration from the neuroepithelium (see also (28)).

Studies using chimaeric mice

Since the neural crest consists of clones with variable potential, cells within a lineage may be derived from different progenitor cell types. For example, a melanoblast may have been derived from an initially fate restricted cell (M cell), or a GM cell of an equivalent age. They may vary, for example, in proliferative or migratory potential. Melanoblasts are particularly amenable to clonal analyses because mice of different coat colours can be used to make chimaeras, where clones of different parental origin are easily distinguished. Several pioneering studies of such chimaeric mice were done by Mintz. She suggested that many embryonic derivatives are likely to be multiclonal in origin, and that different clones, termed phenoclones, may exhibit mitotically heritable differences in gene expression (55). She further suggested that an evolutionary advantage was conferred by having organs and tissues derived from multiple founder cells. Mintz generated aggregation chimaeras using embryos carrying different pigmentation alleles (56). The patterns generally consisted of broad transverse bands of colour, independently arranged on the left and right sides of the body. Mintz proposed each band was derived from a single melanoblast progenitor. After studying the arrangement of bands in the coats of many chimaeric animals, she postulated there were 34 primordial melanoblasts. These conclusions will be considered more fully in Chapter 4.

Evidence for stem cells in the neural crest

If all of the epidermal melanocytes are derived from a small number of founder cells, these founder cells must be capable of extensive proliferation (clonal expansion). Melanoblast and melanoblast/glial (GM) progenitors generate large clones *in vitro* (31), and neural crest progenitors labelled *in vivo* are capable of generating large clones within two days of culture (7). This proliferative capacity, and the diversity of cells types generated, has led to the suggestion that the neural crest contains stem cells. A stem cell must be undifferentiated, and capable of proliferation, self-maintenance, and parenting large numbers of undifferentiated progeny, and it should be able to regenerate following tissue damage.

Certainly, early neural crest cells exhibit some characteristics of stem cells. That some crest cells can generate many derivatives suggests cells have the capacity to self-renew. Early

crest cells tend to generate ventral derivatives and late cells generate dorsal ones (57). This ventral to dorsal development occurs because the first cells to migrate ventrally fill the ventral-most targets and later migrating cells colonise more dorsal targets. If early cells are ablated, late migrating cells populate both ventral and dorsal sites. In addition, wild type cultured neural crest cells injected *in utero* into embryos lacking melanoblasts can populate more than half of the host skin surface (58). In these embryos, injected cells migrated longitudinally, as well as dorsoventrally, undergoing extensive clonal expansion. Cells injected into wild type embryos contributed to host pigmentation in a limited manner, but they mainly migrated dorsolaterally. Together, these results suggest neural crest cells can respond to damage and proliferate beyond normal requirements and therefore self-renew (57).

These results hold for chick and mouse, but not for zebrafish. Although individually labelled zebrafish trunk crest cells can generate multiple cell types, they undergo limited division prior to differentiation. Also, late migrating and cephalic crest cells are only unipotent. Therefore, zebrafish neural crest cells are not thought to constitute a stem cell population (57).

Stemple and Anderson (59) have shown there are stem cells in the rat neural crest population. They cultured neural crest cells, enriched for cells expressing low affinity nerve growth factor receptor (LNGFR), a marker expressed by most neural crest cells, and re-plated cells at clonal density. Surviving cells generated subclones containing multiple cell types: neurones, glia, and an unidentified type, probably melanoblasts since explants were taken from the trunk. When these subclones were re-plated at clonal density, most generated at least one multipotent secondary subclone (i.e., at least one secondary subclone contained three different cell types). Ten per cent of all secondary subclones were multipotent. Half of the primary subclones generated multiple multipotent secondary subclones, and one generated 15 multipotent secondary subclones. This suggested that cells were not simply undergoing asymmetric divisions, as this would limit them to only one multipotent secondary subclone.

Cell divisions that maintain a stem cell population can be asymmetric or symmetric. One stem cell may undergo an asymmetric division to generate a stem cell and a fate-restricted blast cell. Alternatively, a stem cell could divide symmetrically to generate either two stem cells or two blast cells. A population of stem cells undergoing symmetric divisions can

exhibit asymmetry if half the cells generate stem cells and half generate blast cells. Some symmetric divisions must have happened in these experiments to generate multiple multipotential subclones. Environmental cues may control the pattern of stem cell divisions in the population, and this pattern would determine whether or not the stem cells become exhausted (59). Evidence suggests that pluripotent neural crest derivatives are present at terminal sites of differentiation in the quail, suggesting that crest cells may retain the capacity for self-renewal until late stages. Indeed, stem cells present in the adult mouse epidermis re-populate the hair bulb at the beginning of each new hair growth cycle (47;60).

Pigment mutations and the genetics of melanoblast development

Mouse pigmentation mutations

Spontaneous and targeted mouse mutations have revealed many gene loci essential for melanoblast development. Since pigmentation defects do not affect the viability of domesticated animals, there are multiple naturally occurring alleles for many of the genes that affect pigment cell development and function (47). Loci important for the early events of melanoblast development affect more than one neural crest lineage and late acting genes may affect melanocyte function and pigment biosynthesis specifically. For example, *Splotch* mutant mice have disrupted dorsal root ganglia and neural tube defects in addition to pigmentation defects, while a point mutation in the *Tyrosinase* gene which inactivates the enzyme, only affects pigment production. Over 70 pigmentation loci have been identified that affect melanoblast survival and migration, melanosome morphology, and pigment synthesis in the mature melanocyte (47).

Many mutations affect the specification, proliferation, and survival of melanoblasts as they migrate from the neural crest to the epidermis. Mutations in the genes encoding the tyrosine kinase receptor, KIT, its ligand, KIT ligand (KITL), the G protein-coupled receptor, Endothelin receptor B (EDNRB), and its ligand, Endothelin-3 (EDN3) have revealed that these signalling pathways are essential for melanoblast proliferation, migration, survival, and differentiation. Manipulation of the signalling pathways downstream from these genes has begun to reveal how these different effects may be mediated. The phenotypes of mutations in these genes and the information they provide about melanoblast development will be introduced and discussed separately in Chapter 3.

Many of the mutations that only affect melanocytes affect melanosome structure and enzymes in the melanin biosynthetic pathway. Expression of some of these melanocyte-specific genes is thought to be regulated by the Micropthalmia transcription factor (MITF). The *Mitf* gene encodes a basic helix-loop-helix leucine zipper transcription factor. There are more than 20 alleles of *Mitf* and mutations cause the *micropthalmia* phenotype, leading to a lack of pigmentation in the hair or eyes, and small eyes when homozygous. Heterozygotes have white belly spots (47). The *Mitf* gene product is thought to upregulate expression of melanoblast and melanocyte-specific genes.

Mutations at other loci affect the quality of pigment produced. These mutations affect enzymes in the pathway that converts tyrosine to DOPA and DOPAquinones and then to eumelanin (black/brown) or phaeomelanin (red/yellow). Tyrosinase is the key enzyme in the melanogenic pathway. There are several mutant alleles of the *Tyrosinase* gene resulting in coat colours ranging from white to pale to gray. Mutations in *Tyrosinase-related protein 1* (*Tyrp1*) cause eumelanin to look brown rather than black, while mutations in the *Dopachrome tautomerase* (*Dct*) gene cause pigment to look dark gray (47). Mutations in the *Myo5a* gene cause the *dilute* phenotype in which animals have a general dilution of coat colour. The *Myo5a* gene encodes an unconventional myosin required for transporting pigment-containing melanosomes into keratinocytes.

Other mutations affect the regulation of pigment production. Dorsal hairs of wild type mice are banded with yellow and black melanin. This agouti pattern is affected by mutations in the *Agouti* and *melanocortin receptor 1* (*Mc1r*) genes. Dominant *agouti* alleles cause predominantly yellow hair, while recessive *agouti* alleles produce black hair. The reverse is true for *Mc1r*. *Mc1r* encodes a G protein-coupled receptor expressed by mature melanocytes. This receptor controls the switch between production of yellow/red phaemelanin and black/brown eumelanin. The *Agouti* gene encodes a competitive antagonist of α–MSH, the ligand for Mc1r. The relative activities of these proteins determine whether black or yellow melanin is produced.

Zebrafish pigmentation mutations

Orthologues for several mouse pigmentation genes have been identified in the zebrafish genome. Pigmentation patterns in zebrafish are due to the presence of multiple pigment cell types: melanin-producing melanophores, iridophores containing silver and gold reflective

platelets, and xanthophores containing yellow pterodine or carotenoid pigments (61). Larvae are patterned with four longitudinal stripes of melanophores, the dorsal, lateral, ventral, and yolk sac stripes (62). The adult pigmentation pattern consists of longitudinal melanophore and silver iridophore stripes alternating with gold iridophore stripes (63). Xanthophores are present over the iridophores, except in the melanophore-containing blue-black stripes (64). The three chromatophores are thought to share a common precursor (61).

In *sparse* embryos, which have a mutation affecting the zebrafish *Kit* gene (65), melanoblasts fail to survive or migrate normally, while iridophores and xanthophore numbers are unaffected (63;65). Adults are severely deficient in epidermal melanophores, which normally darken the dorsal surface of the fish, and dermal melanophores are reduced to approximately 50% of the wild type complement (63). The *leopard* mutation affects melanophore patterning in adults such that they fail to coalesce into stripes and remain distributed in the dermis as spots. In *rose* mutants, adult iridophores are missing (63). Zebrafish mutations have been identified which affect specific or multiple cell types, and as in the mouse, mutations can affect the specification, proliferation, survival, and differentiation of pigment cells (62;66). The *colourless* phenotype affects multiple but not all neural crest cell types. There are reduced numbers of enteric neurones with disrupted DRG patterning, as well as pigmentation defects, however, ectomesenchymal derivatives are unaffected (66). This suggests that in zebrafish, as has been shown to be the case in avian and mouse embryos, neural crest cells are progressively restricted in their fate.

Human pigmentation mutations

Homologous pigmentation mutations in humans are associated with a variety of hypopigmentation disorders and syndromes characterised by multiple defects. Some diseases, for example, Waardenburg syndrome, can be caused by mutations in one of several genes. Patients with Waardenburg syndrome suffer from deafness and pigmentation defects of the skin, hair and iris (2;67). There are four subtypes of Waardenburg sydrome, defined by the presence or absence of other anomalies. Types I and III are due to mutations in the *PAX3* gene (which causes the *Splotch* phenotype in mice). Type II is caused by mutations in *MITF* (2;67). Mutations in the *EDNRB*, *EDN3*, or *SOX10* genes can result in Type IV Waardenburg syndrome (Waardenburg-Hirschprung disease), in which patients also suffer from aganglionic megacolon. Mutations in mouse *Sox10* cause the *Dominant megacolon* phenotype and mutations in human and mouse *EDNRB* and *EDN3* cause Hirshprung's

disease (aganglionic megacolon and piebaldism). The SOX10 and PAX3 transcription factors have recently been shown to interact directly, binding to and transactivating the *MITF* promoter, resulting in the upregulation of this transcription factor (68).

Mutations in the many genes whose products regulate the production of pigment in mature melanocytes of the skin and eyes cause various forms of oculocutaneous albinism (OCA). OCA-I is caused by mutations in the *Tyrosinase* gene (2;67). OCA-II is caused by mutations in the P gene (which causes the *pink-eyed dilution* phenotype in mice), and OCA-III is caused by mutations in *Tyrosinase-related protein-1* (2;67).

Dct as a marker for early melanoblasts

An early marker for migrating melanoblasts was needed to study the effects of different mutations on melanoblast numbers and migration. The expression of several different enzymes involved in pigment biosynthesis identify mature melanocytes, but one of these enzymes, Dopachrome tautomerase (Dct), also known as Tyrosinase-related protein 2, is expressed particularly early in melanoblast development, before pigment production is initiated (69). *Dct* is also expressed in the developing telencephalon and in the retinal pigmented epithelium (RPE). *Dct* expression can be used to identify melanoblasts in embryos from E10 to E16.5, and several groups have used *Dct* expression to identify migrating melanoblasts in mouse (25;69-71) and zebrafish embryos (25;62;69). In this thesis, melanoblast development was followed *in vivo* and *in vitro* using a *LacZ* reporter gene expressed under the control of the *Dct* promoter (70).

Chapter 2

Materials and Methods

'Hence, we cannot categorically deny that perhaps we may be able to grind genes in a mortar and cook them in a beaker after all.'

H.J.Muller (1922).[3]

[3] Quoted from Gilbert, S. (1994). **Developmental Biology** (fourth edition). Sinauer Associates Inc. Massachusetts, U.S.A.

Manipulation of nucleic acids

General reagents used in molecular biology procedures

All chemicals were analytical grade and were supplied by Sigma, Promega, Gibco BRL, BDH, Fisher Scientific, Flowgen, and Boehringer Mannheim. Nucleic acid manipulations were done in 1.5ml centrifuge tubes unless otherwise stated. General solutions were prepared by HGU technical staff and autoclaved and stored at room temperature.

Tris.HCl

Tris base (tris[hydroxymethyl]aminomethane) was dissolved in sterile water. HCl was used to adjust the pH to the required value.

EDTA

EDTA (ethyldiaminetetra-acetic acid di-sodium salt) was dissolved in sterile distilled water. The solution was adjusted to pH 8.0 by adding solid NaOH.

TE buffer

10mM Tris.HCl (pH 7.5); 1mM EDTA.

TBE buffer, 20X stock

Tris base	216g
Boric acid	110g
0.5M EDTA	80mM

Distilled water was added to a final volume of 1 litre. Stock was diluted to 1X with distilled water.

TAE 50X stock

Tris base	242g
Glacial acetic acid	57.1ml
0.5M EDTA	100ml

Distilled water was added to a final volume of 1 litre. Stock was diluted to 1X with distilled water.

Electrophoresis

Agarose gel loading buffer

Loading buffer was prepared as a 10X stock and stored at room temperature.

	Final concentration
Ficoll	20%
Orange G (Sigma)	1%
EDTA	100mM

Made to required volume with distilled water.

For preparing gels, the required amount of agarose (High pure, BioGene) was dissolved in either 1X TBE or TAE by heating. Molten agarose was cooled and ethidium bromide added to a final concentration of 50µg/100ml agarose. DNA size markers were run alongside experimental samples to estimate the size and amount of DNA in the samples. The size markers used routinely were bacteriophage lambda DNA digested with *Hin*dIII ('λ') (Gibco BRL) and ϕX174 digested with *Hae*III ('ϕX') (Promega). Samples were run in 1X loading buffer. Electrophoresis was used when DNA fragments of a particular size needed to be purified. To do this, samples were electrophoresed using low melting point agarose and the DNA was recovered using a gel extraction kit (Qiagen), according to the manufacturer's instructions.

Determining the concentration of DNA samples

DNA concentrations were determined in one of two ways: by agarose gel electrophoresis or by measuring the absorbance in a spectrophotometer at 260nm (A_{260}). To determine the concentration by electrophoresis, several different volumes of the DNA (e.g., 1,3 and 5µl) were run alongside standard amounts of DNA (usually DNA size markers). An estimate of the concentration was made by visual comparison of the samples with the known amounts of DNA under UV illumination.

To determine the concentration with a spectrophotometer, the DNA sample was diluted 1:100 with dH_2O. The spectrophotometer was calibrated using a water only blank sample. The samples were placed in clean cuvettes and the absorbance at 260nm (A_{260}) was measured. The concentration of the original sample in mg/ml was calculated as follows.

Concentration (mg/ml) = A260 x 100(dilution factor) x 50.

Restriction enzyme digestion

All restriction enzymes were purchased from Boehringer Mannheim unless otherwise stated. Digests were ideally carried out in a large volume (usually 50-100µl) to minimise effects of evaporation. Enzyme was added at a concentration of 5-10u/µg DNA, depending on the duration of the digests. For overnight digests, 5u/µl were used. The manufacturer's guidelines were followed to determine the correct buffer and incubation temperature for each enzyme.

Klenow enzyme was used at a concentration of 1u/µg DNA to end fill digested ends of DNA following digestion with certain restriction enzymes. The reaction was done at room temperature for 15 minutes and it was stopped by heat inactivation at 75°C for 10 minutes, as recommended by the manufacturer.

Removal of buffer salts

In cases where multiple restriction digestion steps were done and the enzymes required different buffers, digests were done separately. Buffer salts were removed between digests by drop dialysis and new buffers were added. A nitrocellulose filter (Millipore) was placed in a petri dish containing filter sterilised dH_2O. The digestion reaction was carefully placed on the filter (a maximum of 50µl per filter) and salts were left to diffuse through the filter for at least 1 hour at room temperature. Following dialysis, the liquid was removed to a fresh 1.5ml centrifuge tube and the appropriate enzyme and buffer were added for the subsequent reaction.

As an alternative to using a filter, salts were removed using either a PCR cleanup kit or a nucleotide removal kit (Qiagen).

Ligations

In order to maximise the ligation efficiency, ligations were set up with the following vector: insert molar ratios: 1:3, 1:5, and vector only (to control for re-ligation of the vector). The amount of vector in each case was 25ng, and the total reaction volume was 10µl. Ligations were done at 16°C overnight using DNA Ligase and ligation buffer (Boehringer Mannheim).

Microbiology

Aseptic technique was observed for all steps involving the growth of bacterial cells (setting up cultures, pouring agar plates, selecting single colonies, and storing bacterial stocks). Liquid cultures were grown at 37°C with vigorous shaking and dry cultures were grown on inverted agar plates at 37°C. All bacterial growth media stocks were prepared by HGU technical staff as follows:

L Broth

Amounts per litre:

Tryptone	10.0g
Yeast extract	5.0g
NaCl	10.0g
Glucose	1.0g

L Broth with Mg^{2+}

L broth with 2.5g magnesium sulphate per litre.

L Agar

Amounts per litre:

Tryptone	10.0g
Yeast extract	5.0g
NaCl	10.0g
Agar	15.0g

Production of electrocompetent cells

A single colony of XL1 Blue *E.coli* cells from an agar plate was used to inoculate approximately 10ml L broth supplemented with 10μg/ml tetracycline (Sigma) for overnight growth. The culture was used to inoculate 2 X 400ml fresh L broth the following morning. Cells were grown to an absorbance at 600nm (A_{600}) of 0.15-1.0. Flasks were chilled on ice for 15-30 minutes and cells were centrifuged at 4°C, 4000g for 15 minutes. Pellets were re-suspended in 800ml ice cold sterile 10% glycerol. The centrifugation step was repeated and cells were re-suspended in 400ml 10% cold glycerol. Following a further centrifugation step, cells were re-suspended in 20ml 10% glycerol. Cells were centrifuged once again and

re-suspended in 2-3ml 10% glycerol. The final concentration of cells was approximately $3x10^{10}$ cells/ml. Aliquots of cells were frozen in liquid nitrogen and stored at –70°C.

Transformations

Competent cells were transformed with DNA by electroporation. For each ligation, 1µl DNA was placed in an ice cold centrifuge tube. Electrocompetent cells were thawed on ice and 50µl were added to each DNA sample. The mixture was transferred to ice cold electroporation cuvettes and allowed to sit for 1 minute on ice. Cells were electroporated using a BioRad electroporator set at 25µF, 2.5kV, and 200Ω. 1ml L broth/ Mg^{2+} was added to the cells immediately following electroporation and cells allowed to recover for 1hour by shaking at 37°C prior to plating on selective medium.

Isolation of plasmid DNA

Plasmid DNA was prepared using commercially available kits (Qiagen or ABI). For the extraction of small amounts of plasmid DNA (minipreps), a single colony was used to inoculate approximately 10ml L broth with antibiotic selection (ampicillin) for overnight growth. The following morning, plasmid DNA was extracted using the kit according to the manufacturer's instructions. Plasmid DNA was eluted in 30 or 50µl elution buffer. The DNA concentration was determined either by agarose gel electrophoresis or by spectrophotometer.

PCR

DNA molecules were amplified by polymerase chain reaction (PCR).

dNTPs

dNTPs were purchased as stocks of 100mM. Working stocks of 10mM were made by mixing 10µl of each of the dNTPs (dATP, dCTP, dGTP, dTTP) with 60µl dH_2O to a final volume of 100µl. Stocks were stored at –20°C. dNTPs were used in PCRs at a final concentration of 0.2mM.

Primers

Primers were purchased from Genosys as lyophilised desalted compounds. Stocks were made up to 1mg/ml using sterile dH_2O. Working stocks were diluted to 100ng/µl. Primers were used in PCRs at a final concentration of 2ng/µl (1:50 dilution).

Taq polymerase, PCR buffer, and Mg^{2+}

These reagents were purchased (Applied Biosystems). Ampli*Taq* (5u/µl) was used at 0.2µl per 25µl reaction. PCR buffer was a 10X stock and therefore diluted 1:10 for reactions. Mg^{2+} was used at a final concentration of 1.5mM unless otherwise stated. Routine PCRs were done in a Hybaid Omnigene thermocycler.

Sequencing

Plasmid DNA used for sequencing was prepared using either a Qiagen midiprep kit or an ABI miniprep kit, both according to the manufacturer's instructions. DNA was linearised using an appropriate restriction enzyme and salts were removed using either a PCR cleanup kit or a nucleotide removal kit column (both supplied by Qiagen). DNA was sequenced using dye-labelled terminators for cycle sequencing. The dye used was either dRhodamine or Big Dye Terminator RR mix. Reagents were thawed on ice and dyes were protected from light as much as possible. Reactions were set up in 0.2ml centrifuge tubes as follows.

200-500ng plasmid DNA in dH_2O	11µl
dRhodamine or Big Dye Terminator RR mix	8µl
primer (3.2 pmoles)	1µl
	20µl

Cycle sequencing was performed using an ABI PCR machine (Gene Amp PCR system 9700). The sequencing program was as follows: [96°C, 30 seconds; 50°C, 15 seconds; 60°C, 4 minutes] for 24 cycles per reaction. Two primer sequences were used for sequencing: either 5' CTTTATGGCAGGGTGAAACG 3' (forward) or 5' ATTCATTGGCACCATGCCGT 3' (reverse).

Reactions were ethanol precipitated following transfer to a fresh 1.5ml centrifuge tube containing 50µl ethanol and 2µl sodium acetate, pH 5.2. Reactions were left at room temperature to precipitate for one to eight hours, then centrifuged at 13,000g at 4°C for 30 minutes. Pellets were washed with 200µl 70% ethanol. The supernatant was removed following a second centrifugation step and pellets were allowed to dry at room temperature with the caps off for approximately 20 minutes. Samples were submitted to the sequencing service to be run on the an ABI machine.

Animal husbandry

All animals were maintained in a specific pathogen free (SPF) environment and experiments were carried out under Home Office licence. Wild type animals (CD1 and CBA x C57Bl6 F1) were either bred in-house or obtained from Charles River Laboratories. Breeding animals were maintained on a mixed CD1/ CBA x C57Bl6 F1 background. Embryos for all experiments were generated from timed matings, with the morning of vaginal plug detection being counted as embryonic day 0.5 (E0.5).

Reagents and equipment used during the manipulation of preimplantation embryos

Equipment

Embryos were transferred between dishes using pulled pasteur pipettes and mouth pipette tubing. A Zeiss Stemi SV11 dissecting microscope was used to aid in manipulating embryos in sterile glass staining blocks and petri dishes.

Microinjection apparatus:
The microinjection apparatus consisted of a Zeiss Axiovert 100 microscope with a variable temperature stage set to 37°C, and mounted holders for the microinjection and holding pipettes (Narashige, Eppendorf). The equipment rested on an anti-vibration table (Carl Zeiss). Embryo holding pipettes were either made in-house using a microforge (MF90) (Narashige) and capillaries (size GC100 T15, Harvard Apparatus) or purchased (Eppendorf). Microinjection pippetes were either made in-house using an automated pipette puller (Sutter model p87, Harvard Apparatus) and capillaries (size GC100 TF 10, Harvard Apparatus) or purchased (Eppendorf). Microinjection needles were filled with DNA at a concentration of 2ng/µl using pipette filler tips (Eppendorf). DNA was microinjected with the aid of an automated microinjector (Narashige IM 300) to allow a constant flow of DNA at variable pressure.

Solutions

Embryo growth media

H6 media was used for handling embryos outside of the incubator. T6 media was used for growing embryos in the incubator (5% CO_2, 37°C). Media was either purchased (Sigma) or prepared in-house by Transgenic Unit staff using embryo culture grade reagents.

Compound	Media (g/100ml)	
	T6	H6
NaCl	0.472	0.472
KCl	0.011	0.011
NaH_2PO_4	0.0047	0.0047
Sodium pyruvate	0.003	0.003
Glucose	0.1	0.1
$MgCl_26H_2O$	0.01	0.01
$CaCl_22H_2O$	0.026	0.026
Penicillin	0.006	0.006
Streptomycin	0.005	0.005
$NaHCO_3$	0.2106	0.2106
Sodium lactate	0.34ml	0.34ml
Hepes		0.50
Phenol red	0.001	0.001
BSA	0.4	0.4

Table 1. Composition of media for manipulating preimplantation embryos. All values are expressed as g/100ml media. Media was made using embryo culture grade dH_2O and filter sterilised. Media was embryo tested prior to use.

Acid Tyrode's solution

Acid Tyrode's solution was used to removed the *zonae pellucidae* from eight-cell embryos prior to aggregation. The working aliquot was kept at 4°C. The solution was warmed to 37°C for use.

Compound	Tyrode's Solution	
	g/litre	Molarity
NaCl	8.0	0.14M
KCl	0.2	2.6mM
$CaCl_2$	0.2	1.4mM
$MgCl_26H_2O$	0.1	0.5mM
$NaH_2PO_4H_2O$	0.05	0.2mM
Glucose	1.0	5.5mM
$NaHCO_3$	1.0	0.12M

Table 2. Composition of Tyrode's solution. For Acid Tyrode's solution, polyvinyl pyrrolidone (Mr 40,000) (Sigma) was added to a final concentration of 0.4%. The pH was adjusted to 2.5 using 5N HCl. The solution was filter sterilised and stored in aliquots at –20°C.

Production of aggregation chimaeras

Aggregation of embryos

[CBA x C57Bl6] F1 females were superovulated by intraperitoneal injection of 10 units of PMS (Intervet) at noon on the first day, followed by 10 units of human chorionic gonadotrophin (hCG) (Intervet) at 2pm two days later. Half of the females were mated to [CBA x C57Bl6] F1 males, and half to *Dct-LacZ* (transgenic line A12) males. Plugged females were sacrificed by cervical dislocation on E2.5 and the uteri and oviducts were removed and rinsed in warm sterile saline (Sigma). Uteri and oviducts were then placed in small petri dishes containing H6 media. Embryos were harvested by flushing the uteri and oviducts with H6. The flushings were done using 2ml syringes and either a narrow bore needle (Beckton Dickinson, microlance 3, No. 18) (uteri) or a Luerlock flushing needle (gauge 34 x 10mm, Coopers needle works, ltd.) (oviducts). The *zonae pellucidae* were removed by transferring embryos to Acid Tyrode's solution, warmed to 37°C, for a minimal period. Pairs of embryos were aggregated in individual drops of phytohaemagglutinin (M form, Gibco BRL) in H6 (1:20) under paraffin oil (BDH) by gently pushing embryos together with the sealed end of a pulled pasteur pipette. Aggregates were washed in H6 followed by T6 media and cultured to the blastocyst stage in drops of T6 under oil overnight at 37°C, 5% CO_2.

Uterine transfers

Ten to 14 blastocysts (E3.5) were transferred to the uteri of E2.5 pseudopregnant recipient CD1 females. Pseudopregnant recipients were prepared by selecting CD1 females in oestrous and mating them to vasectomised CD1 males on the fourth day of the experiment. Plugged females were used for uterine transfer. Recipients were anaesthetised with an intraperitoneal injection of 0.4-0.6 ml anaesthetic [0.75ml of Hypnorm (Fentanyl 0.315mg/ml / fluanisone10mg/ml): 4.5ml water: 0.2ml Hypnovel (Midazolom 10mg/2ml)]. The fat pad adjacent to the ovary and uterus was isolated and held in autoclips (Brownes Diagnostics). The proximal end of the uterine horn was held with forceps while a needle was used to make a small hole in the uterine horn. A pulled pasteur pippette carrying the chimaeric embryos in H6 media was inserted into the hole to deliver the embryos by mouth pipette. Bubbles on either side of the embryos confirmed their successful delivery. The fat pad was released and tucked back into the abdominal cavity and the peritoneum was closed

with sutures (HM&S). The skin was closed using Dieffenbachs bulldog clips (Holborn surgical and medical instruments, ltd.) and the animal was allowed to recover in a warmed post-operative cage with solid drink pouches (BS&S). Chimaeric embryos were re-harvested from E11.5 to E16.5 and processed for Xgal staining.

Production of transgenic animals

Preparation of recombinant DNA for microinjection

Plasmid DNA was digested (10μg DNA in a 100μl reaction) with enzymes to release the transgene. The two enzymes, *Xho*1 and *Bam*H1, require different buffers, so digests were carried out separately. Reactions were drop dialysed between digests to remove salts. For each digest, a sample of DNA was run on a 1% agarose gel in TBE alongside an equivalent amount of undigested DNA to ensure the DNA was completely digested and products were the predicted size. Once the transgene had been released, the remainder of the reaction was run on a 1% agarose gel in TAE buffer. The remaining steps were done using solutions that had been filter sterilised using 0.2μm filters (Schleicher & Schuell), gloves rinsed in dH_2O, and with pipette tips rinsed 3 X in sterile dH_2O. A band-sized well was cut in front of the transgene band using a sterile scalpel blade. The well was lined with dialysis tubing (that had been boiled for 10 minutes in dH_2O) such that the tubing rested on top of the gel in front of the band and underneath the gel behind the band. Fresh sterile TE was placed in the well and the DNA was electrophoresed for a further 20 minutes at 80V. Then the direction of current was reversed to release the DNA from the surface of the dialysis tubing and into the well. TE containing transgenic DNA was recovered and the gel was checked under UV to ensure all of the DNA had migrated into the well. This collection process was repeated until all of the DNA in the band was recovered.

The DNA was purified and concentrated using microcon 30 columns (Amicon) according to the manufacturer's instructions. Briefly, the DNA was passed through a microcon column and washed three times using 0.1mM EDTA/1mM TRIS pH7.4. DNA was eluted in 10μl 0.1mM EDTA/1mM TRIS pH7.4. The eluant was diluted 1:10 in transgenic buffer (0.1mM EDTA/10mM TRIS pH7.4). The DNA concentration was determined by electrophoresis. DNA was stored at –20°C until the day of microinjection. For microinjection, DNA was diluted in transgenic buffer to a final concentration on 2ng/μl and spun through a Spinex 0.22μm column (Costar).

Microinjection of recombinant DNA into fertilised eggs

Embryos used for microinjection were derived from [CBA x C57Bl6] F1 x [CBA x C57Bl6] F1 matings. Females were superovulated as described above for chimaera production. They were then mated to F1 males. Plugged females were sacrificed the following morning (E0.5) and oviducts were removed and rinsed in warm saline. Oviducts were placed in H6 media and fertilised eggs were removed by tearing the swollen ampullae with fine forceps. Several drops of hyaluronidase (1mg/ml PBS) (Sigma) were added to the media for approximately three minutes to remove the cumulus cells from the outside of the eggs. Fertilised eggs were identified by the presence of two large pronuclei and often polar bodies.

Eggs awaiting microinjection were kept at 37°C, 5% CO_2 in drops of T6 media under paraffin oil in sterile petri dishes. Eggs were microinjected in batches of 30-50 in a large drop of H6 media under oil in a glass dimple slide (the injection dish).

During microinjection, embryos were picked up and held on the holding pipette using mouth pipette tubing. The microinjection needle on the automatic injector was set such that a constant stream of DNA left the pipette. Once the (usually male) pronucleus was in focus, the injection needle was brought into the same plane of focus and used to pierce the *zona pellucida* and egg cell membrane, before entering the pronucleus. The needle was held until the pronucleus swelled slightly, and then removed quickly and cleanly. Following microinjection, eggs were returned to drops of T6 media under paraffin oil and kept at 37°C, 5% CO_2 overnight. For each experiment, five to ten uninjected embryos were retained and cultured overnight to control for problems with media, oil, and incubation conditions.

Oviducal transfers

Microinjected embryos were screened the following morning. Only embryos that had developed to the two-cell stage were transferred into recipient females. E0.5 CD1 recipients were prepared, anaesthetised, and the ovarian fat pad isolated and held as described for uterine transfers of chimaeric blastocysts. The bursa surrounding the oviduct was broken carefully to expose the infundibulum of the oviduct. The end of the pulled pipette containing the embryos was inserted into the infundibulum and embryos were delivered by mouth pipette. The successful delivery of the embryos was confirmed when bubbles that had been placed at either end of the embryos in the pipette were seen in the swollen ampulla. Ten to

20 embryos were transferred to each side of the recipient. The mother was closed and allowed to recover as described for uterine transfers. Embryos were allowed to develop to term.

Harvesting of postimplantation embryos

Postimplantation embryos were harvested for neural tube culture, wholemount *in situ* hybridisation, wholemount Xgal staining, and cryostat sectioning. The mothers were sacrificed by cervical dislocation. The abdominal cavity was opened and uteri were removed to petri dishes containing phosphate buffered saline (PBS) (Oxoid, Unipath). Embryos were removed from the uteri and freed of extraembryonic membranes using scissors and forceps. For some experiments, extraembryonic membranes were retained to genotype embryos by PCR. Embryos were rinsed in fresh PBS prior to subsequent processing.

Primary tissue culture of E9.5 neural tubes

Primary neural crest cells were grown in tissue culture from the explantation of E9.5 neural tubes. The procedure used here is based on one described by Opdecamp *et al* (72). All dissection tools were sterilised using 100% ethanol and flaming, and the work surface was wiped clean with ethanol. E9.5 embryos were dissected with the aid of a Zeiss Stemi disstection microscope and immediately placed in fresh PBS on ice. The posterior trunk (equivalent to 10 somites in length) was removed using sharp forceps. Trunks were cut in batches of 3-5 embryos while the other embryos remained on ice. Embryo heads were retained for genotyping by PCR in some experiments. Dissected trunks were kept in 10% foetal calf serun (FCS) (Sigma) in DMEM (Life Technologies) on ice until all of the trunks had been dissected. Trunks were rinsed in cold PBS to remove the FCS and then digested in 1% trypsin (Boehringer Mannheim) in PBS for three minutes on ice. Digested trunks were returned to 10% FCS in DMEM on ice to stop the digestion reaction. Digestion with trypsin facilitated the removal of tissues surrounding the neural tube. Sharp forceps were used to remove the somites and notochord, leaving a clean posterior neural tube segment. Neural tubes were dissected under the microscope individually while remaining tubes were kept on ice.

Neural tubes were transferred to 13mm glass coverslips (Sarstedt) previously coated with poly-L-lysine (Sigma) and 40μg/ml human recombinant fibronectin (Promega) and placed in 24-well plates (Greiner, Cellstar). Neural tubes were grown in 1ml 10% FCS in DMEM in a

humidified incubator at 37°C, 5% CO_2, for three days. This basic growth medium and all supplements (growth factors and inhibitors) were added to cultures in a tissue culture hood. At the end of the growth period, neural tubes were washed in fresh PBS and processed for Xgal and DAPI staining.

Genotyping of mice and embryos

Tail tip lysis buffer

	Final concentration
Tris.HCl pH8.0	100mM
EDTA	50mM
NaCl	100mM
SDS	1%

Proteinase K (stock 10mg/ml) (Sigma) was added to a final concentration of 0.2mg/ml.

Genotyping of breeding mice

Breeding animals were genotyped by PCR amplification of *LacZ* and *LaacZ* sequences from genomic DNA extracted from tail biopsies. Approximately 1cm tail tissue was removed from the ends of the tails of anaesthetised animals. Tail tips were digested in 1.5ml microfuge tubes at 55°C overnight in 500µl tail tip buffer/ proteinase K. The following day, tubes were vortexed and centrifuged at full speed for 10 minutes. 750µl ice cold ethanol was added to the supernatant and tubes were shaken to mix the solutions. Genomic DNA was spooled out to a fresh centrifuge tube containing 500µl dH_2O using a sterile pipette tip. The solution was pipetted gently to resuspend the DNA. PCR was done using 1µl of DNA (approximately 50ng) and either of the following pairs of primers: 5'GTGACTACCTACGGGTAACA3' (*LaacZ* F) and 5'ATTCATTGGCACCATG-CCGT3'(*LaacZ* R), or 5'GAATTATTTTTGATGGCGTT3' (*LacZ* F) and 5'CGCTGATTTGTGTAGTCGGTT3' (*LacZ* R).

Primer Name	Product size in *Dct-LacZ* mice	Product size in *Dct-LaacZ* mice
LacZ F		
LacZ R	} 252bp	}252bp
LaacZ F		
LaacZ R	} 520bp	} 810bp

Table 3. Primers used to amplify *LacZ* DNA.

PCRs were set up in 200µl centrifuge tubes. Reactions were overlaid with approximately 25µl mineral oil (Sigma).

Reaction mix:

DNA	1µl
dH_2O	18.3µl
10 X Buffer	2.5µl
25mM Mg^{2+}	1.5µl
Forward primer (100ng/µl)	0.5µl
Reverse primer (100ng/µl)	0.5µl
dNTPs (10mM)	0.5µl
Amplitaq polymerase	0.2µl
	25µl

Program:

94°C	7 minutes	
94°C	1 minute }	
58°C	1 minute }	X 35 cycles
72°C	1 minute }	
72°C	10 minutes	

Genotyping of embryos

Embryos from neural tube cultures were genotyped using genomic DNA derived from E9.5 embryo heads. Embryos processed for *in situ* hybridisation (both cryostat sections and wholemount) were genotyped using DNA derived from extraembryonic membranes. In both cases, DNA was extracted and amplified using the same procedure as described for tail biopsies.

Histology

Staining embryos and tissues with Xgal and DAPI

Solutions

Paraformaldehyde

4% paraformaldehyde (PFA) (Sigma), used to fix embryos and tissues, was made by dissolving 20g PFA in 500ml PBS at 65°C overnight. Aliquots were stored at –20°C.

Phosphate buffer

Both detergent wash and the Xgal staining solutions were made up in phosphate buffer. 1M phosphate buffer (pH 7.3) was made by mixing 1M Na_2HPO_4 and 1M NaH_2PO_4 at a ratio of seven to three.

Detergent wash

Compound	Per 500ml	Final concentration
1M phosphate buffer, pH 7.3	48.5ml	0.1M
1M $MgCl_2$ in phosphate buffer	1.0ml	2mM
5% sodium deoxycholate in phosphate buffer	10ml	0.1%
10% Nonidet P-40 in phosphate buffer	1ml	0.02%
1% BSA in phosphate buffer	2.5ml	0.05%

Table 4. Composition of detergent wash. The solution was made up to a final volume of 500ml using dH_2O.

Xgal stain solution

Compound	Per 250ml	Final concentration
Detergent wash	236ml	
NaCl, 5.3% stock in phosphate buffer	4ml	0.085%
$K_3Fe(CN)_6$, 250mM in dH_2O	5ml	5mM
$K_4Fe(CN)_6$, 250mM in dH_2O	5ml	5mM
Xgal substrate, 100mg/ml in DMF	750µl	0.3mg/ml

Table 5. Composition of Xgal stain solution. Staining solution, $K_4Fe(CN)_6$, and $K_3Fe(CN)_6$ were stored in the dark. Staining solution was stored at 4°C.

Xgal and DAPI staining procedure

Both whole embryos and neural tube cultures were processed for Xgal staining. Embryos of all gestational stages were dissected in PBS and fixed in 4% PFA at 4°C for at least 1 hour. Neural tube cultures were fixed for at least 20 minutes. Following fixation, embryos and neural tubes were first rinsed in PBS and then washed in detergent wash three times for at least 20 minutes each time. Tissues were stained overnight in Xgal stain at 37°C in the dark. The following morning, the staining solution was removed and tissues were rinsed in detergent wash then re-fixed in 4% PFA at 4°C overnight. The fix was removed and tissues were washed in PBS.

Neural tube cultures were stained with DAPI after Xgal staining. Neural tubes were flooded with 0.05% Triton X-100 and 0.1µg/ml DAPI in PBS for approximately five minutes. Coverslips (on which the neural tubes were attached) were rinsed in PBS, drained on tissue paper, and then mounted in Mowiol for microscopy.

Preparation, sectioning, and staining of paraffin-embedded embryos

Embryos for paraffin sectioning were treated as follows:

Solution	Treatment time
50% ethanol	1:00 hour
80% ethanol	1:00 hour
95% ethanol	1:00 hour
IMS99	1:00 hour
IMS99	1:00 hour
100% ethanol	1:30 hour
100% ethanol	2:00 hour
Xylene	1:00 hour
Xylene	2:00 hour
Xylene	2:00 hour
Wax	1:00 hour
Wax	1:00 hour
Wax	1:00 hour
Wax	1:00 hour

Table 6. Treatment steps for paraffin wax embedding embryos.

10μm sections were cut using a microtome and sections were floated out onto glass slides at 42°C. Sections were stained with eosin as follows. Sections were dewaxed with two five-minute washes in xylene, then washed in two five-minute washes of 100% ethanol, and hydrated in one five-minute wash each in a series of washes of increasing water concentration (90%, 70%, 50%, and 30% ethanol), followed by a final wash in distilled water. Slides were incubated in eosin stain for two minutes, then dipped in 100% ethanol and washed twice in 100% ethanol for one minute each. Slides were cleared by washing in xylene twice for five minutes and mounted using D.P.X. Eosin (Surgipath) stain was made up using three parts 1% aqueous eosin, one part 1% ethanol, and acetic acid was added to a final concentration of 0.05%.

RNA in situ *hybridisation*

Labelling riboprobes with digoxygenin

Riboprobes were labelled with digoxygenin for non-radioactive *in situ* hybridisation. The polymerases, DIG labelling mix, and transcription buffer were purchased (Boehringer Mannheim). RNA products were kept on ice as much as possible and gloves were worn

throughout to prevent exposure to RNAses. Electrophoresis equipment was soaked in 0.1% SDS and rinsed in DEPC-treated water to destroy RNAses.

The plasmid containing the riboprobe was linearised with an appropriate enzyme. The labelling reaction was set up as follows:

dH_2O	8µl	
10X Transcription buffer	2µl	
linearised DNA	5µl	
dNTP (from DIG RNA labelling kit)	2µl	
Human placenta RNAse inhibitor	1µl	
Polymerase (T7 or T3)	2µl	
	20µl	37°C 2 hours

Template DNA was digested by adding 2µl RNAse-free DNAse1 for 15 minutes at 37°C. This reaction was stopped by adding 2µl 0.2M EDTA, pH8.0. The labelled RNA was precipitated by adding 2.5µl 4M LiCl and 75µl 100% ethanol and incubating overnight at –20°C. The following day, the RNA was centrifuged for ten minutes at maximum speed and the pellet was washed with 50µl cold 70% ethanol. The pellet was resuspended with 110µl DEPC-treated dH_2O. 1µl RNAse inhibitor was added. The RNA was checked by electrophoresis and 10µl was used routinely for a probe.

Wholemount in situ hybridisation

E12.5 embryos were processed for wholemount *in situ* hybridisation. Embryos were dissected in PBS and the extraembryonic tissues were used for genotyping. All steps were done at room temperature unless stated otherwise. Solutions were made up using DEPC-treated water and PBS for steps up to and including the hybridisation step. These solutions were DEPC-treated by adding 1µl/ml DEPC (Sigma) to sterile PBS or water, gently mixing the solutions, and allowing them to sit at room temperature for several hours (usually overnight) prior to re-autoclaving.

Solutions for wholemount *in situ* hybridisation

PBT

PBT was prepared fresh each time by adding 0.5ml 10% Triton X-100 to 50ml DEPC-treated PBS (final concentration: 0.1%).

Prehybridisation solution (prehyb)

Compound	Amount added for 50ml	Final concentration
Deionised formamide (Sigma)	25ml	50%
20X SSC (3M NaCl, 0.3M Na_3Citrate, DEPC-treated)	12.5ml	5X
Blocking powder (Boehringer Mannheim)	1g	2%
10% Triton X-100	400µl	0.08%
10mg/ml Heparin	250µl	50µg/ml
50mg/ml yeast tRNA	1ml	1mg/ml
0.5M EDTA	0.5ml	5mM
10% CHAPS (Sigma)	2.5ml	0.5%

Table 7. Prehybridisation solution for wholemount *in situ* hybridisation. The solution was made up to 50ml with DEPC-treated sterile dH_2O and all components were dissolved by gentle mixing at 4°C.

Posthyb solution:

Compound	Amount added to 50ml	Final concentration
Formamide	25ml	50%
20X SSC	12.5ml	5X
10% Triton X-100	0.5ml	0.1%
10% CHAPS	2.5ml	0.5%

Table 8. Composition of posthyb solution used to remove riboprobe.

Solutions were made up to a final volume of 50ml using sterile dH_2O.

TBT:

Compound	Amount added to 50ml	Final concentration
1M Tris.HCl, pH 7.5	2.5ml	50mM
5M NaCl	1.5ml	150mM
10% Triton X-100	0.5ml	0.1%

Table 9. Composition of TBT.

NTM

Compound	Amount added to 50ml	Final concentration
5M NaCl	1ml	100mM
1M Tris.HCl, pH 9.5	5ml	100mM
1M $MgCl_2$	2.5ml	50mM

Table 10. Composition of NTM. The solution was made up to 50ml using dH_2O.

NBT and BCIP

NBT stock was made up to 75mg/ml in 70% dimethylformamide (DMF). BCIP stock was made up to 50mg/ml in DMF. Both were purchased from Boehringer Mannheim and stored in the dark at –20°C.

Procedure for wholemount *in situ* hybridisation

Embryos were first fixed in 4% PFA at 4°C overnight. PFA was removed and embryos were washed with PBT twice for ten minutes each. Embryos were dehydrated by washing for 20 minutes in increasing concentrations of methanol: 25%, 50%, 75% methanol/PBT, then 2X 100% methanol and kept at –20°C overnight. Embryos could be stored at this stage for use later.

Embryos were rehydrated by washing in solutions with decreasing concentrations of methanol/PBT: 75%, 50%, 25%. Embryos were washed in PBT 3X for five minutes each and digested in 10µg/ml proteinase K in PBT for one hour. Embryos were re-fixed in freshly prepared 4% PFA, pH 7.4, for 45 minutes on ice. The fixative was replaced with prehybridisation solution (prehyb) and embryos were washed 2X 5 minutes in 2ml screw cap tubes. Embryos were incubated in prehyb for one hour at 65°C. This was replaced with fresh prehyb for a further two to four hours. 10µl probe was denatured by heating in 100µl prehyb at 80°C for three minutes. Probe was added to the embryos in prehyb and embryos were hybridised overnight at 60°C.

The following day, the probe was removed by a series of washes, each for five minutes at room temperature: 100% posthyb, 75% posthyb/ 25% 2X SSC, 50% posthyb/ 50% 2X SSC, 25% posthyb/ 75% 2X SSC. Embryos were then washed twice in 2X SSC/ 0.1% CHAPS for 30 minutes at 65°C and twice in 0.2X SSC/ 0.1% CHAPS, also at 65°C for 30 minutes. Embryos were washed in fresh TBT twice for ten minutes at room temperature. Embryos were preblocked with 15% sheep serum (previously heat inactivated at 65°C for one hour) and 2% BSA in TBT for at least three hours at 4°C. Embryos were incubated with anti-DIG AP fab fragment at a 1:2000 dilution in 15% sheep serum and 2% BSA in TBT with gentle rocking overnight at 4°C.

The next day, the antibody was removed by washing embryos five times in TBT with 0.1% BSA for 1 hour each time. Embryos were then washed at 4°C for up to two days in 0.1% BSA. Embryos were prepared for staining by washing twice for 30 minutes each in NTM with 0.1% Triton X-100 and 3X 10 minutes in NTM. Embryos were stained in NTM with 4.5µl NBT and 3.5µl BCIP per ml NTM. Embryos were stained in the dark and checked every half-hour until the stain developed. The stain was fixed using 4% PFA.

In situ hybridisation on cryostat sections

Solutions used for preparing cryostat sections

Fish fix buffer

4% sucrose in PBS with 12mM $MgCl_2$

Fish fix

4% PFA dissolved in fish fix buffer

Preparation of sections

E13.5 and E14.5 embryos were used for *in situ* hybridisation on cryostat sections through the telencephalon. Embryos were dissected in PBS and extraembryonic membranes were retained for genotyping. Embryos were fixed overnight at 4°C in fish fix, then rinsed three times for five minutes in fish fix buffer. Embryos were embedded in 1.5% agarose and 5% sucrose in PBS. Blocks were trimmed and then transferred to 30% sucrose in PBS and embryos were allowed to sink overnight at 4°C. Embryo blocks were frozen on dry ice and stored at –70°C until ready to section.

10µm sagittal sections were cut on a cryostat machine (Leica Jung CM3000) and sections were placed onto slides coated with 3-aminopropyl-triethyloxysilane (TESPA). Sections were air dried for at least one hour and stored at –70°C until ready for hybridisation.

Solutions for *in situ* hybridisation on cryostat sections

10X Salt

Compound	Amount for 1 litre PBS
NaCl	114g
Tris.HCl	14.0g
Tris base	1.34g
NaH_2PO_4 H_2O	7.8g
Na_2HPO_4	7.1g
0.5M EDTA	100ml

Table 11. Composition of 10X Salt. The solution was made up in PBS.

Hybridisation buffer

Compound	Final concentration	Amount required for 1ml
10X Salt	1X	100µl
Formamide	50%	500µl
50% Dexamethosone SO_4	10%	200µl
10mg/ml yeast tRNA	1mg/ml	100µl
50% Denhardt's	1X	20µl
dH_2O		80µl

Table 12. Composition of hybridisation buffer for RNA *in situs* on cryostat sections.

10X TBST

Compound	Amount for 100ml
NaCl	8g
KCl	0.2g
1M Tris.HCl, pH 7.5	25ml
10% Tween-20	10ml
dH_2O	Balance to 100ml

Table 13. Composition of 10X TBST.

NTMT

Compound	Amount per 50ml
5M NaCl	1ml
1M $MgCl_2$	2.5ml
10% Tween-20	0.5ml
1M Tris pH 9.5	5ml
Levamisole	10 drops
dH_2O	Balance to 50ml

Table 14. Composition of NTMT.

Procedure for *in situ* hybridisation of cryostat sections

Sections were thawed for at least one hour at room temperature. Probes were diluted 1:500 in hybridisation buffer and denatured at 70°C for ten minutes. 200µl hybridisation mix was added to each slide followed by a coverslip to prevent evaporation. Slides were incubated at 65°C overnight.

The following day, slides were transferred to a coplin jar and washed in 1X SSC, 50% formamide, and 0.1% Tween-20 for 15 minutes at 65°C. They were then washed in fresh solution twice for 30 minutes at 65°C, followed by two washes in 1X TBST for 30 minutes each. Slides were blocked in 10% heat inactivated sheep serum in 1X TBST for one hour. Excess fluid was drained off and 100µl 1:2000 dilution anti-DIG AP fab fragment in 10% serum/ 1X TBST was added. Slides were incubated with the antibody overnight in a humidified chamber at 4°C. Excess antibody was removed by washing five times in 1X TBST for 20 minutes each followed by two ten minute washes in 1X NTMT.

Slides were stained in a clean coplin jar in 4.5µl NBT and 3.5µl BCIP per ml NTMT (+ 5mM levamisole). Slides were stained overnight in the dark. The staining reaction was

stopped by washing slides in water and slides were fixed in 4% PFA/ 0.1% glutaraldehyde for 20 minutes. Slides were mounted using aquamount (BDH).

Microscopy and associated equipment

General microscopy

Dissections of postimplantation embryos were done with the aid of a Zeiss Stemi SV11 dissecting microscope.

Camera lucida drawings were done using a Wild Heerbrugg M7 microscope and associated apparatus (a mirror with a lens).

Photographs of wholemount embryos were taken using a Photometrics ICX205 digital colour CCD camera and a Leica M2F2III stereoscopic microscope with brightfield illumination. Images were captured using IP Lab software.

Images of Xgal stained paraffin sections were captured using a Zeiss Axioplan II with a Xillix microimager 1400 monochrome CCD camera and IP Lab software with brightfield illumination and DIC optics. Images of cryostat sections were captured as for paraffin sections but without the use of DIC.

Images of neural tube cultures were captured using a Zeiss Axioplan microscope and Princeton Instruments Micromax monochrome CCD camera mounted with a Ludl motorised stage and automated focus, shutters, and filter wheels. A multipass Chroma 81000 filterset was used to capture fluorescence images. Paul Perry wrote all scripts for capturing digital images with IP Lab software and he trained me to use all of the equipment.

Capture and analysis scripts for analysing neural tube cultures

Capturing images from neural tube explants

A motorised stage was used for capturing multiple images from each explant to obtain high quality images for analysis. Images were joined to create a montage on which analyses were performed. Two montages were made for each explant, one generated from brightfield images and one from fluorescence images.

Analysis of neural crest cell migration in neural tube explants:

Regions of images can be selected for analysis by marking them with segments. Segments can be drawn onto images manually or automatically. Multiple segments in a single image can be defined by using different colours.

Only cells that migrated away from the neural tube onto the substrate were analysed. The first segment was drawn manually around the explant perimeter. The region enclosed by this segment was filled in automatically in the same colour and none of the data under it was considered during the subsequent analysis. Photographs illustrating the use of the analysis script are presented at the end of this chapter in Plate 1.

The remaining area contained all of the cells that had migrated varying distances away from the tube. This area was subdivided using more segments automatically: using the original perimeter line as a template, the circular segment was dilated out to the edge of the explant on the fluorescence image in previously defined increments of equal width (Plate 1). This generated multiple segments, or annuli, at increasing distances away from the edge of the neural tube. The area of the annulus nearest the explant (the first annulus) was determined by calculating the area under the second segment and subtracting from it the area of the first segment (the segment demarcating the edge of the explant). The areas under progressively distal annuli were similarly calculated by subtracting the area of the next proximal segment. These calculations were performed automatically as the segments were dilating outwards. Since each annulus was separated from neighbouring annuli by a fixed distance, the area of each annulus increased with increasing distance from the edge of the explant.

Individual β-gal+ cells (melanoblasts) were identified by marking them manually with a yellow segment on the brightfield image. Their number was counted and their distance from the explant edge was easily derived using the annuli described above. (Segments drawn on either image were transferrable between brightfield and fluorescence images).

The migration distance and an estimate of the number of β-gal- (non-melanoblast neural crest cells) was determined using the fluorescence images. Counting circles were automatically placed in each annulus (eight per annulus, distributed evenly) (Plate 1). All of the cells (visualised by DAPI staining) within a counting circle were identified manually by segmentation (clicking on them in a colour unique to each annulus). After determining the

area of each counting circle and annulus, the script used the number of cells in each counting circle to estimate of the number of DAPI-stained cells per annulus.

For each explant, the script tabulated the number of β-gal+ cells in each annulus, together with an estimate of the number of β-gal- cells in each annulus. In this way, both the total number and average migration distance (measured in annuli) of each cell population was determined. All of the steps, from capturing multiple images using the motorised stage, to estimating the number of DAPI positive cells in each annulus were automated in scripts written by Paul Perry.

Plate 1. Analysis of neural tube cultures. a. Fluorescence image of a DAPI-stained neural tube explant. The perimeter of the explant was outlined manually on the fluorescence image. Individual β-gal + cells marked manually on the brightfield image (not shown) and the segments were transferred onto the fluorescence image automatically (yellow). Annuli dilated out from the edge of the neural tube to the edge of the culture. b. Eight counting circles are placed in each annulus to generate and estimate of the number of DAPI cells within each annulus. In each annulus, the counting circles have a different segment colour. Within an annulus, the counts of each circle are combined into one count for the entire annulus. This count, and the combined areas of all the counting circles within the annulus, are used to calculate an estimate for the total cell number in that annulus. Annuli represent defined distances away from the edge of the neural tube, based on the manually drawn outline of the explant edge. Examples of brightfield images used for analysis are presented at the end of Chapter 3.

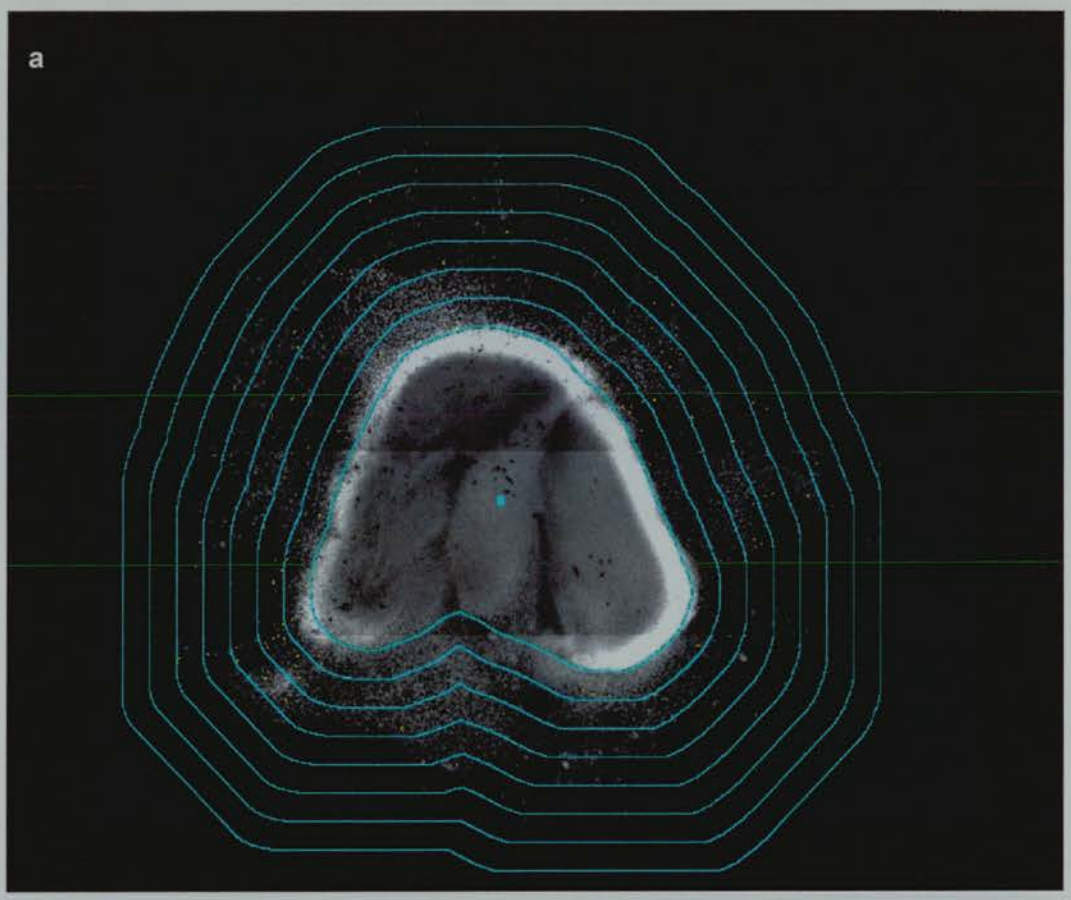

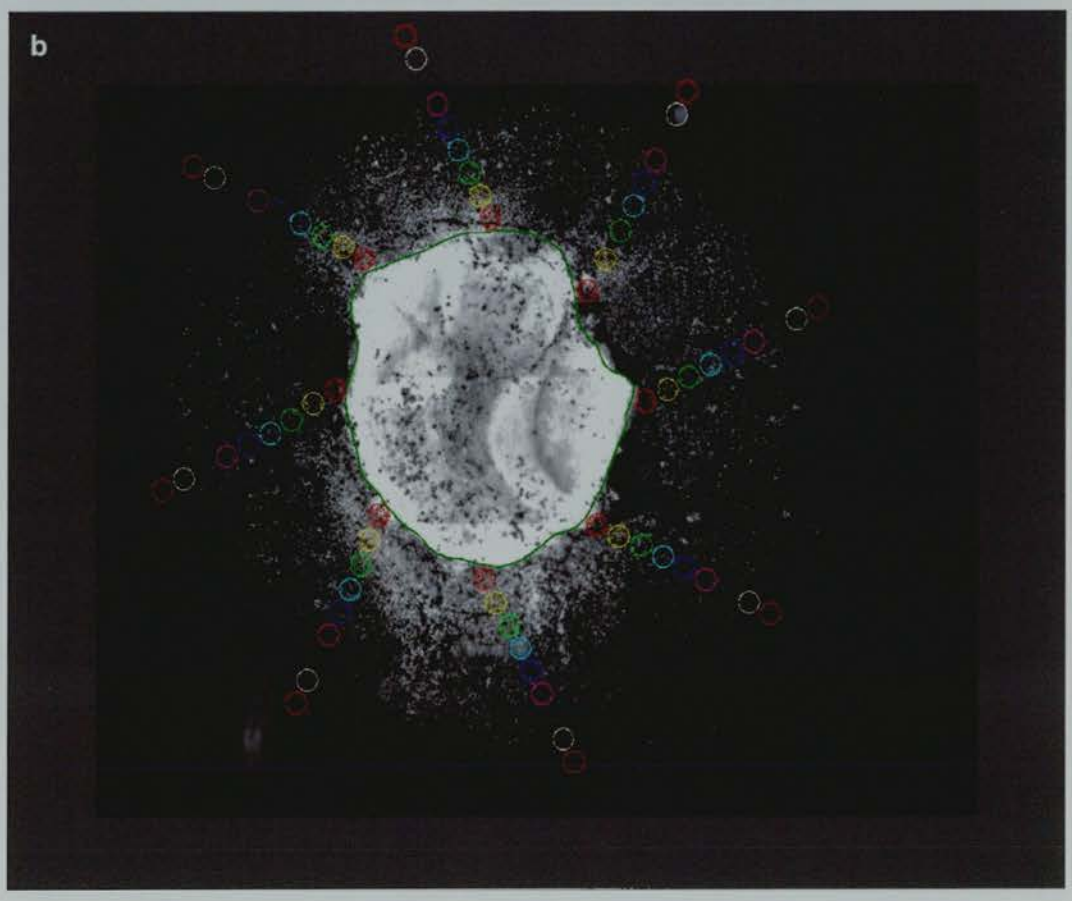

Chapter 3

In vitro manipulation of melanoblast development

Is life worth living? This is a question for an embryo, not a man.

Samuel Butler (1951)[4]

[4] Quote 9472 from (1996). **The Columbia World of Quotations.** Originally from (1951). **Samuel Butler's Notebooks**.

Introduction

The collection of mouse coat colour mutants has illustrated genes and pathways important for melanoblast specification, survival, proliferation, and migration. In addition to studying the phenotypes of mice carrying different mutations, it is informative to manipulate neural crest cells in culture to dissect the sometimes multiple functions of these genes. Manipulation in culture permits direct measurement parameters such as proliferation and migration. By using drugs to block particular branches of known signalling pathways, it is possible to determine the signalling events downstream of growth factor action.

KITL-KIT interactions in melanoblast development

The *Steel* (*Sl*) and *White-spotting* (*W*) mutations affect three developmentally unrelated lineages in the mouse: melanoblasts, primordial germ cells, and haematopoietic cells. A common feature of these lineages is that cells undergo extensive proliferation and migration during embryogenesis. There are many alleles of both *Sl* and *W*, and they affect pigmentation with varying severity, depending on the nature of the mutation (25;47;73). They have provided insights into the signalling pathways required for survival, migration, and differentiation of melanoblasts, as well as highlighting some of the important features of the proteins.

Most homozygous *W* and *Sl* alleles are embryonic lethal due to defects in haematopoiesis, but the common phenotype of mice carrying viable homozygous mutations is a mostly white coat with black eyes (since melanocytes of the RPE are not neural crest-derived and pigment synthesis is unaffected). The white coats are due to an absence of epidermal melanocytes. These mice are severely anaemic and infertile, or have reduced fertility in one or other, or both, sexes. Heterozygotes have a diluted coat colour with white belly and head spots, with varying degrees of reduced fertility and anaemia.

KITL signals through the KIT receptor

The *W* and *Sl* phenotypes result from mutations in genes that encode the receptor tyrosine kinase, KIT, and its ligand, KIT ligand (KITL) (47;74-78). KITL contains an N-terminal signal sequence, an extracellular domain, a transmembrane domain, and a C-terminal intracellular domain (76). The *Kitl* gene encodes two polypeptides by tissue-specific alternate splicing, a membrane-bound and a soluble form (79-81). Both forms are localised

to the membrane initially, and the larger variant is cleaved to produce soluble KITL, while the smaller variant remains membrane-bound.

The dominant negative phenotypes of some heterozygous *Kit* alleles suggested KIT functions as a dimer (82). The simultaneous binding of a KITL dimer to two KIT extracellular domains facilitates receptor homodimerisation, auto-phosphorylation, and subsequent intracellular signalling (83;84;85).

Sites of KIT and KITL expression

KIT and KITL are both expressed in regions predicted by their mutant phenotypes. KIT is expressed by primordial germ cells during their proliferative and migratory phases between E7.5 and E15.5, and by haematopoeitic progenitor cells throughout their development (86). KIT is also expressed in a subset of neural crest cells from E10 and its expression is reported to decline from E15 (87). However, KIT is expressed by mature melanocytes in the dermal papillae of hair bulbs (82) where it is essential for melanocyte maintenance (60;88). While most KIT+ neural crest cells are thought to be melanoblasts, and these cells in culture also express other melanoblast markers, some sensory neurones in the DRG also express KIT (87;89) and are responsive to KITL (89).

As expected, KITL is expressed in the environment of KIT+ cells. It is transiently found in the dermamyotome just before and during dispersal of presumptive melanoblasts onto the dorsolateral pathway (25;27;87;90). As melanoblasts colonise the developing hair follicles, KITL is expressed by skin epithelial and mesenchymal cells. KITL is also expressed by KIT+ neural crest cells both *in vitro* and *in vivo*, and it is thought to act in an autocrine and paracrine fashion (91). In addition, it is expressed by the floor plate from E9.5, by the ventrolateral boundary of the neural tube from E12, and in the DRG from E14. In the developing gonads, KITL is expressed by ovarian follicle cells and Sertoli cells. Both KIT and KITL are expressed in the brain from around E10, and expression here becomes increasingly complex as development proceeds, with expression reported in the cortex, cerebellum, olfactory bulb, and hippocampus. However, no defects in brain development or function are associated with any of the *Sl* or *W* mutations, suggesting KIT signalling is not essential here (87;90).

Mutations in the *Kitl* gene

Different alleles of both *Sl* and *W* have been studied extensively to establish the role of receptor-ligand interactions during melanoblast development. One *Kitl* allele, *Steel-dickie* ($Kitl^{Sl\text{-}D}$), results from an intragenic deletion in the *Kitl* coding region. This deletion removes the cytoplasmic and transmembrane domains. $Kitl^{Sl\text{-}D}$ produces soluble KITL at wild type levels, but no membrane-bound KITL is made (92). Steel *et al* (69) followed the migration of *Dct* positive cells (melanoblasts) to the inner ear in wild type and $Kitl^{Sl\text{-}D}$ homozygous embryos. All melanoblasts disappeared by E13 to E14 in homozygous embryos, suggesting the membrane-bound KITL is required for melanoblast survival. Melanoblasts did undergo early stages of differentiation, since they expressed *Dct*, suggesting membrane-bound KITL is not required for specification, dispersal, and early differentiation events. Also, the identification of KITL expression near the ventral otic vesicle in wild type embryos suggested it may have a role in targeting melanoblasts to their destination. A targeted mutation designed to produce only membrane-bound KITL by disruption of the major proteolytic cleavage site included in the soluble *Kitl* transcript had no pigmentation defects (although the mast cell lineage was affected). Proteolysis of the modified protein at an alternative site may produce sufficient soluble KITL to compensate for the reduced levels of the wild type soluble transcript (79).

In embryos homozygous for $Kitl^{Sl}$ (a null allele), which produce neither the soluble nor the membrane-bound form, individual melanoblasts can be detected in the MSA, but no cells are found in the dermatome (25). This suggested that soluble KITL is required for the initial dispersal of melanoblasts onto the dorsolateral migration pathway and that membrane-bound KITL is required for survival later.

Another allele, $Kitl^{Sl\text{-}17H}$, carries a point mutation which disrupts the splice acceptor site for the exon encoding the cytoplasmic tail of KITL (47;80;93). KITL encoded by $Kitl^{Sl\text{-}17H}$ has a wild type extracellular and transmembrane domain, but a novel cytoplasmic sequence. The phenotype of $Kitl^{Sl\text{-}17H}$ homozygous mice is nearly as severe as the $Kitl^{Sl}$ null homozygotes with almost no coat pigmentation, mild anemia, and sterility in males (47;93). A reduced number of melanoblasts in the MSA in $Kitl^{Sl\text{-}17H}$ homozygous embryos at E11.5 compared to wild type has been demonstrated, and although there are some melanoblasts in the dorsolateral migration pathway initially, they all disappear by E13.5 (80). RNA expression levels in $Kitl^{Sl\text{-}17H}$ and wild type embryos are equivalent, but the amount of KITL protein in mutant embryos is greatly reduced in the dermatome, pronephros, genital ridge, and

floorplate due to its mis-localisation to the apical compartment rather than the basolateral. Therefore, the cytoplasmic domain of KITL is required to localise KITL to the basolateral compartment of epithelia.

Membrane-bound KITL is proposed to act as an adhesion receptor for Kit positive cells, as well as a survival factor (80). Indeed, membrane-bound KITL- mediated signalling facilitates adhesion of primordial germ cells in culture, and this adhesion is reduced in the presence of exogenous soluble KITL, antibodies raised against Kit or KITL, or in $Kitl^{Sl\text{-}D}$/ $Kitl^{Sl\text{-}D}$ cells (94).

Mutations in the *Kit* gene

White-spotting (*W*) mutations in the *Kit* gene have been equally informative in assessing the importance of KIT signalling. The $Kit^{W\text{-}viable\ (v)}$ and $Kit^{W\text{-}41}$ alleles have point mutations in the kinase domains, resulting in normal levels of protein expression but with reduced kinase activity (30;47;86). The $Kit^{W\text{-}sash\ (sh)}$ allele has a 5' DNA rearrangement that affects KIT expression levels in a tissue-specific manner. Mast cells are affected by reduced KIT expression in $Kit^{W\text{-}sh}$ embryos, while KIT is expressed ectopically in the floor plate and dermatome where it affects melanoblast development (82). Mice homozygous for $Kit^{W\text{-}sh}$ are fertile and not anaemic, but they have no mast cells in the skin or intestine, and they are almost completely unpigmented (82). Heterozygotes are pigmented with a white sash in the lumbar region. The distribution of melanoblasts is normal at E10.5 to E11 in homozygous embryos for these *W* alleles, however the number of melanoblasts decreases severely by E12.5 (30). This suggests KIT signalling is not required for initial migration of melanoblasts onto the correct pathway, but only for survival. However, in $Kit^{W\text{-}v}$ and $Kit^{W\text{-}41}$ embryos, melanoblasts still exhibit some kinase activity, and although KIT is ectopically expressed in $Kit^{W\text{-}sh}$ embryos, melanoblasts express functional KIT and they can respond to residual KITL in their environment. It may be that low levels of KIT signalling are sufficient for melanoblast migration but high levels are required for melanoblast survival (70).

In addition to the $Kit^{W\text{-}sh}$ mutation, KIT protein is ectopically expressed in animals carrying the *Patch* (*Ph*) mutation (95). Adult *Ph* heterozygote mice exhibit a white band across the trunk which is devoid of melanocytes. The *Ph* mutation is caused by a deletion of 200kb adjacent to the *Kit* locus. The deletion includes the entire coding region of the *Pdgfra* gene (47). Wehrele-Haller *et al* showed that in *Ph* embryos, melanoblasts initially migrate out normally into the dermal mesenchyme and then disappear. In these embryos, KIT was

ectopically expressed in the somite and lateral mesenchyme. Ectopic expression of KIT in both *Ph* and $Kit^{W\text{-}sh}$ embryos is believed to sequester KITL, effectively reducing the amount of ligand available to melanoblasts (82;95). (The *Ph* mutation also affects development of the cranial neural crest by disrupting Matrix metalloproteinase-2 expression (96). This aspect of the phenotype is due to deletion of the *Pdgfra* gene.)

Artificially induced mutations have also demonstrated a role for KIT signalling in melanoblast survival. In targeted $Kit^{W\text{-}LacZ}$/ $Kit^{W\text{-}LacZ}$ animals (97), no trunk melanoblasts are seen. In heterozygous embryos, β-gal+ cells showed wild type distribution, but in reduced numbers.

MacKenzie *et al* (70) compared the distribution of melanoblasts in wild type and W^v/ W^v embryos. While the spatial distribution of melanoblasts in mutant embryos was similar to wild type at E10.5, there were fewer melanoblasts present. By E11.5, the numbers of melanoblasts in mutant embryos had greatly decreased and virtually all had disappeared by E12.5, confirming a role for KIT in melanoblast survival. In heterozygous embryos, there was also a reduced number of melanoblasts at E10.5 compared to wild type. This difference was more apparent as development progressed, suggesting KIT signalling also promotes melanoblast proliferation. Similar analysis of *Ph* embryos revealed that the region devoid of melanoblasts in the embryo (from the forelimb to the hindlimb) is far greater than predicted by the size of the white patch in adults. This suggests melanoblasts can colonise large unpopulated regions, and it may reflect a second wave of proliferation and migration by a latent stem cell population (98).

Functions of KIT signalling in melanoblast development

Mutations affecting *Kit* and *Kitl* have demonstrated that KIT signalling is essential for melanoblast survival. Other functions mediated by KIT signalling and the timimg of KITL dependence have been elucidated by manipulating melanoblast development in *in vivo* and in primary tissue culture. Nishikawa, *et al* (60) injected the KIT-blocking antibody, ACK-2, intradermally into pregnant mice at different stages of development. They found that KIT signalling is required at around E14, during the time that melanocytes colonise the hair follicles, and postnatally at the beginning of new hair growth cycles, in addition to its previously determined early requirement at around E11-E12.

A clear role for KIT signalling in promoting migration was demonstrated using transgenic mice that ectopically express KITL in the basal layer of the skin (88). In these animals, pigmented melanocytes were found in elevated numbers in sites where there are normally very few (e.g., interfollicular epidermis, lips, and oral epithelium). In addition, they were found in ectopic sites, including pawpads, nails, and even in some teeth. Injection of ACK-2 into newborn animals resulted in complete but transient de-pigmentation. Re-pigmentation occurred following the appearance, expansion, and fusion of small isolated spots, demonstrating that KITL-independent melanoblast stem cells are present in the hair bulb and they are capable of generating large numbers of migratory melanocytes that can repopulate an entire coat. Subsequently, KITL was shown to promote migration by increasing motility during movement of melanocytes from the dermis into the epidermis in an *in vitro* skin culture system (99).

EDNRB2/ EDN3 interaction is required for melanoblast development

Another group of mouse mutations associated with defects in pigment development is the *piebald* class. Mice harbouring these mutations are nearly all white due to the absence of epidermal melanocytes. They occasionally have pigmented patches in the head and tail regions, and they have black eyes due to a pigmented RPE. Mice with severe alleles usually die from aganglionic megacolon which results from defective innervation of the distal colon. The neurones and glia of the enteric nervous system are derived from the vagal and sacral neural crest. They, like melanoblasts, undergo extensive proliferation and migration between leaving the neural tube and reaching their targets.

The *piebald* mutations affect the gene encoding a G protein-coupled receptor, the endothelin B receptor (EDNRB), and its ligand, endothelin-3 (EDN3). A targeted null mutation in the *Ednrb* gene fails to complement the *piebald-lethal* mutation (which confers pigmentation defects and aganglionic megacolon) (100) and is essentially identical to the phenotype of a targeted null mutation in the *Edn3* gene, which fails to complement the *lethal spotting* mutation (101). Both targeted mutations mimic their naturally occurring *piebald* mutations in phenotype.

Ednrb and *Edn3* are members of two gene families. There are two endothelin receptors in mice, EDNRA and EDNRB. In the chick and quail, there is a third member, EDNRB2. There are three ligands, EDN1, EDN2, and EDN3 (102). The founding endothelin, EDN1,

was first described as a potent vasoconstrictor expressed by endothelial cells. Endothelins bind EDNRA with different affinities: EDN1 binds with highest affinity, followed by EDN2, while EDN3 binds poorly. However, these ligands bind EDNRB with equal affinity. Mature endothelins are produced by proteolytic activation of inactive precursor proteins. Preproendothelins are first cleaved by furin to produce big endothelins of 38-41 amino acids. Big endothelins are cleaved by endothelin converting enzyme-1 (ECE-1) to release the mature active endothelins of 21 amino acids (102). Mice carrying the targeted null allele of the *ECE-1* gene show both craniofacial and cardiac defects associated with loss of EDNRA signalling and the pigmentary and enteric nervous system defects associated with loss of EDNRB signalling (103).

Expression of endothelins and their receptors

The *Ednra* and *Ednrb* genes are expressed in different regions of the embryo. EDNRA is expressed by cranial neural crest-derived ectomesenchymal cells of the pharyngeal arches, and EDN1 is found in their migratory environment (104). Mutations in *Ednra* and *Edn1* cause craniofacial abnormalities and defects in the cardiac outflow tract. In humans, these mutations are associated with CATCH22 syndrome, also characterised by these phenotypes (104).

In the quail, EDNRB is expressed early in the neural folds prior to neural crest delamination (105). Later, EDNRB+ cells are found on migrating trunk neural crest cells and then expression is restricted to crest cells on the ventral pathway, including those that colonise the developing gut. Following migration, EDNRB expression persists in the DRG, peripheral nerves, and sympathetic ganglia. No expression is seen in cells on the dorsolateral pathway or in the pigmented cells of primary quail neural crest cultures (105). Avian neural crest cells specified as melanoblasts first express EDNRB prior to migration on the dorsolateral pathway and then switch to expressing EDNRB2 (106). EDNRB2 expression is restricted to melanoblasts. EDN3 is appropriately expressed in the intestinal mesenchyme through which enteric neural precursors migrate, and later in the ectoderm when melanoblasts are migrating underneath through the dermal mesenchyme (107).

Timing of EDNRB/2 and EDN3 action

EDNRB signalling affects more than one neural crest-derived lineage and it is first expressed prior to neural crest delamination, suggesting it is required during the earliest stages of melanoblast development. No Dct+ cells are seen in *piebald-lethal* embryos outside the RPE

and telencephalon, suggesting that EDNRB2 signalling is upstream from *Dct* expression. However, Dct+ cells are seen in $Kitl^{Sl\text{-}D}$ homozygous embryos at E11 before melanoblasts die (105;108). Shin, *et al* (109) used the tet repressor/ activator system to show that EDNRB signalling is essential for melanoblast and enteric nervous system development between E10 and E12.5. The absence of signalling during this period results in mice lacking epidermal melanocytes and exhibiting aganglionic megacolon. Expression of EDNRB between E10 and E12.5 produced mice with pigmentation patterns reflecting the rostral to caudal emigration of neural crest cells.

The HGF/ MET interaction can influence melanoblast development

Another signalling pathway known to influence melanoblast development results from the interaction of hepatocyte growth factor (HGF) with its tyrosine kinase receptor, MET. MET signalling has wide-ranging effects on developmental and physiological processes (110;111). HGF was identified independently as a result of its roles in epithelial-mesenchymal interactions, in growth, survival, and motility stimulation, and through its ability to inhibit tumour growth. MET signalling is essential for muscle, liver, and placental development, and embryos lacking either HGF or MET activity die *in utero* from deficient liver and placental function.

The MET receptor is expressed by epithelial cells as a heterodimer consisting of an extracellular C-terminal α chain, and a β chain with a short N-terminal extracellular domain, a transmembrane domain, and a cytoplasmic kinase domain. The HGF ligand is expressed in a complementary manner in adjacent mesenchymal cells where it acts in a paracrine fashion. HGF is produced by proteolysis of a single polypeptide into a heterodimer consisting of an α chain with a hairpin loop and four kringle domains, and a β chain containing a serine protease. Interaction of HGF with MET activates intracellular signalling cascades that can stimulate proliferation, promote survival, and activate migration.

While MET signalling is not essential for maintaining melanoblast numbers or mediating their migration (112), and animals lacking either HGF or MET show no pigmentation defects (111), ectopic expression of mouse *Hgf* cDNA under the metallothionin promoter has a dramatic effect on pigmentation (113). In addition to inappropriate migration of dermamyotome-derived skeletal muscle precursors, transgenic animals are hyperpigmented with abdominal spots and increased numbers of interfollicular melanocytes in the dermis and

epidermis. Melanocytes are also found in the CNS and lymph nodes, demonstrating that HGF induced inappropriate migration of melanoblasts. These results suggest that, although HGF signalling is not essential for melanoblast development, melanoblasts are influenced by it.

Intracellular signalling

The effects of different growth factors on neural crest cells has been studied extensively *in vitro* (114). One of the benefits of using *in vitro* culturing systems is that the effects of different factors on cell behaviour can be assessed in isolation, and different combinations of factors can be used. These types of studies have suggested that growth factors mainly act in concert to produce particular cellular responses. For example, it has been proposed that KITL alone is a survival factor for melanoblasts, but that it is lethal for differentiated melanocytes. However, the combination of KITL and a neurotrophin such as NGF, NT-3, or BDNF may act as survival factors for differentiated melanocytes, and be lethal to pluripotent neural crest cells (114). Basic fibroblast growth factor (bFGF) acts as a mitogen, increasing the proportion of S phase nuclei in culture, but these cells fail to survive in the absence of a neurotrophin.

The effects of different growth factors on cell behavior depend on the intracellular signalling pathways operating downstream of ligand-receptor binding events. These pathways converge in specific ways when different combinations of growth factors are present. Also, branching points in pathways facilitate multiple and coordinated cellular responses such that, e.g., proliferation and survival are coupled with migration. Specific inhibitors can be used to separate these branches so that each can be studied in isolation. These types of experiments can reveal which branches mediate the different cellular responses.

Growth factor activation results in the phosphorylation of the classical mitogen-activated protein (MAP) kinases (MAPK1, MAPK2), while growth factor withdrawal can lead to the phosphorylation of stress activated protein kinases (SAPKs), such as the JUN kinases which have been implicated in apoptosis. The biological effect of these signalling events depends on the magnitude and duration of the signal, which in turn, depends on the balance between kinases and kinase phosphatases. Phosphatase inhibitors can be used to inhibit kinases selectively. For example, the dual specificity threonine/tyrosine phosphatase inhibitor, M3/6, selectively inhibits the JNK/SAPK pathway. This inhibitor has been used to show

that JNK/SAPK activation is required for proliferation, but not for apoptosis (115). These types of inhibitors are being used to determine signalling events downstream of KIT autophosphorylation (116;117). Together, they have shown that cell survival is mediated by phosphatidyl-inositol-3'-kinase (PI_3 kinase) activity. This pathway also mediates increased cell motility following activation of MET by HGF (111).

In this chapter, a novel method of analysis was used to measure the migration distance of cells in the melanoblast and non-melanoblast neural crest populations, and to determine the proportions of cells that become melanoblasts in different growth conditions. Neural tubes were cultured from *Dct-LacZ* transgenic animals, where β-galactosidase acts as a marker for melanoblasts. A long-term aim of the project was to determine the roles of different branches of the intracellular signalling pathways known to affect melanoblast development with respect to cell migration, proliferation, survival, and differentiation. It was hoped that these pathways would be studied by culturing neural crest cells in the presence of growth factors known to influence melanoblast development, and further, by culturing neural tubes from embryos carrying mutations in genes affecting melanoblast development. Difficulties associated with culturing neural crest cells meant that, for many of the growth factors studied, the results were difficult to interpret. Some factors, such as KITL and EDN3 may have acted specifically on melanoblasts, while others, e.g., HGF, may have had a more general affect on neural crest cells, and α-MSH, which is required for eumelanin synthesis in mature melanocytes, had no effect during the early stages assessed here. Molecules that interrupt intracellular signalling pathways downstream from KIT were also tested using the cell migration assay and these preliminary data are presented.

Results

Initial culture conditions

Neural tubes were cultured from *Dct-LacZ* (A12) transgenic animals which express the *LacZ* reporter gene in melanoblasts. Originally, they were cultured in plastic 24-well plates in wells coated with 10μg/ml human fibronectin for three days using 1ml 10% FCS in F-10 medium. Cultures were grown in a humidified incubator with 5% CO_2, at 37°C. After three days, they were fixed in 4% paraformaldehyde (PFA) and stained with Xgal, as described in Chapter 2. Cultures attached and grew well on the plastic surface coated with fibronectin, with both β-gal positive (β-gal+) and negative (β-gal-) cells migrating away from the explanted neural tube and onto the substratum. A photograph illustrating a typical neural tube culture grown on plastic is shown in Plate 2 at the end of this chapter.

Culturing neural tubes on glass coverslips

While neural crest migration in general and melanoblast development in particular had been studied *in vitro* before (52;72;107;112;118-120), the effects of growth factors on melanoblast migration specifically had rarely been addressed. Also, many studies reported effects on melanoblasts without demonstrating whether there was also an effect on the general crest population. To redress this, a major aim of this project has been to measure the effect of exogenous growth factors on cell numbers and migration distances for both the non-melanoblast and the melanoblast populations.

Melanoblasts were identified easily as the β-gal+ population after staining with Xgal (Chapter 2). Other neural crest cells were not readily distinguishable for counting under brightfield illumination. Therefore, all cells in culture were stained with DAPI in order that they could be visualised and counted using fluorescence microscopy. The plastic dishes on which neural tubes were cultured autofluoresced, precluding their use for fluroescence microscopy. Initial attempts to culture neural tubes on glass coverslips failed because explants did not adhere to glass, even when the glass was coated with 10μg/ml fibronectin. Therefore, a variety of coatings was tested to improve neural tube attachment and growth on glass. The coatings used and growth results observed are presented in Table 15.

Neural tubes attached and grew reproducibly well on poly-L-lysine (100mg/ml) and fibronectin (40μg/ml)- coated coverslips. Therefore, this coating was chosen for all subsequent culturing experiments. Subsequently, DMEM was found to improve growth of cultures and its use replaced that of F-10.

Coating	No. Tubes Cultured	No. Tubes Attaching	No. Tubes Staining	Comments on Stained Cultures
poly-L-lysine (100mg/ml)	7 3 7	0 2 1	_ 0 1	β-gal + cells on top of explant only
2 coats of poly-L-lysine	8	0	_	_
poly-L-lysine + Fibronectin (40mg/ml)	8 8	7 3	1 1	Good growth with cells migrating beyond explant
Laminin (50mg/ml)	8	4	0	Of those that attached, 3 were small cultures
Laminin (100mg/ml)	8	6	0	Of those that attached, 1 was small
poly-L-lysine + Laminin (40mg/ml)	8	6	3	cells migrated beyond explant
poly-L-lysine + Laminin (50mg/ml)	8	4 (small)	2	cells migrated beyond explant in 1
poly-L-lysine + Laminin (100mg/ml)	8	5	2	cells migrated beyond explant in both
poly-L-lysine + Laminin (40mg/ml) + Fibronectin (40mg/ml)	8	4	1	Good growth with migration away from explant

Table 15. Growth of neural tube explants on glass with various coatings.
Coverslips were coated with different concentrations of laminin, fibronectin, or both, in the absence or presence of poly-L-lysine. Neural tubes were cultured on coverslips for three days in 1ml 10% FCS in F-10 medium supplemented with 50ng/ml KITL.

Attachment of neural tubes to the substrates and subsequent growth of neural crest cells was highly variable. Laminin and fibronectin are both permissive for neural crest cell migration, however, cells did not migrate consistently well on these substrates. Efforts to reduce

sources of variability, for example, harvesting litters at the same time of the day, and ensuring that a length of neural tube equivalent to ten somites in length was cultured, were not successful.

Analysing neural tube cultures

Capture and analysis scripts were developed by Paul Perry to derive quantitative data from explants grown under different conditions. Several approaches for analysis were considered and the final method decided on has been described in Chapter 2 (with sample script analysis photographs presented in Plate 1). For each neural tube analysed, the number of β-gal+ cells (melanoblasts) in each annulus, together with an estimate of the number of β-gal- cells (non-melanoblast crest cells) in each annulus was tabulated. In this way, both the total number and migration distance (measured in annuli) of each cell population was determined. An example of the output data produced by the analysis is shown below in Table 16.

Distance from explant edge (Annuli)	Estimated no. DAPI cells	No. β-gal+ cells	Annulus area (pixels^2)
1	2104	136	160768
2	1703.51	122	203168
3	937.29	34	247840
4	94.65	12	292640
5	0	1	337440

Table 16. Sample output data from the neural tube analysis script. This explant was one of seven cultured in medium supplemented with 50nM EDN3.

Are all β-gal+ cells are specified as melanoblasts?

The *Dct-LacZ* transgene is ectopically expressed in caudal nerves. Since caudal-most neural tube sections were used for culture, it was necessary to determine whether only cells specified as melanoblasts expressed the transgene in culture. All β-gal+ cells should also express *Dct* since this is one of the earliest known markers expressed by specified melanoblastasts (69). However, attempts to identify β-gal+ and Dct+ cells using immunofluorescence were unsuccessful.

It is known that signalling through the KIT tyrosine kinase receptor is necessary for melanoblast survival (69;70). In the absence of KIT signalling, melanoblasts should fail to survive.

Therefore, to remove KIT signalling, *Dct-LacZ* wild type neural tubes were cultured with ACK-2, an antibody which blocks KIT signalling (60). Additions of ACK-2 reduced the numbers of β-gal+ cells in culture (Figure 2) (120). The purpose of this experiment was to demonstrate that β-gal+ cells leaving the neural tube were specified as melanoblasts. Since some β-gal+ cells remained in the culture dish, it is not possible to conclude that all β-gal+ cells are melanoblasts. It is possible that the antibody did not fully penetrate the explant. However, this is unlikely because the neural tube is not a thick tissue and the crest cells emigrating from it do so mainly as a monolayer. Alternatively, the antibody may have had limited stability during the culture period. The reduction in the number of β-gal+ cells demonstrates that KITL is present in the neural tube culture (119). KITL is produced by the ventral neural tube (87) and by KIT+ crest cells (91). Examples of a control neural tube culture (with no addition) and one grown in media supplemented with ACK-2 is shown at the end of this chapter in Plate 3 a, b, respectively.

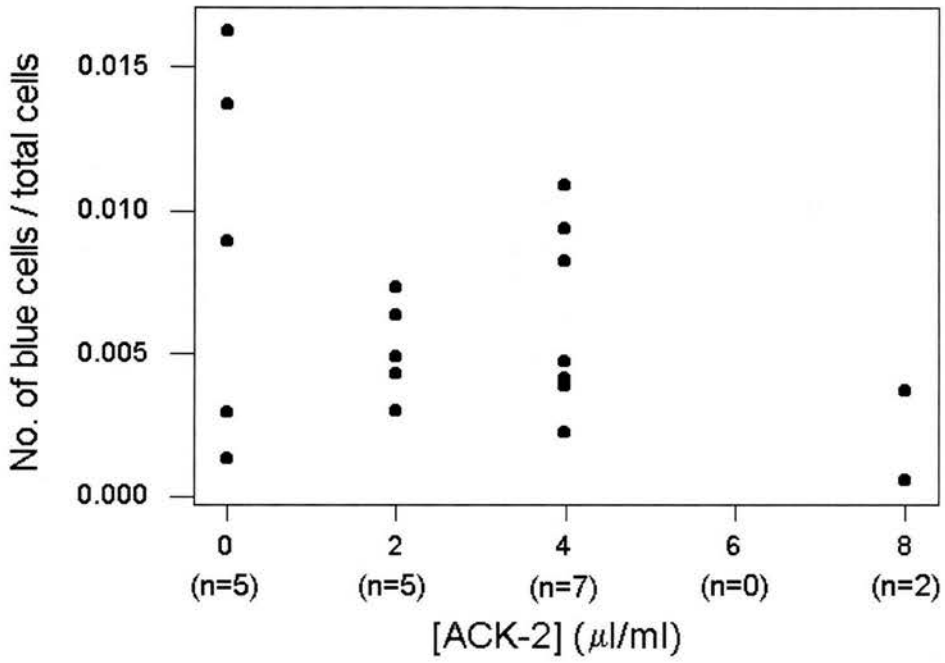

Figure 2. Effect of ACK-2 on the proportion of cells that are β-gal+. Each dot represents data from a single neural tube.

The apparently large spread in the distribution of data points for the no-addition control results from the unusually wide scale of the y-axis, which runs from 0% to only 1.5%. Factors which increase the proportion of cells that are melanoblasts demonstrate there is, in fact, normally little variation among data points representing the no-addition control (see Figure 3). The results of this and later experiments were discussed in detail with the statistician, Andrew Carothers. Preliminary statistical analyses of the data from this and some subsequent experiments suggested that the results were not significant. Therefore, for all growth factor additions, it was decided to present the raw data rather than, for example, mean data values, to avoid producing misleading results.

KIT ligand mildly increased both the number of melanoblasts and the distance they migrate

Neural tubes were grown in medium supplemented with increasing concentrations of KITL. At low concentrations (up to 50ng/ml), KITL mildly increased the proportion of cells that

express β-gal (Figure 3). Since the proportion of cells that are melanoblasts is so small (typically less than 5%), a small increase in this proportion can have a large effect on melanoblast numbers in culture; this effect can be visually striking (Plate 3 a, c). KITL may have had a mild effect on the average migration distance, but again, this effect was only seen at low concentrations. β-gal- cells were unaffected, suggesting any effect of KITL was specific to the melanoblast population (Figure 4). When neural tubes were grown in 10% FCS in DMEM with no exogenous growth factors, melanoblasts do not migrate as far as the non-melanoblast neural crest population. In the presence of low levels of KITL, melanoblasts migrated beyond their non-melanoblast neighbours. KITL acts as a chemokinetic factor in later stages of melanoblast development, where it increases the motility of melanoblasts (99). Cells may exhibit increased motility without necessarily being displaced into the next annulus in this assay. In addition, melanoblasts cultured with medium supplemented with KITL appeared more dendritic compared to controls. An example of neural tube culture grown in medium supplemented with KITL is shown at the end of this chapter in Plate 3 c.

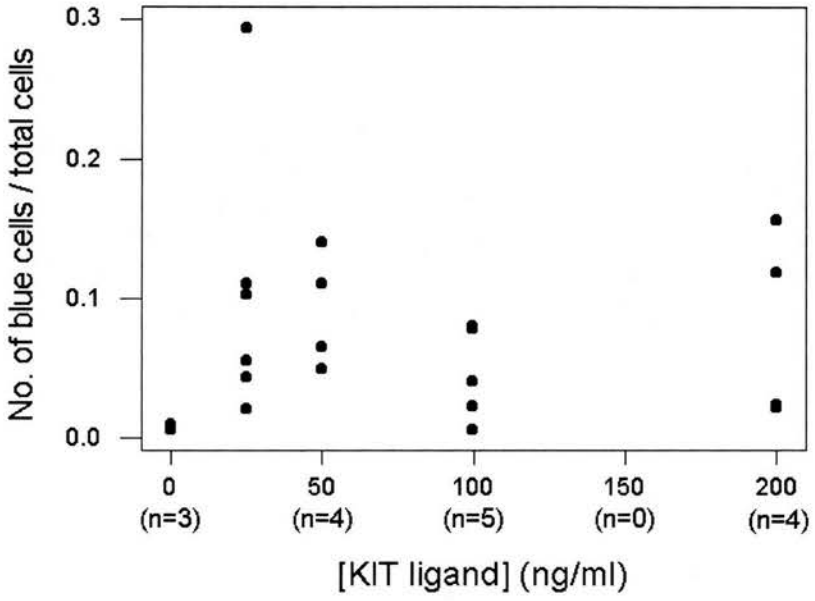

Figure 3. Low concentrations of KITL may have increased the proportion of migratory cells that are melanoblasts. Each dot represents a single neural tube culture.

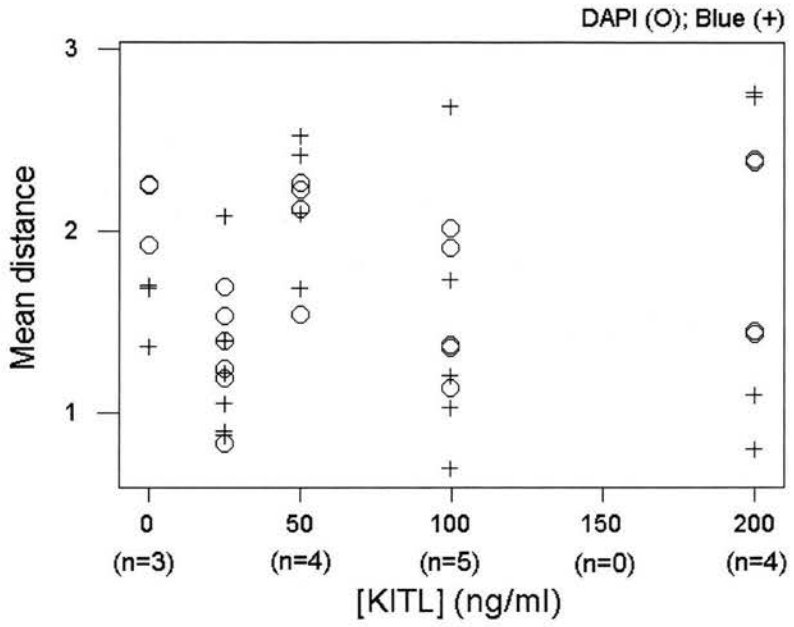

Figure 4. Effect of KITL on melanoblast migration distance. Each + or o represents a single neural tube culture.

KITL acts through the PI-3'-kinase signalling pathway (82). To determine whether activation of this pathway promotes migration or melanoblast survival/ proliferation, neural tubes were cultured in the presence of the PI-3'-kinase inhibitor, LY294002. LY294002 is a reversible classical competitive inhibitor which acts by binding to the ATP-binding site of PI-3'-kinase. In these experiments, the inhibitor did not affect the proportion of cells that are melanoblasts (Figure 5), or the distance that melanoblasts migrated (Figure 6). However, a large proportion of neural tubes grown with the inhibitor (approximately 50%) failed to remain attached to the glass surface. (In control experiments, very few neural tubes detach after the growth period.) This problem was not alleviated by delaying addition of the inhibitor by 24 hours to allow the neural tubes to attach. PI-3'-kinase signalling is likely to be required by multiple cell types in many signalling pathways, and therefore, detachment of neural tubes probably reflects non-specific effects. It is not clear why, in those explants which attached, there was no effect on melanoblasts (β-gal+) specifically. An example of a

primary neural tube cultured with the inhibitor is presented at the end of the chapter in Plate 4.

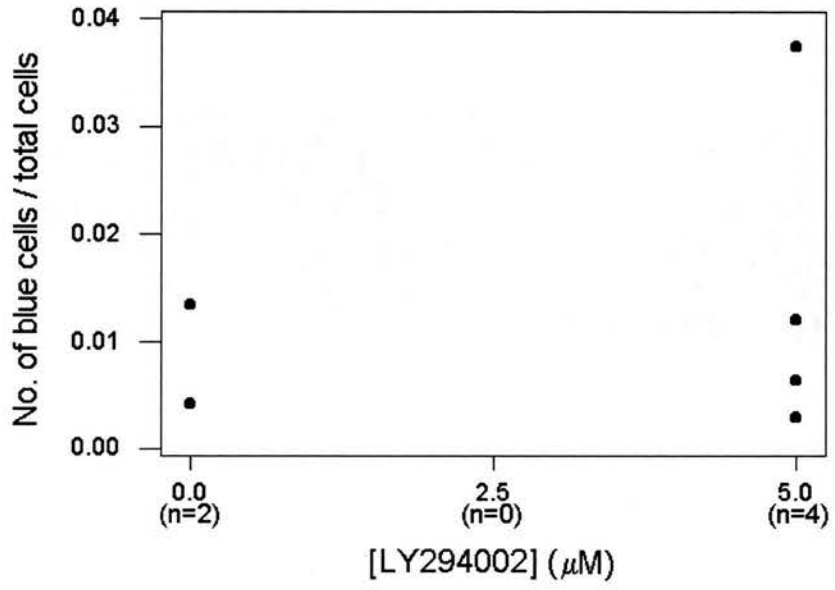

Figure 5. Effect of the PI-3'-kinase inhibitor, LY294002, on the proportion of cells that are melanoblasts. Each dot represents data from one culture.

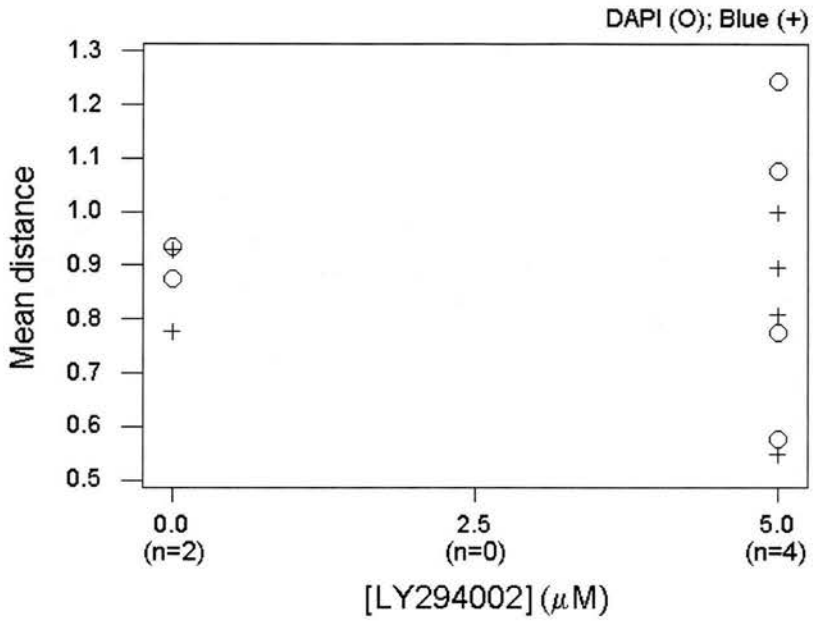

Figure 6. Effect of LY294002 on melanoblast migration distance. Each + or 0 represents data from one neural tube.

Endothelin-3 significantly increased the proportion of cells that become melanoblasts without affecting migration

Neural tubes were grown with increasing concentrations of endothelin-3. EDN3 increased the proportions of cells that were melanoblasts (Figure 7) without affecting the migration of either melanoblasts or the non-melanoblast neural crest population (Figure 8). Regression analysis indicated that the increase in the proportion of cells that are melanoblasts following EDN3 treatment was statistically significant (P= 0.0005), while the effect on migration was not (P=0.37 and 0.16 for the neural crest and melanoblast populations). An example of a neural tube grown in medium supplemented with EDN3 is presented in Plate 3 d at the end of this chapter.

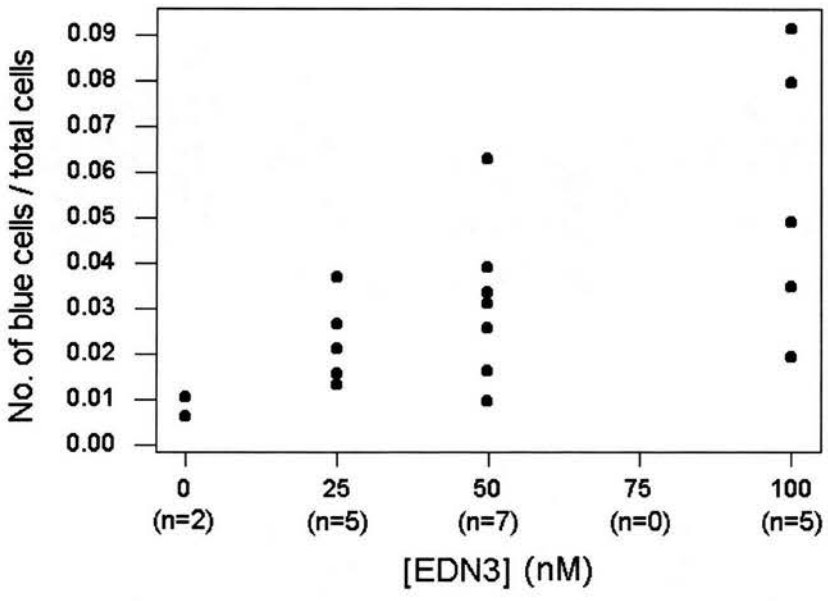

Figure 7. Endothelin-3 increased the proportion of cells that are melanoblasts. Each dot represents data from a single neural tube.

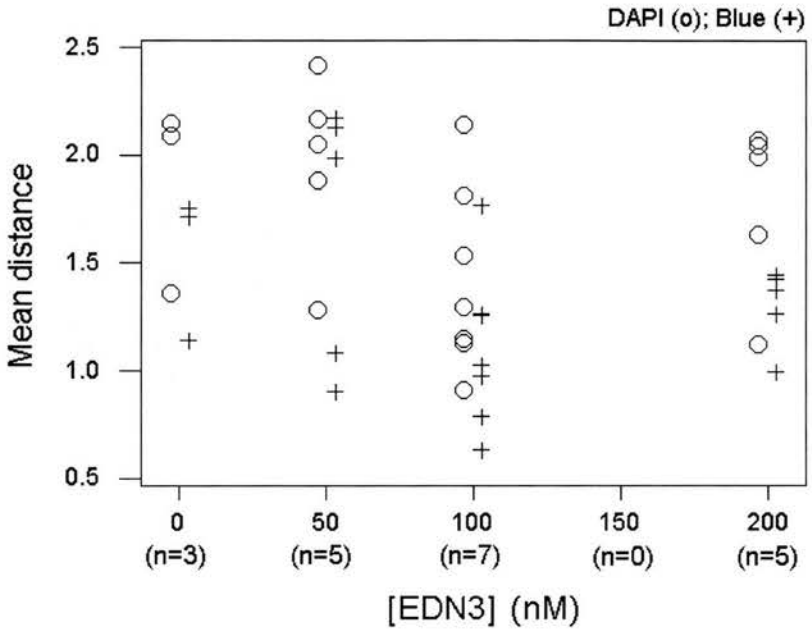

Figure 8. Endothelin-3 had no effect on neural crest migration. Each + or o represents data from a single neural tube.

HGF may affect melanoblast development

Hepatocyte growth factor (HGF) was added to neural tube cultures to assess its effect on melanoblast numbers and migration. Increasing concentrations of HGF may have caused a mild increase in the proportion of neural crest cells that were melanoblasts (Figure 9). HGF also affected migration, but this may not have been specific to melanoblasts since there appeared to be an effect (though milder) on the migration of all DAPI-stained cells (Figure 10). An example of a neural tube grown with HGF is shown at the end of the chapter in Plate 5 a, b.

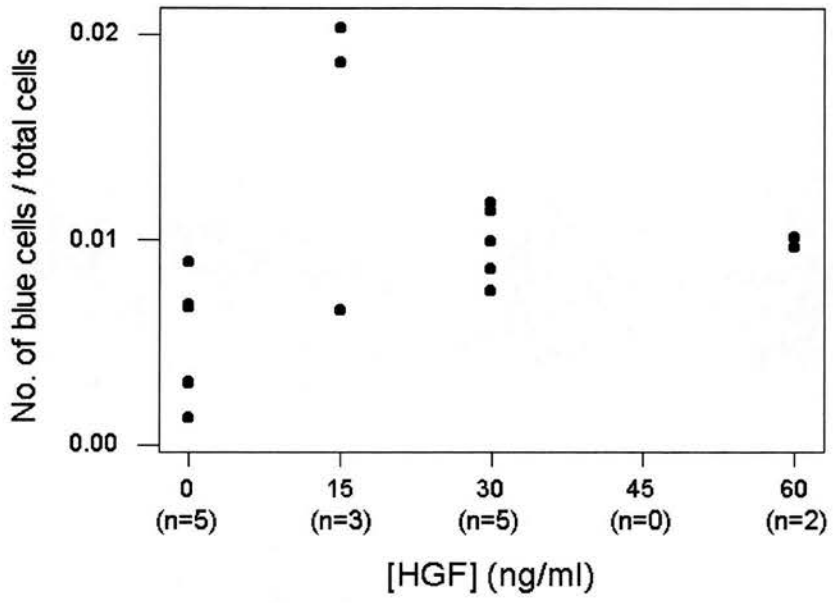

Figure 9. HGF may have mildly increased the proportion of cells that are melanoblasts. Each dot represents data from one neural tube.

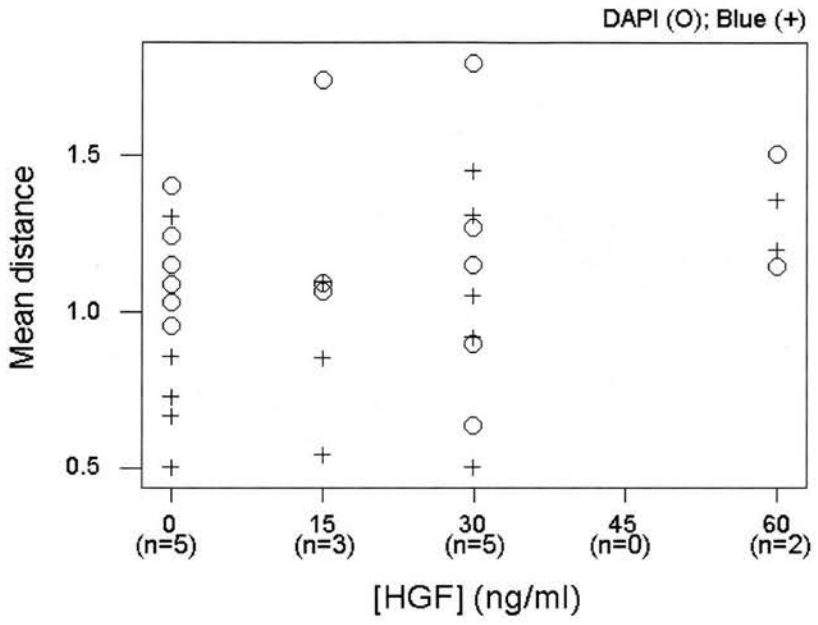

Figure 10. Effect of HGF on neural crest cell migration. Each + or o represents data from one neural tube.

MSH had no effect on melanoblast numbers or migration

The receptor for α-Melanocyte stimulating hormone (α-MSH), the Melanocortin-1 receptor (MC1R), is not expressed by melanocytes until P4. Therefore, the addition of the α-MSH analogue, [Nle^4, D-Phe^7]-α-MSH, was not expected to affect melanoblast migration in the primary tissue culture assay. Therefore, neural tube cultures were supplemented with [Nle^4, D-Phe^7]-α-MSH as a control experiment. As anticipated, additions of this growth factor did not affect the proportions of cells that were melanoblasts or the migration distance of either melanoblasts or non-melanoblast crest cells (Figure 11, Figure 12). An example of a neural tube grown with exogenous [Nle^4, D-Phe^7]-α-MSH is shown in Plate 5 c, d at the end of the chapter.

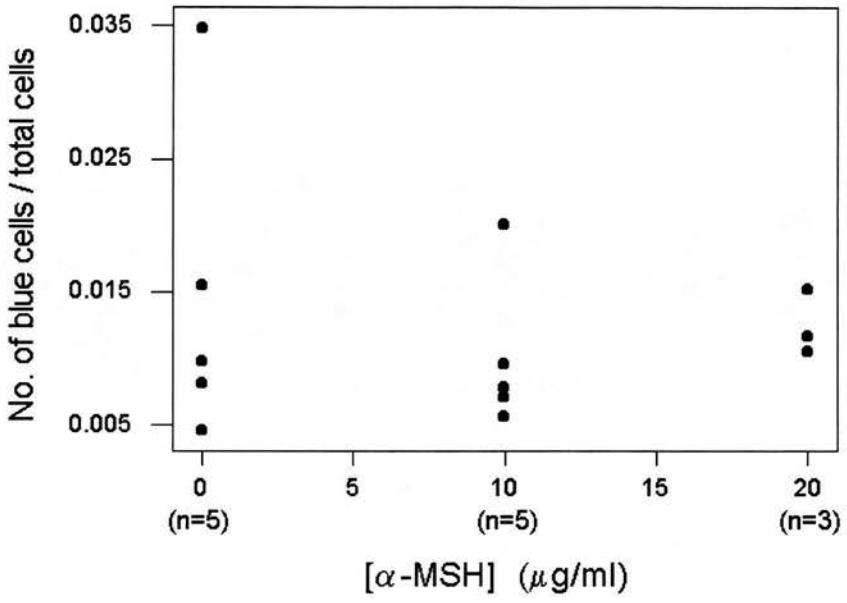

Figure 11. [Nle^4, D-Phe^7]-α-MSH had no effect on the proportion of cells that are melanoblasts. Each dot represents a single culture.

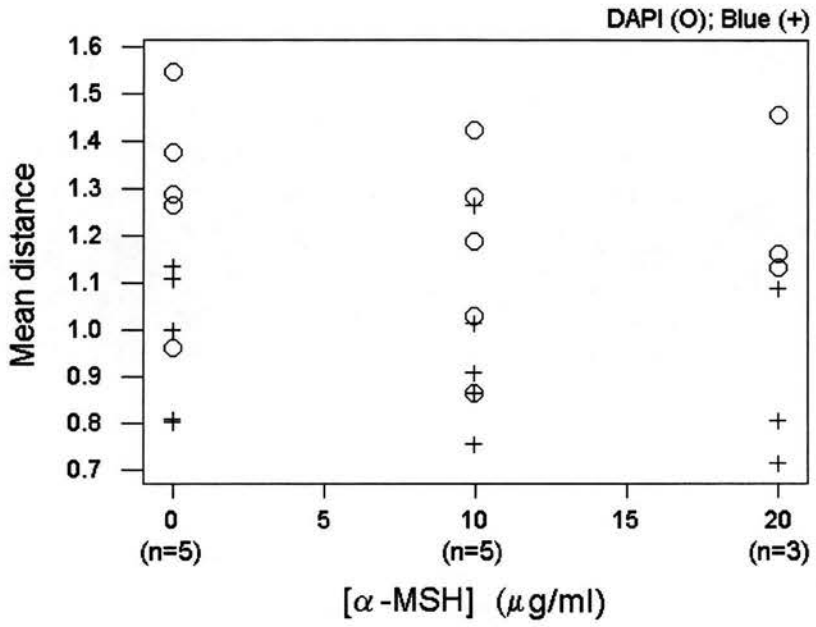

Figure 12. [Nle^4, D-Phe^7]-α-MSH had no effect on neural crest migration. Each + or o represents data from a single culture.

Discussion

Culturing primary neural crest cells allows individual signalling pathways to be manipulated to determine their contributions to melanoblast development. In this study, the effects of signalling through the KIT, EDNRB, MET, and MC1 receptors were determined using a novel assay in which cell numbers and their migration distances were measured for both the melanoblast and non-melanoblast neural crest populations. Signalling through the KIT receptor using exogenous KITL caused a mild increase in melanoblast migration distance and in the proportion of cells that were melanoblasts. EDN3 increased the proportion of cells that were melanoblasts without affecting migration. HGF mildly stimulated migration, but this effect was not specific to melanoblasts, and signalling through Mc1r had no effect on cell numbers or their migration distance.

Proportions of cells that are melanoblasts

Do factors that affect the proportions of cells that are melanoblasts act by influencing melanoblast specification, survival, or proliferation? The counting assay cannot distinguish between these alternatives. Indeed, it is possible that signalling through one receptor has multiple effects. The phenotypes of mice carrying mutations affecting different signalling pathways indicate the most likely explanations for observations made using the counting assay.

Effects of KIT signalling on melanoblast development

KIT mediates survival and promotes the proliferation and migration of melanoblasts

Signalling through the KIT tyrosine kinase receptor is essential for melanoblast maintenance and survival, but not differentiation (120;121). By inhibiting KIT signalling with the blocking antibody, ACK-2, Ito *et al* demonstrated that KIT positive cells died by apoptosis (122). KIT signalling has also been shown to promote melanoblast proliferation *in vivo* (70) and *in vitro* (84;107;120). Here, a novel assay was used to demonstrate that this effect is specific to melanoblasts in primary tissue culture.

Migration of KIT+ germ cells is mediated through the membrane-bound form of KITL (94). However, soluble KITL is as effective at promoting migration of melanocytes into hair follicles as localised KITL (99). Exogenous soluble KITL also promoted migration of

cultured human melanocytes on fibronectin by modulating integrin expression (123). Here, addition of soluble KITL increased the migration distance of melanoblasts, while other neural crest cells were unaffected.

Although KIT signalling is not essential for the early stages of melanocyte differentiation (expression of early markers such as *Dct*), addition of KITL to chick neural crest cultures affected melanoblast morphology with cells being more dendritic than in control cultures (91). In this study, melanoblasts cultured with KITL also appeared more dentritic than those in control cultures.

Intracellular signalling downstream from KIT

Signal transduction pathways downstream of tyrosine kinase receptor activation have been studied intensively. The different cellular effects of KIT signalling are mediated by branches of these downstream mediators. Cells transfected with human KIT and cultured with KITL exhibited increased proliferation, downregulation of KIT expression, and actin reorganisation (84). Subsequently, addition of soluble KITL promoted proliferation or survival, but not differentiation, of pigmented cells in long term primary neural crest cultures (121). Following activation and autophosphorylation, KIT associates with intracellular signalling molecules containing SH2 domains, including phosphatidylinositol-3'-kinase (PI-3'-kinase), which has been shown to mediate cell survival (116). PI-3'-kinase activation permits phosphorylation of other serine/ threonine kinases, e.g., MAP kinase. In addition to its role in cell survival, low levels of PI-3'-kinase activation promote adhesion and migration (81). In this study, addition of LY294002, the PI-3'-kinase inhibitor, prevented attachment of neural tubes to the fibronectin-coated surface, therefore, other processes mediated by PI-3'-kinase signalling could not be addressed.

Effects of EDN3/ EDNRB signalling on melanoblast development

Signalling through EDNRB is essential for the early stages of melanoblast development (109). EDN3 is likely to increase the proportion of cells that are melanoblasts by either increasing the proportion of neural crest cells that are specified as melanoblast progenitors or by selectively expanding the melanoblast progenitor population at early stages. Studies using neural crest cultures in the mouse (107) and avian system (106;124;125) have shown that addition of exogenous EDN3 increases the proliferation rates of melanoblasts in primary neural crest culture. However, KITL must be present in the culture in order for EDN3 to

promote melanoblast differentiation or proliferation (119). EDN3 is also highly mitogenic for cultured melanocytes derived from embryonic skin which already contain pigment granules (126).

EDNRB signalling also affects the differentiation state of melanoblasts in culture. EDN3 induced pigment production earlier than α–MSH in long-term mouse neural crest cultures, and pigment production was dramatically enhanced in cultures supplemented with both EDN3 and α–MSH (107). In the quail, however, EDN3 delayed pigment production, increased the re-plating efficiency of primary neural crest cells, and increased the numbers of multipotent cells within the re-plated population (125). Lahav *et al* showed that EDN3 increased the growth and re-plating efficiency of glial progenitors, melanoblasts, and GM progenitor cells, without affecting neurone progenitors, NG cells, or NGM cells (106). These results suggest EDN3 plays a central role in determining the differentiation state of melanoblasts.

Furthermore, EDN3 can influence the morphology of 'determined' melanocytes and glial cells. EDN3 induces the appearance and proliferation of KIT+ pigmented cells in E10 quail sciatic nerve cultures containing Schwann cells and initially no melanoblasts (124). Conversely, EDN3 induces de-differentiation of cultured embryonic epidermal melanocytes and stimulates the generation of unpigmented cells that express glial markers (126). Clonal cultures demonstrated that EDN3 increases the proliferation rate of pigmented cells. Cells become elongated and transiently depigmented, and then they recover pigmentation. Almost half of the epidermal melanocyte clones cultured with EDN3 produced glial cells compared to just 10% of clones grown in control medium. Together, these results suggest that long-term treatment with EDN3 restores and maintains cells in a bipotential state, and that even differentiating melanocytes and glial cells retain bipotency until late stages.

In this study, EDN3 additions increased the proportion of cells that were melanoblasts, consistent with findings reported previously. However, EDN3 had no effect on melanoblast migration. Cultures were not grown sufficiently long to demonstrate pigment synthesis. The increase in proportions of cells that are specified as melanoblasts probably results from the combined effects of expanding the GM precursor pool, and increasing the proliferation rate of melanoblasts. Nataf *et al* proposed that EDN3 expands the progenitor population and prevents early differentiation so that sufficient cell numbers are generated to colonise distant and widespread targets (skin and gut) (105).

KITL and EDN3 act synergistically

Combined additions of KITL and EDN3 to neural tube cultures can be used to determine whether these growth factors act in concert (107;124). In mouse neural crest cultures, EDN3 and KITL acted synergistically to increase the number of KIT+ cells, but their effects on melanoblast proliferation (measured by % [^{3}H]-thymidine incorporation) were only additive (107). However, EDN1, which also acts through EDNRB in primary melanoblast cultures, and KITL did act synergistically to increase DNA synthesis in cultured human melanocytes (127).

Activation of EDNRB by EDN3 results in the mobilisation of intracellular calcium and 1,2-diacylglycerol (DAG). DAG, in turn, activates protein kinase C (PKC) (107). These effects of EDN3 addition are also mediated by EDN1 (127), and mimicked by phorbol esters such as TPA (121). Activated PKC phosphorylates intermediate kinases which activate MAPK, and they also phosphorylate receptor tyrosine kinases, including KIT. PKC-mediated phosphorylation of KIT inhibits KITL-induced autophosphorylation and associated kinase activity (128). This reduces KITL-induced mitogenicity, but is necessary for actin reorganisation and cellular motility (128). PKC is thought to act in a negative feedback loop to control KIT activity. Therefore, the two distinct pathways may interact to coordinate adhesion and migration with proliferation. However, in this study, EDN3 affected melanoblast numbers without affecting migration.

Effect of HGF on melanoblast development

In this study, addition of HGF to neural crest cultures increased the proportion of cells that were melanoblasts and increased their migration distance, although the latter effect may not have been specific to melanoblasts as β-gal– crest cells also exhibited a comparatively mild increase in average migration distance in response to HGF. Since HGF affects epithelial-mesenchyme interactions generally, and epithelial to mesenchyme transitions in particular (111), it is expected that other neural crest cells may also express MET and be able to respond to locally available HGF.

HGF can increase the number of melanoblasts in mouse neural tube culture and promote their differentiation into melanocytes (112). This increase in melanoblast numbers is only

partly explained by a stimulation of melanoblast proliferation, suggesting HGF promoted survival as well (112).

Effect of α-MSH on melanoblast development

Cultured neural crest cells were not expected to respond to exogenous α–MSH since its receptor, Mc1r, is not expressed until after birth (S. A. Jordan, unpublished observations). Neural tubes were grown with α–MSH as a negative control for the analysis method. α–MSH induces DOPA-positive cells to become fully pigmented between 12 days and three weeks of culture (107;118;121), and although EDN3 alone produces cultures with more pigmented cells than α–MSH alone, the effect of EDN3 is enhanced by the presence of α–MSH (107). Since signalling in both pathways is initiated by stimulation of a G protein-coupled receptor, some signalling molecules may be common to both and they may act together.

Observing melanoblast development in living primary tissue culture

With the vast array of mouse mutants affecting coat pigmentation, the large number of growth factors known to influence melanoblast development *in vitro*, and the complexity of their intracellular signalling cascades, the ability to directly observe living melanoblasts migrating in the presence of exogenous growth factors and intracellular signalling inhibitors would enable a fuller understanding of the roles of different proteins at different stages of development. To this end, a *Dct-GFP* transgenic line was generated and this line will be used to continue the analysis of *in vitro* melanoblast development in the future. Live cell imaging will allow the cell shape changes to be recorded in real time and it will be possible to distinguish more readily between factors that promote directed migration and those that increase cell motility.

Plate 2. Example of a neural tube cultured on plastic coated with 10mg/ml fibronectin. The explant was grown for three days and stained with Xgal.

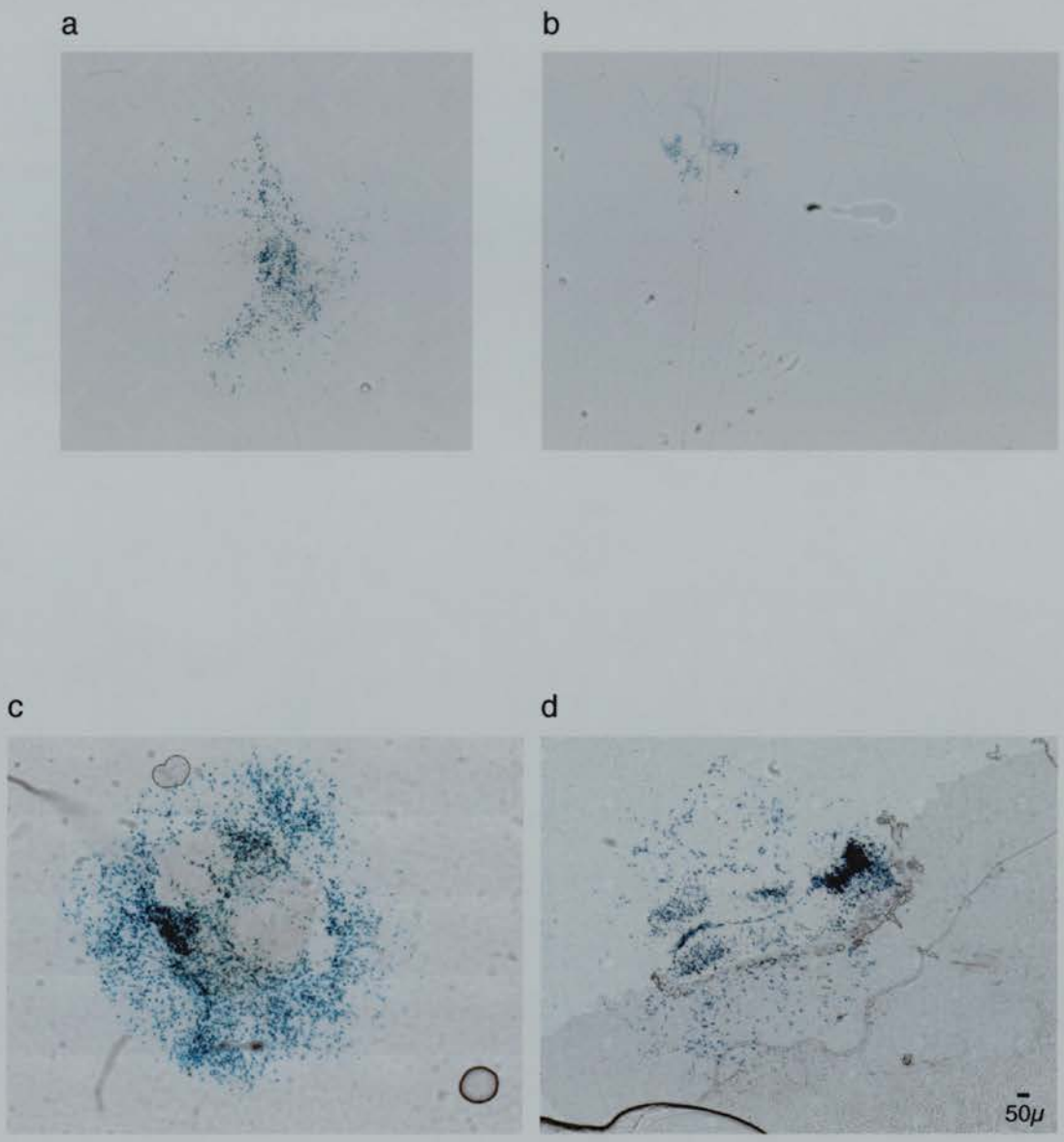

Plate 3. Effect of KITL and EDN3 on melanoblast migration and numbers in the primary tissue culture assay. a. No addition control culture, b. Neural tube cultured with 2μg/ml ACK-2, c. 200 ng/ml KITL, d. 100 nM EDN3. Neural tubes were cultured on glass coverslips coated with 100mg/ml Poly-L-lysine and 40 μg/ml human recombinant fibronectin for three days and then stained with Xgal and DAPI. (Fluorescence images not shown).

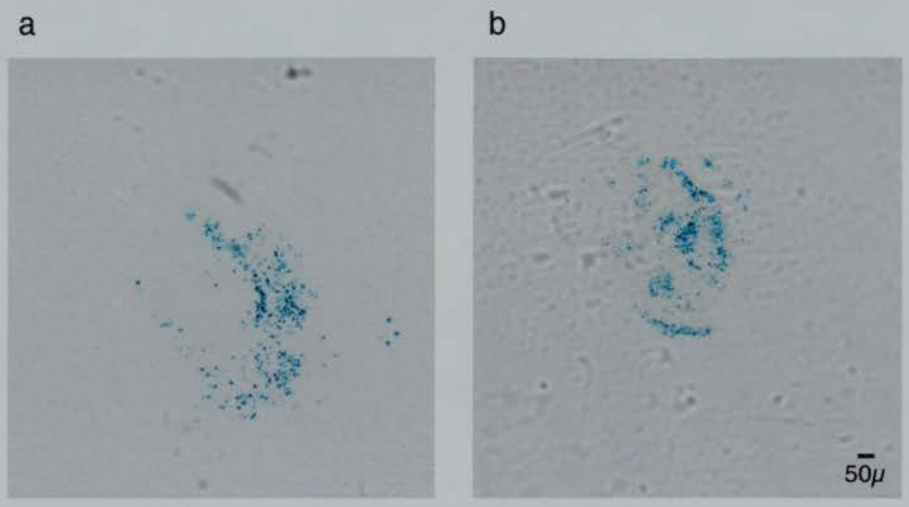

Plate 4. Effect of the PI-3'-kinase inhibitor, LY294002 on melanoblast migration and numbers. a. no addition of LY294002, b. 10μl/ml LY294002. Neural tubes were cultured on glass coverslips coated with 100mg/ml Poly-L-lysine and 40 μg/ml human recombinant fibronectin for three days and then stained with Xgal and DAPI. (Fluorescence images not shown).

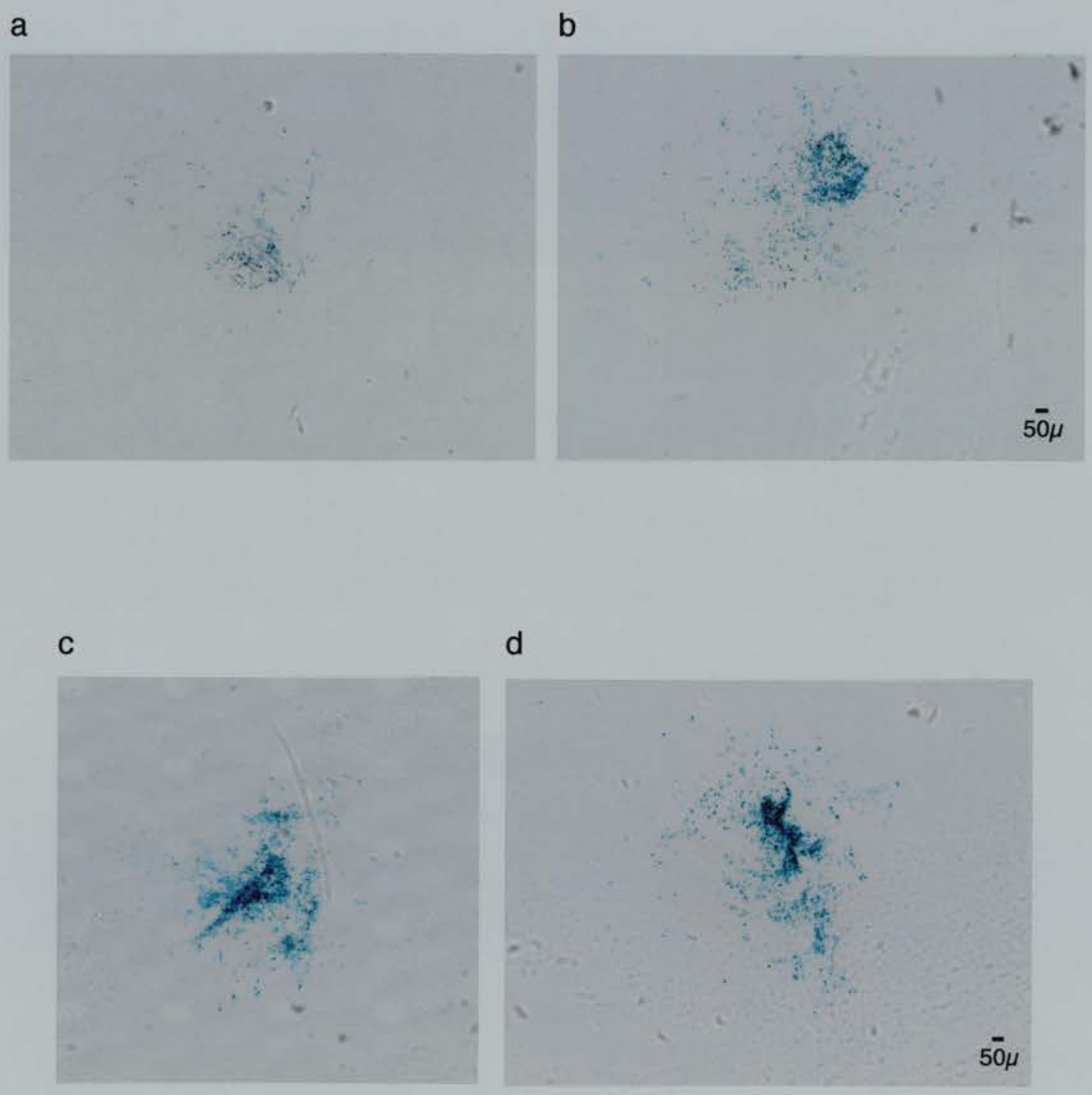

Plate 5. Effect of HGF and αMSH on melanoblast migration and numbers.
a. no HGF, b. 30 ng/ml HGF, c. no αMSH, d. 10 μg/ml [Nle^4, D-Phe^7]-α-MSH. Neural tubes were cultured on glass coverslips coated with 100mg/ml Poly-L-lysine and 40 μg/ml human recombinant fibronectin for three days and then stained with Xgal and DAPI. (Fluorescence images not shown).

Chapter 4

Clonal Analysis of Melanoblast Development

'Thus, beyond all questions of quantity there lie questions of pattern which are essential for understanding Nature.'

Alfred North Whitehead (1934).[5]

[5] Quoted from Gilbert, S. (1994). **Developmental Biology** (fourth edition). Sinauer Associates Inc. Massachusetts, U.S.A.

Introduction

Most tissues in mammalian embryos are multiclonal in origin. Having organs and tissues that are derived from multiple progenitors provides a selective advantage: the accidental loss of one progenitor does not affect the development of the tissue as a whole (55), and plasticity allows modification of developmental mechanisms through evolution.

Because melanoblasts are derived from the neural crest, and neural crest cells delaminate from the neural tube at all axial levels, it is reasonable to assume that the neural crest and the melanoblast population as a subset, are derived from multiple progenitors. How many melanoblast progenitors are there and how are their progeny distributed? Specifically, how much mixing is there between cells from different progenitors, how large a region can one melanoblast progenitor populate, and what is the proliferative potential of one melanoblast precursor?

Genetic chimaeras have been used to address these types of questions in many tissues in the mammalian embryo. They have been used to estimate the number of founder cells in an organ, and to study the phenotypic interactions between clonal progeny. Estimating the number of founder cells is extremely difficult for several reasons. Most statistical methods cannot account for clonal selection mechanisms, such as the allocation of cells to either the trophoblast or inner cell mass lineages. There may be genotype-dependent tissue-specific selection, which would result in cells of one embryonic origin being favoured to contribute to a particular lineage. Also, founder cells may acquire mitotically heritable differences in proliferative potential (129), thus the contribution of one founder may be over-represented in the mature organ. Cell death during organogenesis also complicates the interpretation of data from experiments using chimaeras. However, mosaics and chimaeras can be used successfully to study other patterns of tissue growth, including cell mixing, proliferation, and migration within and between clones.

In vivo clonal analyses using lysinated rhodamine dextran to label individual dorsal neural tube cells (presumptive neural crest) (6), and migratory crest cells (50), in the chick have shown that many neural crest cells give rise to diverse cell types and highly variable clone sizes. The same experiments in the mouse gave similar results (7). Multipotent neural crest cells have also been isolated and grown *in vitro* (31;51;52). These studies demonstrated heterogeneity in the neural crest by illustrating the range of diverse phenotypes and

proliferative capacities that crest cells exhibit. They also showed that the developmental potential of crest cells is progressively restricted. However, since they did not study melanoblasts specifically, no information regarding the distribution patterns of clonally related melanoblasts across the surface of the embryo was obtained.

By making a series of aggregation chimaeras between genetically distinct morulae differing at various coat colour loci, Mintz (55;56;130) endeavoured to make quantitative and qualitative statements to explain melanoblast ontogeny. The coats of the adult chimaeric mice showed a spectrum of phenotypes depending on the degree of chimaerism. Mintz explained the phenotypes by using a model or 'standard' coat pattern which itself was rarely seen. This pattern consisted of alternating broad transverse bands of colour extending from the dorsum to the midventrum, and it was believed to reflect the migratory history of melanoblasts in the embryo. While no mouse exactly matched the standard pattern, all phenotypes could be explained by it. For example, three adjacent clones of one genotype would generate a very wide band, and bands in the face were thought to be distorted as a result of regional growth differences. The patterns on the left and right sides were asymmetrical, suggesting they were determined independently. Mintz concluded that each band represented the progeny of a single melanoblast progenitor from the neural crest. Melanocytes at the borders of adjacent bands were intermingled, sometimes extensively. By assessing the patterns of many chimaeric coats, Mintz proposed that if bands were arranged alternately by chance, the maximum number that could be generated on either side of the body was 17: three in the head, six in the body, and eight in the tail. Mintz therefore concluded there were 34 melanoblast progenitors in total (55;56).

Similar coat colour patterns in chimaeric mice have been observed by others (131), but they were interpreted differently (132). The transverse bands of colour were frequently interrupted and broken by neighbouring bands, suggesting individual melanoblast precursors did not generate discrete bands, but rather extensive mixing occurred. It has been suggested that 34 melanoblast progenitors would generate 34 bands in a chimaeric animal in less than one in one million random arrangements of progenitor cells. Other mathematical approaches have been used to suggest a variety of progenitor numbers that could generate 17 bands on each side of the embryo (132). However, despite conflicting interpretations, Mintz's proposal that there are 17 melanoblast progenitors on either side of the embryo was recognised to have become widely accepted (133).

Recently, a new, non-invasive technique was developed to label clones *in vivo* (134;135). Using a modified *LacZ* reporter gene, called '*LaacZ*', it is possible to label cells at low frequency and randomly during development. The modified transgene contains a 290 base pair duplication which introduces an in-frame termination codon. This results in the translation of a non-functional, truncated β-galactosidase protein in all cells that express the transgene. By homologous recombination, either intra- or intergenically, the 290bp duplication reverts to wild type *LacZ*, restoring the normal reading frame and resulting in the translation of functional protein in expressing cells. Therefore, a single founder cell and all its progeny can be labelled genetically. Reversion events occur sufficiently rarely to ensure that, normally, only single labelling events occur in an embryo. Reversion events can occur in any cell and at any time during development, and labelled clones in expressing lineages can be identified easily by Xgal staining. This technique has been used successfully to perform lineage analyses in the developing somites, neuroepithelium, and cerebellum (136-138). This technique is particularly amenable for use in the melanoblast lineage since Xgal staining provides a visual presentation of the arrangement of clonally related cells on the surface of the embryo.

While previous studies only examined coat colour patterns in adults, here two complementary approaches have been used to study the distribution of melanoblast clones in the embryo as development proceeds. Chimaeric embryos were made by aggregating morulae carrying a *LacZ* reporter gene expressed in melanoblasts (70) with non-transgenic morulae. In addition, *Dct-LaacZ* transgenic lines were generated in order to mark melanoblast clones randomly (134). The patterns of melanoblast distribution in chimaeric and mosaic embryos suggest that 1.) the melanoblast population, in general, is derived from a large number of progenitors and that 2.) the head and face region is populated by a larger number of progenitors than the trunk, 3.) a pool of melanoblasts may reside in the cervical region of the embryo, and 4.) melanoblasts within a clone show considerable longitudinal migration, suggesting there is more axial mixing than was previously thought.

Results

Chimaeras

Production of chimaeras

Aggregation chimaeras were made between eight-cell morulae carrying the *Dct-LacZ* transgene (morulae from A12 mice) and non-transgenic morulae, as described in Chapter 2. Embryos were harvested between E11.5 and E16.5 and stained with Xgal. For analysis, chimaeric embryos were compared with Xgal stained age-matched A12 (*Dct-LacZ*) embryos.

Although many embryos were harvested during the course of each aggregation experiment (Table 17), only eight-cell embryos containing round (not compacted) cells were used for aggregation. Chimaeras made from compacted embryos do not aggregate well and cells do not mix well subsequently. In the first experiment, an excess of embryos derived from A12 X F1 matings were recovered. Since, on average, half of these embryos will have been non-transgenic, the excess embryos were aggregated with each other with the expectation that at least some of the aggregations will have been between a transgenic and a non-transgenic embryo.

Table 17. Summary of chimaera aggregation experiments.

Experiment no.	No. F1 X F1 plugs	Total no. healthy embryos harvested	No. A12 X F1 plugs	Total no. healthy embryos harvested	No. F1/A12 aggregations	No. A12/A12 aggregations	Age at harvest	No. embryos transferred	No post-implantation embryos harvested	No. embryos staining	No. informative embryos
1	8	70	8	149	44	24	E12.5 E13.5	28/ 2 mice 33/ 2 mice	16 20	11 13	6 3
2	10	157	6	103	40	0	E12.5 E13.5	20/ 1 mouse 20/ 1 mouse	4 13	3 6	3 3
3	8	168	7	185	80	0	E14.5 E15.5 E16.5	20/ 1 mouse 20/ 1 mouse 37/ 2 mice	5 10 12	3 3 4	1 1 1
4	8	80	8	131	35	0	E10.5 E12.5	14/ 1 mouse 14/ 1 mouse	5 5	too young 3	0 0
5	8	145	8	137	75	0	E14.5 E15.5 E16.5	14/ 1 mouse 28/ 2 mice 21/ 2 mice	7 14 11	2 9 5	1 4 4
6	8	143	8	90	25	0	E10.5 E14.5	14/1 mouse 9/1 mouse	9 1	2 0	too young 0
7	3		7		16	0	E11.5	16/1 mouse	3	2	2
8	5	97	6	146	74	0	E10.5 E14.5	14/1 mouse 40/2 mice	3 6	0 3	too young 1
										Total	30

Distribution of labelled melanoblasts in Dct-LacZ ↔ non-transgenic chimaeric embryos

A total of 30 chimaeric embryos were informative. Informative embryos were defined as those that contained labelled melanoblasts but that did not appear exactly like *Dct-LacZ* transgenic embryos. Uninformative embryos either had no labelled melanoblasts, or were indistinguishable from *Dct-LacZ* transgenic embryos. Informative embryos were informally classified as either high grade (HG) or low grade (LG), according to the density of labelled melanoblasts. Those in which a large proportion of the melanoblast population (when compared to age-matched *Dct-LacZ* transgenic embryos, Plate 7) was labelled were classified as high grade, and those with low levels of labelling were low grade (Table 18).

Table 18. Results summary of chimaera analyses. The degree of chimaerism was estimated visually and embryos were categorised as being either high grade (HG) or low grade (LG).

Age	Total no. informative embryos	Degree of chimaerism	No. embryos	General description
E11.5	2	LG	1	Embryo had two labelled cells in the trunk.
		HG	1	General dilution with trunk gap
E12.5	9	LG	3	All embryos have labelled clusters in the face; some also have a trunk/tail stripe
		HG	6	All embryos have a dilution or complete gap in the trunk; some also have a dilution in the face
E13.5	6	(LG)	(1)	(No labelled melanoblasts; only telencephalon staining)
		HG	5	One embryo had patches and gaps of about equal size, the others had a general dilution, either with or without gaps.
E14.5	3	LG	1	Severe dilution down length of body with a mid-trunk gap.
		HG	2	Both embryos had a general dilution with no complete gaps, but with particularly diluted trunks.
E15.5	5	LG	1	Labelled cells on pinna, snout, and around eye only.
		HG	3	All showed a general dilution; 1 had stripes and gaps along body; all three had a reduced no. labelled cells on one side of the snout.
E16.5	5	LG	1	Labelled cells in pinna, snout, around eye, and at hindlimb.
		HG	4	One embryo had a general dilution; three showed clearer stripes and gaps.
Total	30			

General appearance of chimaeric embryos

Both high and low grade chimaeras were informative. In high grade chimaeras, areas consistently lacking labelled melanoblasts ('gaps') identified regions populated by a small number of progenitor cells. In low grade chimaeras, areas that consistently contained labelled cells indicated that a large number of progenitor cells populate the region. A very low grade chimaera can illustrate the number and distribution of the progeny of a single clone (Plate 6 a. i-iii). Chimaeras can be compared directly to age-matched A12 (*Dct-LacZ*) embryos (Plate 7.). In wild type E13.5 embryos, melanoblasts appear more densely populated in the rostral and caudal areas, with a comparatively lower density of labelled cells between the limbs. This observation has been documented previously (82). Some mid to high grade chimaeras looked similar to control *Dct-LacZ* embryos except that there was a general dilution of labelled cells. This suggested there are many melanoblast progenitors generally, and that cells mix extensively between clones. There were no low grade chimaeras showing a low but uniform distribution of melanoblasts; they all had large regions lacking labelled melanoblasts. The left and right sides of chimaeric embryos were patterned independently, as expected.

Patterns of labelled melanoblasts in the head and face

In the head and face, low grade chimaeras almost always had labelled melanoblasts around the eye and pinna, suggesting these regions are populated by the progeny of more than one precursor (Plate 6 b). Medium and high grade chimaeras occasionally lacked labelled melanoblasts on one or other side of the snout. The face patch in one low grade embryo (Plate 6 c.) suggests that one clone may cross the ventral midline in the snout. The higher concentration of melanoblasts in control embryos (Plate 7 e.) indicates this region is normally populated by more than one clone.

Medium grade chimaeras almost always had labelled melanoblasts in the cervical region (Plate 6 di, ii), suggesting this area is populated by the descendants of multiple progenitors, while other regions of the same embryo have a reduction or absence of labelled cells compared to age-matched *Dct-LacZ* embryos (Plate 7 c).

Patterns of labelled melanoblasts in the trunk

In the trunk, high grade chimaeras frequently show single or multiple gaps between the limbs (Plate 6 d, e, marked by arrows) when compared to age-matched A12 embryos (Plate 7 b,c). In high grade embryos lacking gaps, there is a general dilution of labelled cells, and this dilution may be stronger between the limbs. In older embryos (E15.5 and E16.5), labelled cells are arranged into more discrete patches with sharper boundaries (Plate 6 f) comapred to A12 age-matched embryos (Plate 7 f). These patterns in older embryos are more reminiscent of the patterns seen in adult chimaeric coat patterns reported by Mintz and McLaren (56;131). The distribution of melanoblasts may mature into a more fixed, adult pattern at this stage of development.

Discussion of chimaera data

Chimaeric embryos have been used here in an attempt to study the extent of cell mixing in the melanoblast lineage during embryogenesis, and to estimate the number of melanoblast progenitors there are. Rather than study adult coat patterns to draw conclusions about events that happen during embryogenesis, patterns of melanoblast dispersal were studied in embryos directly. This was made possible by aggregating embryos carrying the *Dct-LacZ* transgene with non-transgenic embryos. In total, 30 informative chimaeric embryos were generated, ranging in age from E11.5 to E16.5. Embryos of all ages were informative, and both low and high grade embryos provided unique information.

There are several caveats associated with studying chimaeras. Chimaeras are derived from more than one animal and so the aggregate must undergo cell number regulation prior to implantation. This regulation might result in the selection of one genotype over another by the chance position of cells in the morula at early stages of lineage allocation (129). Alternatively, one genotype may have a growth advantage and therefore be more likely to contribute to embryonic tissues. Here, the two groups of embryos used in the aggregations were derived from an F1 background. Therefore, they should have similar growth properties and, so far, no observations have suggested that the presence of the transgene affects cell viability.

The use of aggregation chimaeras allows cells to be labelled from the earliest stages of embryogenesis, prior to the allocation of cells to the melanoblast lineage. The advantage of this is that one can be sure that all branches of the lineage are labelled. Therefore, in embryos with the fewest labelled cells, an entire single clone can be visualised. The disadvantage is that, in other embryos with many labelled cells, multiple progenitors were labelled; therefore, one can not conclude that only a single clone has been represented.

However, chimaeras are invaluable for studying interactions between clonally related cells. In this study, chimaeras were classified into two groups, low grade and high grade. In low grade chimaeras, melanoblasts were consistently found in regions near the eye, pinna, and cervical region, suggesting these areas are normally populated by a large number of progenitors. In high grade chimaeras, labelled melanoblasts were frequently missing from the region between the limbs, indicating that a small number of progenitors populate the trunk. Some high grade chimaeras did not have obvious gaps, but rather showed a more general dilution in cell labelling when compared to age-matched A12 (*Dct-LacZ*) embryos,

indicating there is a high degree of mixing within and between clones. A similar effect has been documented in $Kit^{W\text{-}sh}$ heterozygous embryos, where there is a general dilution of melanoblasts throughout the developing dermis, resulting in an almost complete loss in the interlimb region which, even in wild type embryos, has a lower melanoblast density compared to rostral and caudal regions (82). No low grade chimaeras had a uniform but low level of cell labelling; all low grade chimaeras had large areas devoid of labelled cells. This indicated that, while there is a high degree of cell mixing, clones do not completely overlap.

The patterns of labelled cells changed with embryonic age. As embryos matured, patterns of labelled cells changed from being distributed over widespread areas with poorly defined boundaries, to being organised in discrete patches of labelled cells with more clearly defined boundaries. This shift may reflect changes in proliferation and migration patterns, or it may simply be the result of the growth of the embryo as a whole, and the associated shape changes that this brings. While it is difficult to reconcile the early patterns with patterns in the coats of adult chimaeras, the patterns later in development are an intermediate pattern. This suggests that the early widespread patterns somehow become condensed into tight discrete blocks.

Dct-LaacZ-LacZ *mosaic embryos*

A new method of labelling lineages genetically was developed recently (134). It is based on reversion by homologous recombination of a modified reporter gene ('*LaacZ*'), whose product is a non-functional β-galactosidase protein, to its functional wild type reporter (*LacZ*). This method has been used here to label progenitor cells in the melanoblast lineage at different stages of embryogenesis.

Production of *Dct-LaacZ* transgenic mouse lines

The construct was generated from a plasmid vector containing the *Dct* promoter and the *LacZ* transgene (pPB2, Figure 13). This vector had been used previously to generate the *Dct-LacZ* transgenic line (A12) (70). The methods used to manipulate the vector are described in Chapter 2.

In order to create a 290bp duplication in the *LacZ* sequence, the *Xho*1/*Eco*RV fragment was ligated to the *Cla*1/*Xho*1 fragment (134) (see Figure 13). The *Xho*1/*Eco*RV fragment was prepared by digesting 10μg pPB2 with *Eco*RV and *Bam*H1. Electrophoresis confirmed that the predicted bands of 2.6kb and 7.7kb were produced. Buffer salts were removed using a millipore filter and the DNA was digested with *Xho*1, producing the expected 2.6kb, 2.9kb, and 4.7kb fragments. The 4.7kb band contained the *Dct* promoter and the 5' end of the *LacZ* gene. The *Cla*1/*Xho*1 fragment was prepared by first digesting 10μg pPB2 with *Cla*1. This produced the expected 847bp and 9.5kb fragments; these are due to the presence of two *Cla*1 sites. The digested ends were filled in using klenow enzyme. Subsequent *Xho*1 digestion cut the 9.5kb fragment into a 3.6kb and a 5.9kb fragment. This 5.9kb fragment contained the 3' end of the *LacZ* gene and vector DNA (see Figure 13).

Both bands (the 4.7kb *Xho*1/*Eco*RV band and the 5.9kb *Cla*1/*Xho*1) were gel purified and the DNA concentrations were assessed before setting up ligations. The ligation products were transformed by electroporation, and transformants were screened by digesting plasmid (miniprep) DNA with *Cla*1 and *Eco*RV. Two clones produced the correctly sized digestion products and sequencing across the duplicated region confirmed that the duplication had been made correctly.

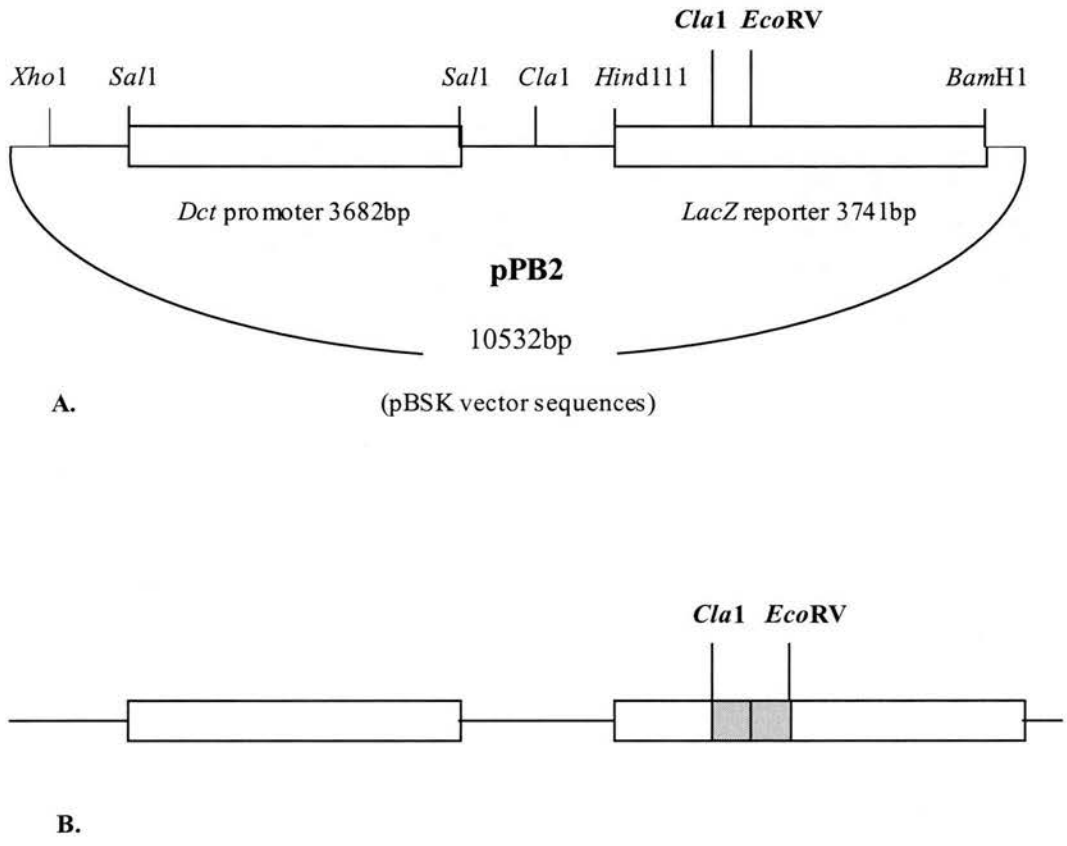

Figure 13. Modification of pPB2 to generate a 290bp duplication in the *LacZ* gene. A. Diagram of pPB2 showing the position of restriction sites used to manipulate the construct. B. Diagram showing changes in the reporter construct following manipulation. The *Cla*1/*Eco*RV fragment in *LacZ* was duplicated by ligating the *Xho*1/*Eco*RV fragment to the *Cla*1/*Xho*1 fragment, as described by Bonnerot *et al* (134).

Experiment No.	Total No. Embryos	Total No. Injected Embryos	Total No. Cultured	Total No. Transferred	Total No. Born	Total No. Transgenic
1	102	69	47	24	1(died)	0
2	70	65	50	30	0	0
3	229	203	165	138	3	0
4	191	186	135	110	0	0
5	144	120	102	75	16	2
6	179	173	123	123	6	5
7	277	200	173	100	16	4
8	177	164	119	70	17	4
Totals	1369	1180	914	670	58	15

Table 19. Summary of microinjection experiments for the *Dct-LaacZ* construct.

The construct was microinjected at a concentration of 2ng/μl into [CBA x C57Bl6] F1 x [CBA x C57Bl6] F1 fertilised eggs. Fifteen out of 58 founders were identified as transgenic by PCR amplification of the duplicated sequence from tail biopsy genomic DNA (Table 19). Founders were bred onto a mixed CBA x C57Bl6 F1-CD1 background. Breeding animals were genotyped by PCR amplification of *LacZ* sequences from genomic DNA.

Assessment of transgenic lines

The transgene must integrate into a region of chromatin in which it can both be expressed and undergo reversion, in order for individual clones to be labelled. In addition, homologous recombination can occur both intra- and intergenically (134). Therefore, the copy number also affects the frequency of clone labelling because there are statistically more opportunities for reversion with increasing copy number.

In order to draw conclusions about the distribution of cells in labelled melanoblast clones, many clones at different stages of development needed to be generated and analysed. Of all *Dct-LaacZ* expressing lineages (melanoblasts of the skin and eye, and telencephalon cells), the melanoblast lineage produced clones with the lowest frequency. Therefore, it was necessary to select the transgenic line that generated labelled clones most frequently.

Timed matings were set up for each line and E13.5 and E14.5 litters were harvested and stained with Xgal in order to identify the line which would generate labelled clones most frequently. Matings were set up between one transgenic animal and one CD1 so that, on average, one half of the progeny was transgenic. (Genotyping results from breeding animals confirmed that the transgene was transmitted as predicted by normal Mendelian genetics for all lines studied). Embryos within a litter were pooled together for staining in the same vial. Initially, several litters were harvested from each of the 15 transgenic lines. Labelled clones were identified in embryos representing six of the 15 lines in these preliminary studies (Table 20). The different lines produced labelled clones at different frequencies. This presumably reflected differences in copy number or locus-dependent variations in recombination potential. Clones were labelled in all lineages that express *Dct*: melanoblasts of the skin and eye, and the developing telencephalon. (Telencephalon clones are considered separately in Chapter 5).

Founder Name	No. Litters Stained	No. Embryos Stained	No. Embryos with Labelled Clones	Total No. Clones	Overall Labelling Frequency
A188	Failed to breed				
A188.1	7	81	0	0	0
A189	5	52	0	0	0
A189.1	16	193	3	3	0.031
A189.2	7	91	3	3	0.066
A189.3	3	42	0	0	0
A189.4	6	76	0	0	0
A194	7	71	0	0	0
A194.1	5	42	0	0	0
A195	29	339	23	28	0.165
A195.1	11	132	4	4	0.061
A202	19	248	3	4	0.032
A202.1	8	96	5	6	0.125
A202.2	7	92	0	0	0
A202.3	5	60	0	0	0

Table 20. Summary of preliminary studies of the 15 *Dct-LaacZ* transgenic lines. Embryos from each line were harvested at E13.5 or E14.5, and stained with Xgal.

Melanoblast clones were only observed in lines A195 and A202 in these initial litters. These early clones are presented in Plate 8 at the end of this chapter. Clones varied in size, shape, and cellular distribution. Comparison with age-matched A12 embryos (Plate 7 c) suggests unlabelled melanoblasts are present among labelled melanoblasts in mosaic embryos.

Line A195 was selected for further analyses because it had the highest clone labelling frequency (CLF). In order to generate a large number of clones in the melanoblast lineage from A195 embryos, a large-scale series of timed mating was set up. (These matings were also set up to study large numbers of embryos at different developmental stages for analyses in the telencephalon, as described in Chapter 5.) A195 litters were harvested from E10.5 to E14.5. Over 3300 embryos were stained with Xgal and screened for the presence of labelled clones. This corresponds to approximately 1650 transgenic embryos, in which a reversion event can occur. Within these, 46 labelled melanoblast clones were identified. A list summarising all mosaic embryos harvested and clones recorded can be found in the appendix. Only the most informative clones are discussed below.

Distribution of melanoblasts in labelled clones

To assess the degree of cell mixing between clones, it would be necessary to compare *Dct-LaacZ/LacZ* mosaic embryos containing labelled melanoblasts with age-matched control *Dct-LacZ* embryos. These two groups can only be compared if the transgenes have equivalent expression domains. Wholemount *in situ* hybridisation was done on E13.5 and E14.5 A195 (*Dct-LaacZ*) and A12 (*Dct-LacZ*) embryos using a *Dct* riboprobe to label the entire melanoblast population, and with a *LacZ* riboprobe to assess whether the entire melanoblast population expresses the transgenes in the respective lines. These results are presented in Plate 9. *Dct* was expressed strongly in both lines in neural crest-derived melanoblasts, as expected. *LacZ* was expressed strongly in melanoblasts in A12 embryos. In A195 embryos, *LacZ* expression was much weaker than in A12, however, the domain of expression appeared to have been conserved. Despite low *LacZ* RNA levels, β-galactosidase activity levels were sufficiently high in mosaic embryos to see labelled clones easily, and even one-celled labelled clones were identified. However, expression levels in A195 were sufficiently low to prevent labelled cells from being visible in photographs. Therefore, clones were recorded using *camera lucida* apparatus, or by mapping labelled cells onto pre-drawn embryos. The *in situ* results suggest that direct comparisons between A12 and A195 mosaic embryos are valid.

Examples of clones

In A195 *Dct-LaacZ/LacZ* mosaic embryos, labelled clones were found in a sufficiently small proportion of transgenic embryos to provide confidence that each group of labelled cells represented a clone resulting from a single recombination event (see below). Therefore, the distribution pattern of labelled cells illustrated the proliferative capacity of the founder cell, and migratory capacity of its descendents. Fifty-nine per cent of clones were in the head/face, 27% were in the head-trunk region, and 14% were in the body. This suggests a large number of melanoblast progenitors populate the face and head. Clones were almost always confined to either the left or right side of the embryo, as predicted by Mintz's suggestion that melanoblasts migrate independently on the left and right sides of the body and do not normally cross the midline (56).

Clones in the head and face

In the head and the face (Plate 8 a, b, Plate 10 a), labelled cells were distributed across relatively large areas. Within a clone, melanoblasts could be grouped into small clusters, or arranged in lines. Cells were not organised into discrete patches or stripes, and clones did not have sharp boundaries. Comparison with A12 (*Dct-LacZ*) embryos (Plate 7) suggested that unlabelled melanoblasts were distributed among the labelled ones in many widespread clones.

Cells in clones at the head-trunk boundary were dispersed widely, covering regions as broad as the forelimb bud to the eye. Clones did not have sharp boundaries (Plate 10 b). Again, comparison with age-matched A12 embryos indicated there were unlabelled melanoblasts between labelled cells.

Clones in the trunk

In the trunk (Plate 10 c), clones were arranged as broad patches of widely distributed cells, or as transverse bands that appeared to have split into narrower bands. In one embryo (Plate 10 c i and ii), three separate patches of melanoblasts were labelled on one side of the embryo, with smaller patches in the same locations on the contralateral side. It is likely that, in this case, a particularly early reversion event occurred in the ectoderm, giving rise to labelled premigratory neural crest cells at different levels of the neural tube. However, this embryo did not contain marked cells in the telencephalon, another ectodermally-derived tissue which

also expresses the transgene. Labelled cells were rarely organised into stripes; in those that were (e.g., Plate 10 ciii), the stripes were broad and cells were widely distributed within the stripe. Again, comparisons with age-matched A12 embryos suggest there must be extensive longitudinal mixing because unlabelled melanoblasts are present among labelled clone members.

The trunk clone labelled in line A202 (Plate 8 c) comprised more discrete, but still widely distributed, clusters of labelled cells, suggesting longitudinal migration occurs over great distances. These results are not predicted by Mintz's interpretation of adult chimaeric coat patterns. The pattern of labelling in the A202 clone also indicated that, in order for clusters to be separated in this way, melanoblasts would have to undergo distinct phases of migration and proliferation. Such a pattern is not observed in the head and face, but in this region, melanoblasts must migrate over longer distances to reach their destinations.

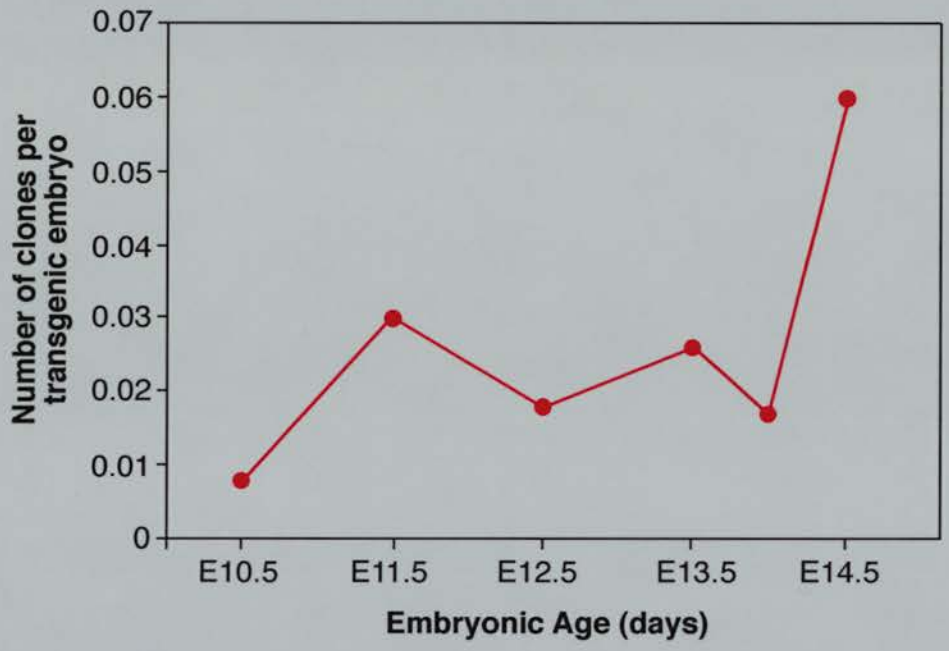

Figure 14. Clone labelling frequency in the melanoblast lineage of A195 *Dct-LaacZ* mosaic embryos varies with embryonic age.

The frequency of clone labelling varies with embryonic age

Bonnerot, *et al*, (134) showed that the rate of homologous recombination per cell division in cells transfected with the modified *LaacZ* construct was approximately 5 x 10^{-6}. In line A195, the occurrence of clones varied with embryonic age. Since the rate of homologous recombination per cell division should remain constant throughout an A195 animal's life, any apparent changes in clone labelling frequency must reflect changes in cell proliferation and death patterns.

In the melanoblast lineage, the clone labelling frequency (CLF) varied between E10.5 and E14.5, from a minimum of 0.008 labelled melanoblast clones per transgenic embryo at E10.5, to a maximum of 0.06 at E14.5. (This value considers only the presence or absence of a clone, and does not reflect the size of the clone.) This very low labelling rate suggests that labelled cells within an embryo result from a single recombination event.

Between E10.5 and E11.5, the CLF increases from 0.008 to 0.03, by nearly a factor of four, suggesting there is a phase of proliferation in the progenitor population at this time. This increased CLF is not statistically significant (see Chapter 5, page 147). Because cells in the melanoblast lineage become labelled so infrequenty, many more embryos would have to be screened to achieve statistically significant results. Nevertheless, this observation is consistent with the increased number of melanoblasts seen between E10.5 and E11.5 (70). During this time, melanoblasts have left the dorsal neural tube and are dispersing onto the dorsolateral pathway between the ectoderm and the dermamyotome. Over the course of the next few days (E12.5-E14.0), the CLF fluctuates between 0.017 and 0.026 labelled clones per transgenic embryo. Cells are migrating through the developing dermis towards the ventrum. They may not be cycling as frequently in this environment or cell division may be balanced by cell death. Over just a 12-hour period between E14.0 and E14.5, the CLF increases from 0.017 to 0.060 labelled clones per transgenic embryo. At this stage, melanoblasts are entering the epidermis prior to colonising the developing hair follicles and melanoblasts undergo a further phase of cell proliferation. This increase in melanoblast numbers can be visualised directly by comparing Xgal-stained E13.5 and E14.5 A12 embryos (Plate 7, c and d).

Discussion of mosaic embryo data

Mosaic embryos have been used in addition to traditional chimaeras in an effort to study the interaction between and within individual melanoblast clones, and to estimate the number of melanoblast progenitors. Mosaic embryos have the advantage over chimaeras that individual cells can be labelled at very low frequency, ensuring that multiple labelled clones are not found in the same embryo. This allows an assessment of the proliferative potential of melanoblasts and the size of region they can populate.

In these experiments, a modified *LacZ* reporter gene, *LaacZ* (134), was used to label cells spontaneously. By driving *LaacZ* expression under the *Dct* promoter, labelled clones were generated in all *Dct* expressing lineages: neural crest-derived melanoblasts, melanoblasts of the RPE, and cells of the developing telencephalon. The modified transgene contains a 290bp duplication which introduces an in-frame termination codon. Therefore, cells expressing *Dct-LaacZ* produce a truncated non-functional β-galactosidase protein. The duplicated sequence undergoes homologous recombination spontaneously and at low frequency. This restores the wild type *LacZ* reading frame, functional protein is produced in expressing cells, and the founder cell and all its daughters are labelled and can be followed retrospectively.

Of the 1600 transgenic embryos aged between E10.5 and E14.5 that were screened for the presence of labelled clones, 46 melanoblast clones were labelled in total. Most labelled clones were in the head and face. This suggests that either the head and face are populated by a large number of progenitors, or that melanoblasts in the head and face have a higher proliferative capacity than those in the rest of the embryo, making them more likely to be labelled. There were also many labelled clones in the cervical region (head-trunk region).

The position of cells within a clone provides information about cell movements within and between clones. In most clones, labelled cells were broadly distributed within a region and comparison with A12 embryos suggested unlabelled melanoblasts were present among labelled cells, indicating there is extensive mixing between clones. Although melanoblasts migrate on the dorsolateral pathway towards the ventrum, clear transverse stripes of labelled cells were rarely seen. Most clones did not have distinct boundaries and they varied in shape. In those embryos that did have stripe-like clones, the stripes were broad and labelled cells were widely distributed within the stripe. These clones were mainly seen in older embryos (E14.5). For those clones with patches varying in shape, it is possible that the often

round patches may be precursors of more mature stripes which would not be apparent until later in development.

Discussion

Two different approaches have been used to investigate the distribution of melanoblast clones in the mouse embryo. *Dct-LacZ* ↔ non-transgenic chimaeric embryos and *Dct-LaacZ/LacZ* mosaic embryos have shown that the melanoblast population is derived from a large number of progenitor cells in the neural crest. Melanoblasts migrate extensively in an axial direction such that cells from neighbouring clones normally overlap, and descendants of a single precursor can be distributed over a large area. A large proportion of the progenitors populates the head and face region of the embryo, while the region between the limbs is populated by only a few progenitors.

What information can be extracted from chimaeras and mosaics?

The two different approaches used here have generated results that are complementary and partially overlapping. Each technique provides unique information, and each has limitations. Melanoblast patterns in chimaeric embryos identify which regions of the embryo are populated by a large and small number of progenitors, and suggest there is a high degree of cell mixing. On the one hand, chimaeric embryos generally contain the progeny of multiple labelled progenitors, so they cannot illustrate the proliferative capacity of single precursors or the size of region a single progenitor populates. On the other hand, mosaic embryos label single cells at undefined times during development. These embryos depict the distribution of a single clone and they demonstrate the proliferative capacity of single progenitors. However, in mosaic embryos, the labelled cell is not labelled from the beginning. While some reversion events will have occurred prior to the allocation of cells to the melanoblast lineage, many will have occurred afterwards, and not all of the melanoblast clone will have been labelled. Unfortunately, there is no way to determine when a reversion event occurred. Even by counting the number of cells within a clone and determining the cell cycle time, it is possible that clone members die, which would lead to an underestimate of the clone's size and age.

Cell mixing in the melanoblast lineage

Each technique can give an indication of the extent of cell mixing and migration patterns. Chimaeric and mosaic embryos both suggested there is a high degree of cell mixing between clones with cells migrating extensively in an axial direction, in addition to their established lateral migration.

The predominance of head and face clones in mosaic embryos can be explained by one of two possibilities. Either this region is populated by more progenitors than the rest of the body, or progenitors in the head and face proliferate more than those in the trunk, making them more likely to be labelled. Low grade chimaeras always have labelled cells in the head and face.

While it has not been possible to determine exactly the number of progenitor cells there are in the melanoblast lineage, Mintz's predictions of three progenitors in the head, eight in the body, and six in the tail is highly unlikely. The rostral region of the embryo is populated by a large number of progenitor cells, with fewer colonising the trunk. It is not clear why different areas should be populated unevenly, although, several possibilities have been proposed (82). Firstly, melanoblast progenitors may be produced in different numbers along the body axis, with fewer progenitors leaving the neural crest between the limbs than elsewhere. Alternatively, growth rate variations along the axis may account for differences in melanoblast density. Finally, differences in the migratory environment could affect relative melanoblast numbers in different regions. For example, in the trunk, the dermis is derived from the somites (dermamyotome), however, in the head, the dermis is derived from the cranial neural crest in the absence of somites (82).

Some naturally occurring mutations label melanoblast progenitors

Some naturally occurring mutations recapitulate the coat colour patterns seen in chimaeric animals and they must be reconciled with the data presented here. *Chinchilla-mottled* (c^m/c^m) (139) mice carry a chromosomal rearrangement upstream from the *Tyrosinase* coding region. The rearrangement confers mitotically heritable transcriptional instability such that adult coats comprise transverse bands of lightly pigmented (grey) and pale hairs. Another naturally occurring mutation, the *pink-eyed dilution (unstable)* (p^{um}) allele is very like the *Dct-LaacZ/LacZ* mosaics. It is caused by a 75kb tandem duplication that interrupts a gene encoding a 12-membrane spanning protein expressed in melanosomes which may be involved in pigment biosynthesis (47). The duplication can revert to wild type by homologous recombination at a frequency of about 1.8% (140). Adult animals appear cream with usually a single pigmented patch of variable size and position. Pigmented patches must consist of clonally related melanoblasts, and their shapes are not limited to broad transvese bands.

Cell mingling within and between melanoblast clones

Studies in which cultured melanoblasts were injected into embryos *in utero* have suggested migrating melanoblasts respond to melanoblast density in the local environment. Donor melanoblasts can contribute to host pigmentation (58). If the hosts are wild type, donor cells show limited contribution and apparently migrate predominantly dorsolaterally. However, if the host lacks viable melanoblasts, as in *W* mutant embryos, donor cells undergo extensive clonal expansion and longitudinal migration occurs in addition to dorsolateral migration, such that donor cells can pigment more than half of the adult coat. If two populations of differently pigmented melanoblasts are introduced into *W* host embryos, the resulting dual-coloured mice exhibit bands with either extensive mixing at the boundaries, or regions of fine intermingling of the two colours within a 'band' (58). This fine intermingling suggests that neighbouring bands overlap almost completely. These data also suggest melanoblasts mix extensively between clones and they are consistent with the chimaera and mosaic data presented here.

Another pair of mutations interrupts correct signalling between the tyrosine kinase receptor, KIT, and its ligand, KITL. The mutations *rump-white* and *patch* are caused by chromosomal rearrangements in regions upstream from the *Kit* gene (47;95;98). These rearrangements cause aberrant expression of the receptor in the dermamyotome, where it is thought to sequester KITL (95). *rump-white* adults have unpigmented areas that are devoid of melanoblasts in the rump, while *patch* coats show unpigmented areas of variable shape and size in the abdomen, sometimes with discrete pigmented spots in the middle of an unpigmented area. However, the adult coats have smaller unpopulated areas than do embryos, suggesting regions devoid of melanoblasts are partially repopulated later in development. This occurs either by migration and proliferation of melanoblasts from regions of high to low cell density, or by rapid clonal expansion of surviving melanoblasts in the middle of regions largely devoid of melanoblasts (98). Together, these results indicate that melanoblasts have proliferative and migratory capacities beyond those they normally exhibit. The *Dct-LacZ* ↔ non-transgenic chimaeras and *Dct-LaacZ/LacZ* mosaic embryos permit visualisation of some of this proliferative and migratory capacity directly.

The results of mosaic and chimaeric experiments described here are compatible with observations made during the analysis of mutant pigmentation phenotypes. They are not compatible with Mintz's interpretations of adult coat patterns in chimaeras, however, they do

agree with the alternative interpretations proposed by McLaren *et al.* In addition, the results presented here suggest a large number of melanoblast progenitors populate the mouse coat.

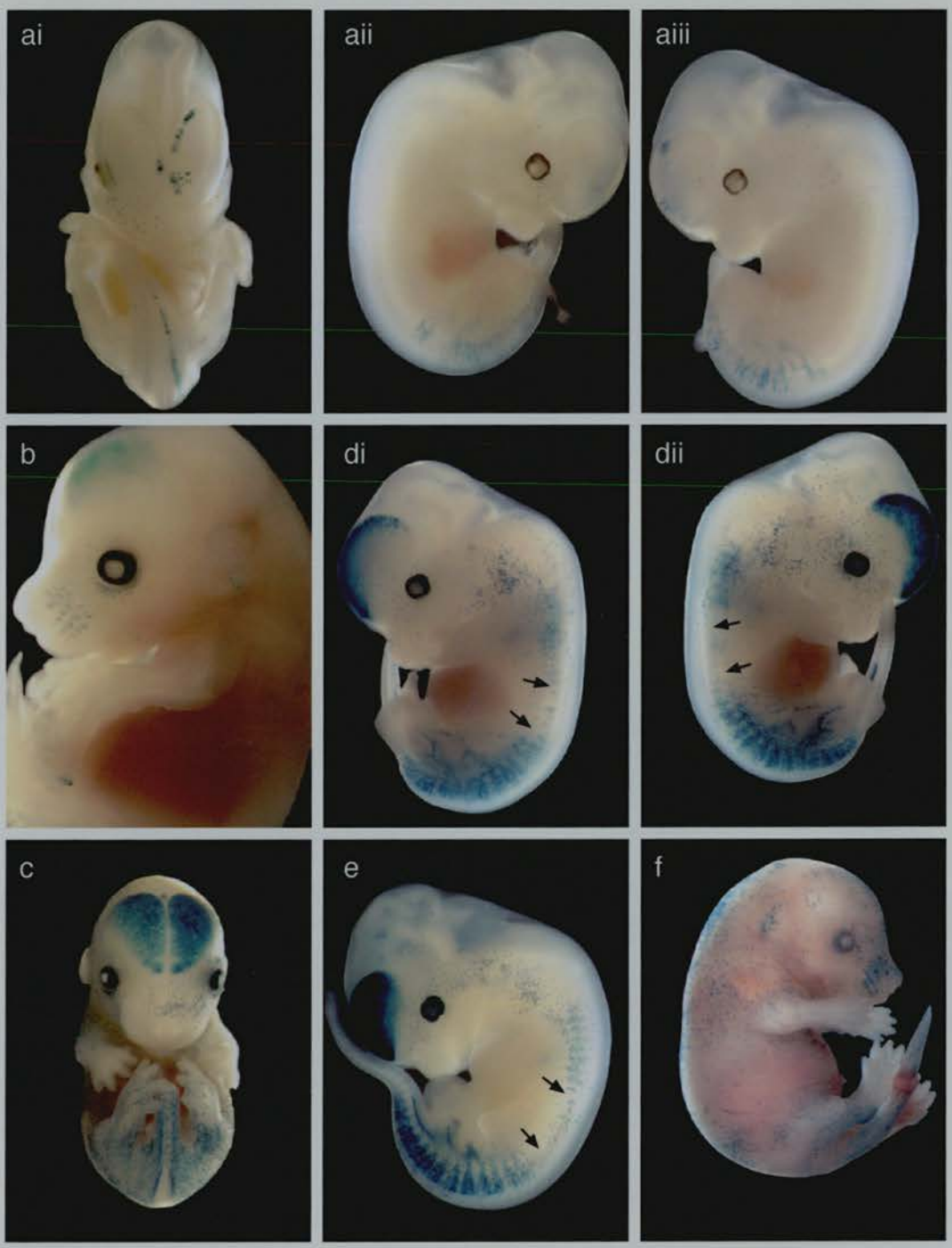

Plate 6. Examples of *Dct-LacZ* ↔ non-transgenic chimaeric embryos.
a. i. Ventral view of low-grade E12.5 chimaera with labelled melanoblasts in the face and tail. ii. and iii. side views of the same embryo. b. Head and face of low-grade E15.5 chimaera showing labelled melanoblasts in the snout, pinna, and around the eye. c. High-grade E15.5 chimaera showing labelled melanoblasts across the ventral midline of the snout. d. i and ii Left and right sides of an E13.5 high-grade chimaera showing distinctive gaps lacking labelled melanoblasts between the limbs. e. High-grade E12.5 chimaera showing a dilution of labelled melanoblasts between the limbs. f. E16.5 high-grade chimaera showing discrete patches of labelled melanoblasts. Arrows indicate regions between the limb buds that lack melanoblasts in high grade chimaeras.

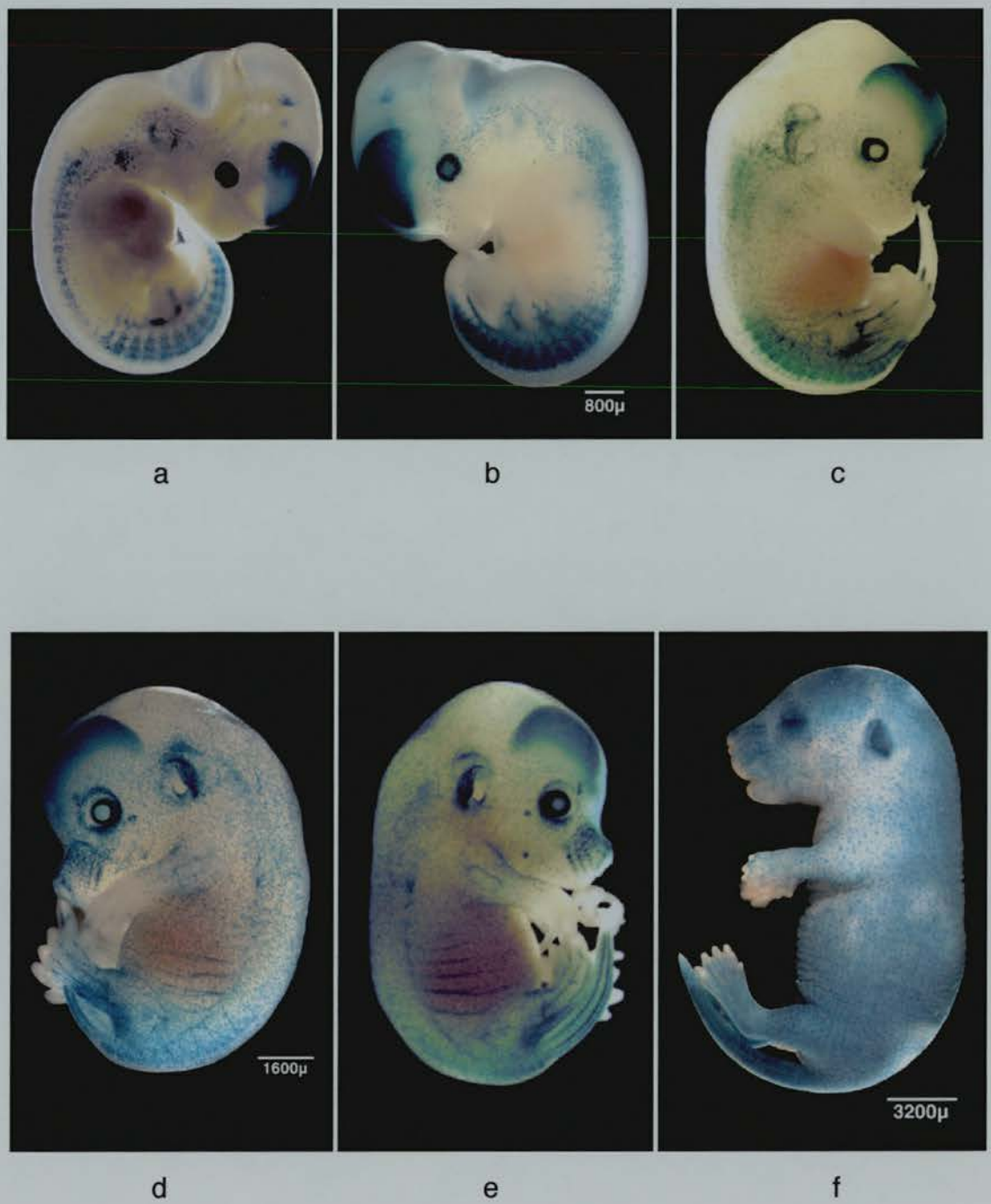

Plate 7. Labelled melanoblasts in A12 (*Dct-LacZ*) control embryos of different ages.

a. E11.5. b. E12.5. c. E13.5. d. E14.5. e. E15.5. f. E16.5.

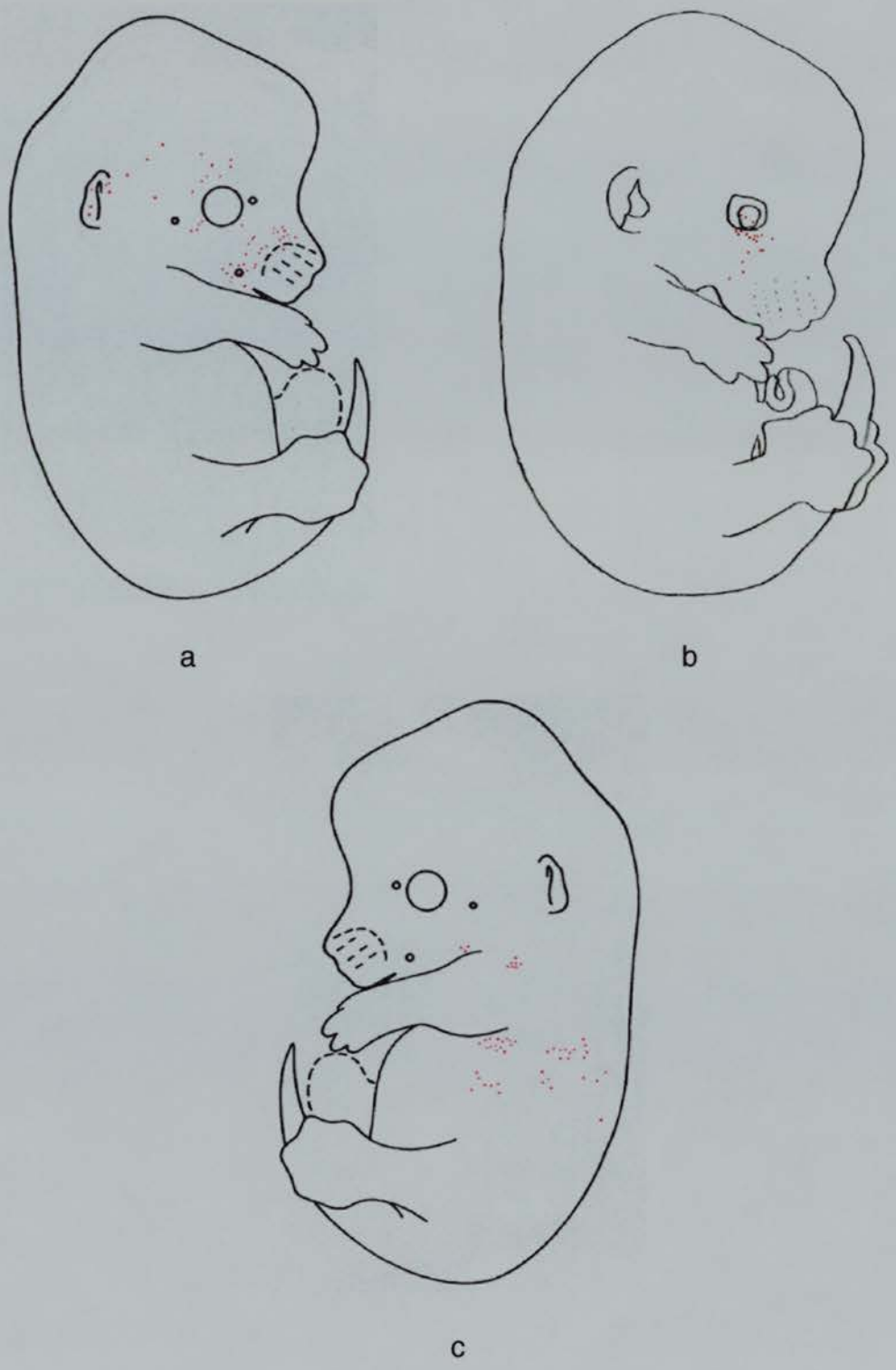

Plate 8. Examples of melanoblast clones generated in preliminary screening of *Dct-LaacZ* transgenic lines.

a. Large E13.5 face clone in line A195 (clone 2.1) (recorded in Table 25). b. Small E13.5 face clone in line A195 (clone 21.1) (recorded in Table 25). c. E13.5 clone at the forelimb level in line A202.

a

b

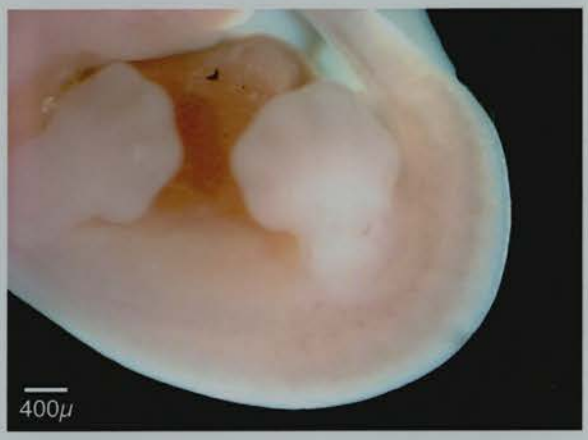

c

Plate 9. Wholemount *in situ* hybridisation in A12 and A195 embryos.
a. *LacZ* expression in A12 at E12.5. b. *LacZ* expression in A195 at E12.5. c. *Dct* expression in A195 at E12.5.

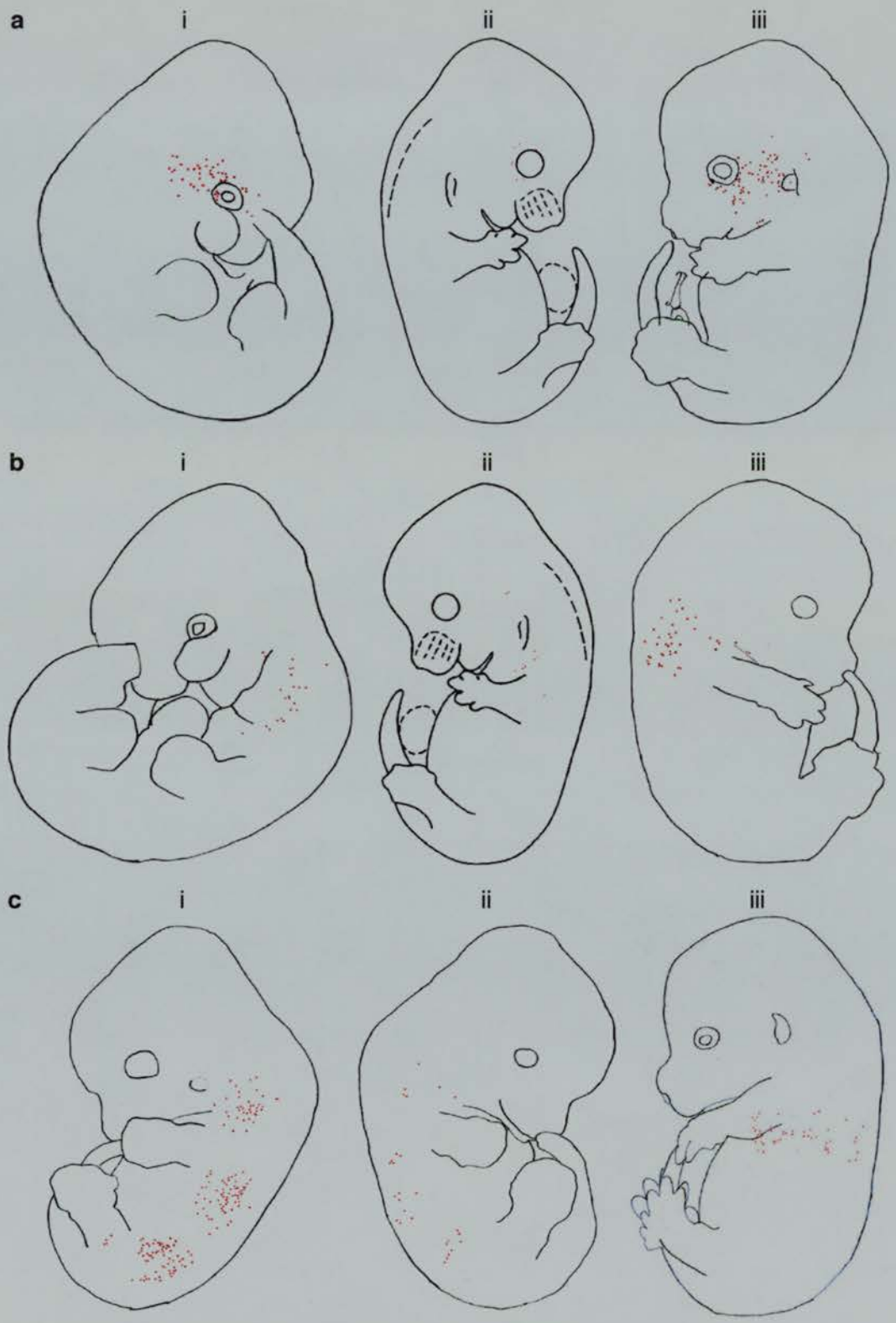

Plate 10. Examples of melanoblast clones in A195 mosaic embryos.
a. Face clones i. E11.5 (clone 35.2), ii. E13.0 (clone 204.3), iii. E13.5 (clone 98-100.2). b. Clones in the cervical region i. E11.5 (clone 31.1), ii. E12.5 (clone 191.2), iii. E13.5 (clone 93-98.3). c. Trunk clones i. and ii. E12.5 (left and right hand sides of clone 207-211.4), iii. E14.5 (clone 142-143.3). Clone numbers are recorded in the appendix (Table 23-Table 27).

Chapter 5

Clonal Analysis of Telencephalon Development

'For the real amazement, if you wish to be amazed, is this process. You start out as a single cell derived from the coupling of a sperm and an egg; this divides in two, then four, then eight, and so on, and at a certain stage, there emerges a single cell which has as all its progeny the human brain. The mere existence of such a cell should be one of the great astonishments of the earth. People ought to be walking around all day, all through their waking hours calling to each other in endless wonderment, talking of nothing except that cell.'

Lewis Thomas (1979).[6]

[6] Quoted from Gilbert, S. (1994). **Developmental Biology** (fourth edition). Sinauer Associates Inc. Massachusetts, U.S.A.

Introduction

The adult cerebral cortex is a highly organised, complex structure with an enormous degree of cellular diversity. There are many different types of neurones and glial cells, each with characteristic functional and morphological properties. There are approximately 15 billion cells in the adult human brain, and most of them are derived from an apparently homogeneous germinal layer of cells (141). Understanding how such extraordinary diversity can be generated from these cells is a formidable task. One of the most interesting questions driving developmental neurobiology research asks how progenitor cells behave during neurogenesis. Are there different progenitor cells for the multitude of different cell types, or do diverse cell types share common progenitors (142;143)? What cell division patterns do progenitors exhibit and are these controlled mainly by environmental cues or by an intrinsic genetic programme (142), and how are the progeny of these cells distributed during cortical development? At which point during cortical development do the different functional domains of the adult acquire their identity and what role do progenitor cells play in assigning this identity?

Overview of cortical development

Following neural tube closure, the anterior neural tube becomes morphologically divided in a rostral to caudal manner, producing the telencephalon, the diencephalon, the metencephalon, and the myelencephalon. These regions give rise to further subdivisions which acquire functional identity as neurogenesis proceeds and nuclei emerge (144). The cerebral hemispheres of the adult are derived from the telencephalon, the anterior portion of the prosencephalon (forebrain). The telencephalon is subdivided into regions that surround the lateral ventricles: the medial hippocampus, the dorsal neocortex, the lateral pyriform cortex, and the ventral basal ganglia and septum (144). Early in embryogenesis, the telencephalic vesicles balloon out, generating a thin cortical wall with a large surface area (145). Large numbers of cells can be generated due to this extensive surface area and because neurogenesis occurs over an extended period of time in mammals (146).

Most cells of the telencephalon are derived from germinal cells in the ventricular zone (VZ) which lines the lateral ventricles. Cells of the VZ are part of the pseudostratified neuroepithelium of the neural tube. They maintain attachments to both the lumenal and pial surfaces and their cell bodies move between these two surfaces in a manner that correlates with their position in the cell cycle. Nuclei of S phase cells are positioned near the basal

surface, and those of M phase are at the apical (ventricular) surface. This movement of a cell's nucleus according to its stage in the cell cycle is termed interkinetic migration.

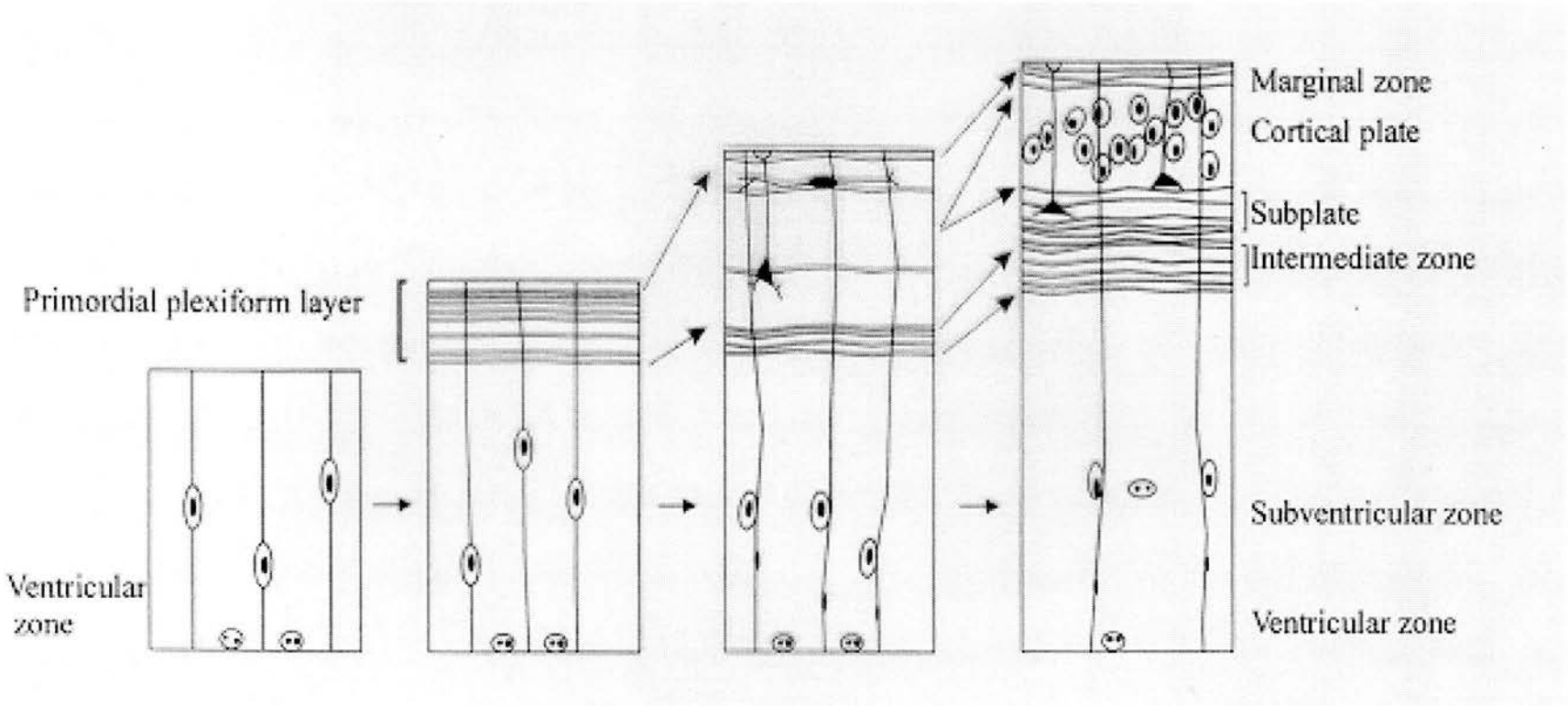

Figure 15. Generation of cortical laminae in the developing forebrain. Progenitor cells reside in the ventricular zone (VZ). Neurogenesis begins at around E12 and continues until about E16 in the mouse embryo. Postmitotic neurones leave the VZ and migrate into the developing cortical plate where they take up their position in the lamina appropriate to their birthdate.

Establishment of the cortical plate and lamination

From around E10, progenitor cells in the VZ undergo predominantly symmetric cell divisions (Figure 15); this expands the pool of progenitors. Later, a second proliferative layer forms immediately superficial to the VZ, the subventricular zone (SVZ). It is from this layer of cells that most glial cells are formed when neurogenesis begins to subside (146). From around E12, there is a gradual transition from symmetric to asymmetric cell division, and the first neurones are born. These postmitotic neurones leave the VZ, migrate radially towards the pial surface along the processes of specialised radial glial cells, and establish the preplate or primordial plexiform layer (Figure 15). This layer subsequently splits into two layers, the deep subplate (layer VII) and the superficial marginal zone (layer I), by the migration of later-born neurones which generate the cortical plate (146-148).

Neurogenesis proceeds until around E16 in the mouse (149). Postmitotic neurones take up their positions in the cortical plate in an inside-out fashion such that the youngest, most recently arriving neurones migrate past older neurones. In this manner, the mature cortical plate consists of layers or laminae, with layer VI being the deepest layer and layer II being the most superficial and containing the most recently born neurones (141;146;147). Although the birthday of a neurone generally predicts its laminar fate, there is a large degree of plasticity early in cortical development, and later-born neurones can occupy deeper layers in the absence of earlier-born cells (149). The arrangement of neurones in each lamina generates a characteristic morphology, allowing each layer to be distinguished histologically. Neurones also establish connections typical of their lamina. For example, neurones in superficial cortical layers tend to make connections with neurones in other cortical regions, while those in deeper layers tend to make connections with subcortical targets (145).

That postmitotic cells migrate radially has been known for some time. Rakic (150) proposed that radial migration was the primary mechanism by which any positional information stored in the VZ could be copied to the cortical plate. By this 'radial unit hypothesis', a protomap of the mature cortex would be established, and the identity of functional modalities in different horizontal regions would be carried in the map. A consequence of this would be that the VZ is actually a mosaic of germinal cells. Any cellular mixing within the VZ or in higher layers would disrupt the fidelity of the map. As cells migrate out of the VZ to the lamina appropriate for their birthdays, they would carry an identity prescribed by the position of their progenitor. Some cell lineage studies do not support the protomap idea very well; instead, they indicate significant tangential cell dispersion occurs both in the

proliferative and non-proliferative layers. However, radial migration is still considered a major method of cell dispersion, as suggested by some retroviral work (151), original cell tracing experiments, and by the overall radial orientation of many cells in the cortex (148;152). Recent work (153) shows that radial glial cells give rise to postmitotic neurones in the VZ and that these cells migrate radially along the processes of their radial glial siblings.

Horizontal organisation in the cerebral cortex

In addition to this vertical organisation, the horizontal plane of the telencephalon is organised into distinct functional regions, for example, the visual, motor, auditory, somatosensory cortex, and cortical regions assigned to the different aspects of language (141;144;146). The overall structure of laminae is preserved across different functional domains, but there are characteristic differences, in for example, the relative thicknesses of the layers in different functional regions (154). Broadman used these variations in cytoarchitecture to map the often sharp boundaries between different functional domains of the human cortex. These domains are reproducibly positioned, and for many regions, they have equivalent locations in other mammals. These domains can be further subdivided into radially oriented arrays with more specialised functions (146).

How functional regions acquire their identity and position is a major question in developmental neurobiology. It has been postulated that regions may be determined by differential expression of genes that may act as morphogens to set up boundaries. However, there are no mouse mutants that exhibit specific defects in cortical arealisation. Despite this, there is evidence that a genetic component influences the reproducible mapping of modalities onto the telencephalon from studies in the primary visual cortex. Sensory cortical areas receive input from particular thalamic nuclei (the lateral genicualte nucleus, in the case of the visual cortex). These connections, which are among the first to be established during cortical development, were also proposed to be the source of positional information for different sensory cortical areas. However, in the absence of a thalamus, the visual cortex is specified in the correct location relative to other cortical areas. In the opposite experiment, if the the primary visual cortex is removed, a visual area will still be specified, demonstrating the plasticity of the developing telencephalon. Cortical grafting experiments have produced conflicting results, but they generally suggest that cortical areas are specified by planar signals intrinsic to the neuroepithelium, rather than by signals from the adjacent thalamus. *In vitro* culture experiments using young cortical explants from different cortical regions

suggest that isolated cortical pieces subsequently express markers appropriate for their site of origin (154).

Several groups of genes are differentially expressed in the telencephalon, including cadherins, ephrins, ephrin receptors, and several members of the *Wnt* family of signalling molecules. The homeobox-containing genes, *Emx1* and *Emx2* are specifically expressed in the dorsal telencephalon. *Emx2* is expressed in a graded fashion along the length of the telencephalon, with the strongest expression posteriorly. Mice lacking EMX2 function have a reduced visual cortex (which is located posteriorly), but other markers show normal expression. *Pax6* is expressed in a complementary graded fashion, with the strongest expression anteriorly. *Pax6* mutant mice have a reduced anterior cortex, but again, the expression of other markers is unaffected. It has been suggested that, rather than specifying functional domains, these and other genes act to proportion cortical areas (154). It is not clear what types of positional information progenitor cells in the VZ carry, when they acquire it, and how it may be subsequently translated into functional domains.

Cell lineage analyses in the developing cortex

Cell lineage analyses have been used to study progenitor cell behaviour, with different approaches providing different types of information. Chimaera studies illustrated general patterns of cell distribution across many lineages and clones (148;152;155), while lineage markers applied at various times during neurogenesis identified distribution patterns of individual clones and their mature cellular phenotypes (151;156-160), and *in vivo* progenitor cell labelling using vital dyes (153;161) recorded the movement of live cells.

Cell lineage using chimaeric and mosaic embryos

Early aggregation chimaera studies suggested there was a large degree of cell mixing between different cell lineages in the developing cortex. More recent chimaera work demonstrated a lack of large homogeneous blocks of clonally related cells in mid-gestation embryos, also suggesting there is cell mixing among progenitors in the VZ (148).

By studying β-galactosidase expression patterns in mosaic females carrying an X-linked *LacZ* reporter gene, Tan and Breen (162) visualised the extent of non-radial cell dispersion. At E12.5, after X-inactivation is complete, stained cortical preparations consisted of alternating radially arrayed blue and white stripes of varying width emanating from the ventricular surface into the preplate, reflecting the radial migration of postmitotic cells. The

authors argued this arrangement indicated daughters of progenitor cells generally remain together as a clone. In adults, however, while radial stripes were widened into bands through clonal expansion, they were blurred by tangentially dispersed cells. Within a band, approximately two thirds of the cells were the one colour, while one third were the other colour. Cells of the minority colour were evenly distributed throughout the band rather than being limited to its edges. Importantly, bands did not correspond to functional domains in the adult cortex (152). Blurred bands indicated that, in addition to the predominantly radial deployment of cells, there is a significant amount of tangential dispersion, and this was proposed to take place in the VZ. The authors proposed that radial migration establishes a scaffold which is embellished by later tangential dispersion.

Tan, et al (155) produced highly unbalanced chimaeras by injecting one to five ES cells carrying a *LacZ* marker into blastocyts. Cerebral hemispheres from four to eight week old animals had labelled radial columns, scattered cells, or both. Most columns contained 600-3000 cells, and only around 10% of cells in a column were labelled, suggesting a high degree of cell mingling during column formation. Most neurones in radial columns were pyramidal (excitatory, glutamergic) in phenotype, while those in scattered clones were mainly non-pyramidal (inhibitory, GABAergic), but with a large minority (one third) of pyramidal neurones. These results suggest there are both restricted unipotent progenitors and multipotent progenitors that generate both pyramidal and non-pyramidal neurones.

Labelling individual progenitor cells during neurogenesis

The advantage of using aggregation chimaeras and X-inactivation mosaics is that a global picture of clonal activity is generated by recording multiple lineages. Ofcourse, the progress of individual lineages is necessarily lost. One way of marking individual progenitor cells at varying stages of neurogenesis has been to use replication-incompetent retroviruses carrying histological markers such as a transgene encoding β-galactosidase or alkaline phosphatase (AP) (157;158;163). These retroviruses are injected into the lateral ventricles of mid-gestation embryos where they have access to progenitor cells in the VZ. Retroviruses are estimated to take one to two cell cycles before they integrate into the genome of a dividing cell and then remain in one or other of the daughter cells (143;151). If they are diluted sufficiently such that only a few progenitor cells are labelled in any one hemisphere, the phenotypes and positions of clone members can be followed in the confidence that labelled cells are members of the same clone.

Many informative studies have been carried out using these types of retroviruses (151;156-160). By labelling and analysing clones at different stages, results can be combined to determine how progenitor dynamics change during neurogenesis. Early studies suggested there were separate progenitors for different cell types (143;158). Grove, *et al* (160) injected the BAG retrovirus (which carries the *LacZ* transgene) into lateral ventricles of E16 embryos and analysed the clones at P14. Nearly all clusters consisted of cells of a single phenotype (neurones, astrocytes, or undifferentiated white matter cells, considered to be oligodendrocyte precursors). Neuronal clusters contained one to four cells, while astrocyte clusters were larger. However, even at this late stage of labelling, a small minority of clusters did contain multiple cell types.

While retroviruses provide a retrospective picture of progenitor cell activity, direct cell labelling using the lipophilic dye, DiI, and time-lapse video fluorescence microscopy (161), illustrated the movements of live progenitor cells in the VZ. The authors showed that progenitor cells move within the VZ at rates of ten to 100μm per hour. Following cell division, labelled siblings moved apparently independently and exited the VZ at different times. While progenitors apparently moved freely within the dorsal telencephalon VZ, they did not cross the boundary believed to separate the dorsal and ventral telencephalon. This supported the suggestion that a physical boundary separates the dorsal and ventral telencephalon, preventing cell mixing between the two regions. The rates of cell movement and the apparently independent trajectories of movement of sibling cells indicates that clonally related progenitors could become widely dispersed in the VZ.

Symmetrical and asymmetrical cell divisions

Cai *et al* (151) generated retrovirally labelled clones in the mouse early, at E11, when neurogenesis is just beginning, and analysed clones mid-way through neurogenesis at E14. They generated an average of 18-19 clones per hemisphere. Most clones were clusters of around 50μm wide and isolated from neighbours by at least 300μm. Nearly half of the clones had cells in the VZ only, one third were outside the VZ (postmitotic), and the remaining clones had cells in both proliferative and postmitotic regions. In almost all cases, clonally related cells in the VZ were in close contact. The authors suggested this tight arrangement of cells in the VZ reflects cell cycle synchrony among clonally related progenitors. They proposed this synchrony explains why clustered clonal relatives in the mature cortex exhibit similar phenotypes. The authors suggest that the VZ is therefore a

mosaic of cells which could facilitate the transfer of any positional information in the VZ to the mature cortex, supporting the protomap hypothesis.

The pattern of symmetrical and asymmetrical divisions in the VZ is crucial for determining the numbers of progenitor cells generated at different stages of neurogenesis and the numbers of postmitotic neurones produced for each lamina. Mione *et al* (159) combined retroviral cell labelling with BrdU incorporation to assess the relationships between cell division patterns, progeny distribution, and cell fate. The retroviruses and BrdU were administered at E16 and resultant clones were analysed at P14. Pyramidal neurones were either early-born from asymmetrical divisions and radially arrayed, or late-born from symmetrical divisions and horizontally arrayed, while non-pyramidal cells were usually late-born from symmetric divisions. Most neurones of either phenotype were found in pairs or as single scattered cells. Most paired clusters contained only one cell type, but a small minority contained both a pyramidal and a non-pyramidal neurone, sometimes with similar BrdU levels, suggesting even terminal symmetric divisions could generate cells of different fate.

Neurogenesis precedes gliogenesis and many retrovirally-labelled clusters contained both neurones and glia, suggesting they share common progenitors. By using time-lapse video microscopy to record the growth of isolated progenitor cells, Qian *et al*, (164) recently showed progenitors do generate both neurones and then glia. Furthermore, the timing of neuro- and gliogenesis *in vitro* reflected the normal *in vivo* situation, suggesting temporal changes in cell division patterns are inherent to progenitor cells.

A model for progenitor cell activity during cortical development

The main difficulty with retroviral work was that it was impossible to be certain individual clones were being identified accurately. Even in low retroviral titres, many labelling events took place in any one hemisphere (151;156;157;159;160) and assumptions regarding progenitor activity were necessary to identify clones. Retroviral libraries were developed which contained a mixture of viruses carrying unique DNA sequences, or tags (163). Following infection, clone members were identified directly by PCR of individual cells dissected from cortical preparations. If the number of unique sequences far outweighed the number of infection events, it would be highly unlikely that two progenitor cells would be infected independently by viruses carrying the same tag. In these heroic and thorough

studies, PCR success rates were low (between 40 and 50% of PCRs were successful), leading to a systematic underestimation of clone sizes.

Walsh and Cepko (156) used a retroviral library to study labelled clones at different stages after labelling in the rat. Clones were labelled at E14-E15 and analysed after three, six, or ten days. At E18, clonally related cells (one to five cells) were closely spaced in radially arrayed columns up to 200μm tall and less than 120μm wide. At E20, nearly half of the clones were dispersed over 500μm; some were dispersed over as much as half of the rostrocaudal length of the forebrain. Widely dispersed cells were found in the VZ and SVZ, suggesting cell dispersion can happen before cells leave the proliferative layers. By P3, more than half of the labelled clones were widely dispersed over as much as 6mm. This study suggested that clonally related cells could be dispersed over increasing distances as cortical development proceeds.

Later, Reid, *et al*, used an AP retroviral library to correlate clone distribution with cellular phenotype (157). Cell processes can be visualised with AP staining, allowing cellular phenotypes to be determined. Clones were labelled by injection at E14, E15, or E17, and analysed at P15. Labelled cells were found in laminae indicative of their time of labelling, such that progeny of cells labelled later in development were found in progressively more superficial laminae. Labelled cells were generally found in localised clusters, or in widespread clones consisting of multiple clusters. In widespread clones, clusters were positioned at regular intervals, usually in the rostrocaudal direction. Later injections labelled progressively higher proportions of non-pyramidal neurones. (Non-pyramidal and pyramidal neurones are generated simultaneously for each lamina; however, superficial laminae contain more non-pyramidal neurones).

After labelling at E15, nearly half of the clones were widespread (distributed over at least 1.5mm). The remaining clones were single-celled or clustered clones. Cells within a cluster had similar morphologies, regardless of whether they accounted for an entire clone or were part of a larger, widespread one. Widespread clones were distributed over different regions of the telencephalon, and most comprised clusters of multiple cell types. However, following E17.5 injections, only 12.5% of clones were widespread and they contained fewer clusters than those labelled at E15, with fewer neurones in each cluster. Only 29% of labelled neurones were found in widespread clones labelled at E17.5 compared to 73% labelled at E15.

Reid *et al* proposed a model (Figure 16) (157;165) to explain both their own data and data from previous retroviral experiments. They suggested that the periodicity they observed could be explained by a migrating pluripotent progenitor in the VZ which would undergo periodic asymmteric cell divisions, generating another migratory pluripotent progenitor and a non-migratory progenitor. This non-migratory daughter would divide further, producing cells that undergo radial migration and establish clusters in the cortical plate with positions and fates appropriate to their birthdays. The migrating cell could account for the periodic spacing in this study and the tangential dispersion in previous cell lineage analyses. It would also explain why progressively later injections in this and previous studies label few widespread clones and mainly label isolated clusters of usually one cellular phenotype. Late injections would be most likely to label the terminal branches of progenitor family trees.

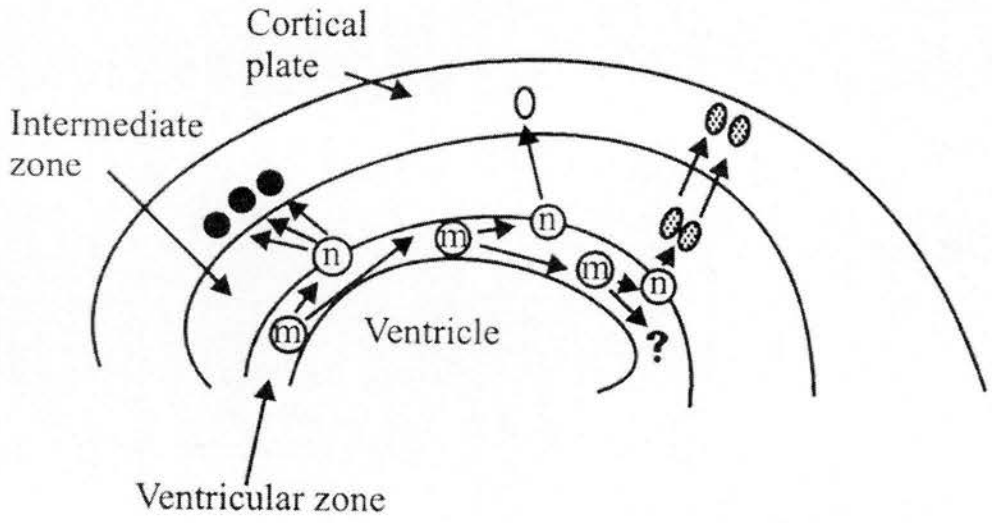

Figure 16. Model of progenitor cell activity in the VZ during neurogenesis. This model was proposed by Reid *et al* (157). A migrating neurogenic stem cell is proposed to move through the ventricular zone, undergoing periodic asymmetric divisions, generating another migratory stem cell (m) and a non-migratory (n) progenitor. The non-migratory daughter divides further generating radial columns in the cortical plate.

Cell death during cortical development

Death is an important cell fate in many developmental processes and its role during cortical development has been particularly difficult to assess. It was believed that cell death mainly affected postmitotic neurones in the cortical plate as they established connections, therefore, most reports detailing the extent of cell death in the cortex concentrated on death of postmitotic cells peri- or postnatally (166;167). While some cell lineage studies acknowledged cell death may be a factor affecting experimental results (151;156;159), few attempted to determine how cell death might affect clone sizes and the relationship between surviving cells (145;159;168). Those studies that did assess the degree of cell death during corticogenesis in the embryo sometimes produced conflicting results (169-172).

Some estimates of cell death in the telencephalon have been very low. Spreafico *et al* (171) assessed the levels of apoptosis between E16 and adulthood by counting the numbers of terminal dUTP nick end labelling (TUNEL) positive cells in sections. They concluded that apoptosis levels peak during the first postnatal week and that there is virtually no apoptosis in the telencephalon during embryonic and adult life.

The TUNEL method involves using terminal deoxynucleotidal-transferase (TdT) to label double stranded DNA breaks with DIG-labelled dUTP. Cell death is difficult to measure because dying cells may be cleared by macrophages quickly, before they are detected (172). In addition, it is not clear what proportion of time apoptotic cells exhibit the detectable phenotype (172). If cells are only detectable for a small fraction of the time taken from being specified to die to actually undergoing apoptosis, and if they are subsequently cleared quickly, low TUNEL positive levels may actually indicate high levels of apoptosis.

Thomaidou *et al* (172), also counted the numbers of TUNEL positive cells in cortical sections at different stages of development. They reported that at E14, only 1:200 cells in the VZ and SVZ stained and this increased to 1:110 at E16 and peaked in newborn rats, where around 3% cells stained. By combining TUNEL staining with BrdU labelling, they showed that most apoptotic cells were part of the cycling population. They used TUNEL, BrdU, and [^{3}H]-thymidine labelling to assess the cell cycle time and the length of time that apoptosis is visible (the cell clearance time). Accounting for these estimates, they suggested that at E14, around 2% of cells in the SVZ and VZ are dying by apoptosis, with an increase to around 9% at E16 and a maximum of one in two cells dying in the newborn SVZ.

Blashke *et al* used a highly sensitive method of detecting double-stranded DNA breaks, the hallmark of cells fated to undergo programmed cell death, to suggest that the extent of apoptosis in the telencephalon is extremely high (169). The method used, *In Situ* End Labelling (ISEL+), is approximately ten times more sensitive than other *in situ* end labelling techniques, but still uses DIG-labelled dUTP and TdT. After confirming that the technique is specific to apoptotic cells, they showed apoptosis affects cells in both the proliferative (VZ and SVZ) and postmitotic compartments. While there is little cell death prior to E12 (around 1% at E10), between E12 and E18, cell death levels vary between 25 and 70% of cells, with an average of around 50%, and a peak at E14 of 70%. Similar percentages of dying cells were found in the cortical plate and VZ, however, since there are more cells in the VZ during these stages, there are higher numbers of labelled cells in the VZ compared to the cortical plate. Cell death levels begin to decline towards the end of neurogenesis. In a subsequent study, these authors also demonstrated that this phenomenon is widespread in the CNS (170).

Previous studies may need to be re-interpretred in light of these findings. For example, a major consequence of the Blashke results is that labelled cells in other studies that appeared to be siblings are actually 'cousins' whose lineage relationship is unclear. In these cases, closely positioned clonally related cells, which may have a different phenotype (e.g., pyramidal and non-pyramidal neurones) would be interpreted to be sibling cells resulting from an asymmetric terminal division. This would indicate that progenitor cells remain bipotential until late stages. However, if cell death levels are high, these cells may represent the only surviving members of a larger clone, and their lineages may have, in fact, segregated several cell divisions back. Therefore, these cells would not have resulted from an asymmetric terminal division. Cell death must be accounted for if the activities of progenitor cells are to be understood.

In this chapter, *Dct-LaacZ* transgenic animals were used to study labelled telencephalon clones in mosaic embryos throughout the early stages of neurogenesis. The overall appearance of clones suggests that clones labelled prior to the onset of or early in neurogenesis are often widely distributed across multiple functional regions within the telencephalon. Serial sections suggest labelled radial columns exhibit a periodic spacing, while 3-dimensional reconstructions of clones permit visualisation of the migratory pathway of progenitor cells in the VZ. In addition, changes in the frequency of clone labelling

throughout these early stages of neurogenesis demonstrate there is indeed a dramatic phase of cell death within the proliferative zones.

Results

Dct-LaacZ *is expressed in the VZ*

In order to determine the expression domain of the transgene, and therefore identify the population of cells in which a reversion event may be visualised, *in situ* hybridisation was done on cryostat sections of E13.5 and E14.5 A195 (*Dct-LaacZ*) and A12 (*Dct-LacZ*) embryos using riboprobes for both endogenous *Dct* and *LacZ*, as described in Chapter 2. The results are presented at the end of this chapter in Plate . They suggest that the transgene is expressed at high levels in the VZ, and this expression does not change between E13.5 and E14.5. Therefore, clones labelled at E13.5 can be compared directly with those labelled at E14.5.

General appearance of labelled telencephalon clones in Dct-LaacZ/LacZ mosaic embryos

The production of *Dct-LaacZ* transgenic animals is described in Chapter 4. Many clones found during the preliminary analysis of the different transgenic lines were generated in the telencephalon. A sample of these clones is presented in Plate . Line A195 produced many telencephalon clones. From the surface of wholemount Xgal stained embryos, clones consisted of visually striking labelled columns projecting from the ventricular zone out towards the surface of the telencephalon (see below). Superficially, columns appeared to be regularly spaced.

Embryos were harvested from E10.5 to E14.5, as described in Chapter 4. Preliminary observations of clones labelled in line A195 suggested labelled telencephalon clones were seen with varying frequency, depending on the embryonic age. To test this, a large scale timed mating programme was set up to determine the clone labelling frequency (CLF) at different stages of development. Since observed recombination events were rare, a large number of embryos were harvested to ensure differences in observed frequencies were significant. This also had the advantage that many more clones were generated in both the melanoblast (Chapter 4) and telencephalon lineages.

Approximately 1680 transgenic embryos aged between E10.5 and E14.5 were screened by Xgal staining and 160 labelled clones in the telencephalon were recorded. A summary list of all *Dct-LaacZ* embryos harvested and labelled clones recorded is presented in the appendix

(Table 24-Table 29). Large clones contained widespread columns positioned throughout the telencephalon and they were assumed to result from early reversion events (Plate 13, a., b.). Small clones, containing five or fewer columns, made up over 60% of all reversions (Plate 13, c.). Clones consisting of even a single column could be visualised easily (Plate 13, c. ii.). Columns in small clones could be adjacent (Plate 13, c. iii.), or widely dispersed (Plate 13, c. i.). Such widely dispersed clones may be the result of extensive cell death pruning a larger, contiguous clone (see below).

Multiple independent reversion events (double-sided clones)

While the CLF is very low, and less than one in ten transgenic embryos (in all age groups combined) had a labelled clone, it was possible to see multiple reversion events in the same embryo. Labelled clones were sometimes found in each hemisphere (see Table 24-Table 29, and Table 31); these were considered to result from independent reversion events, and therefore, they were counted separately in the analyses. In the same way, it is possible that a small proportion of single-hemisphere clones were produced by two or more reversion events. Since there was no way to identify these, all single-hemisphere clones were counted as a single clone.

Although cases in which labelled clones were identified in both hemispheres were counted as resulting from independent reversion events, it was subsequently discovered that this could not be the case. Double-sided telencephalon clones were observed at a frequency much higher than that predicted by the occurrence of two independent reversion events. To test this formally, estimates of the numbers of double-sided telencephalon clones predicted to occur (assuming clones on the left and right hand sides occur independently and with equal probability) at different stages of development were tabulated, then compared with the observed numbers of single and double-sided clones (Table 21). The results indicate that double-sided labelled telencephalon do, in fact, occur much more frequently than would be expected if they were independent labelling events. This suggests that most of the double-sided telencephalon clones actually comprise a single clone.

Age	N_E	N_0	N_1	N_2	X_e	N_{2e}	N_2/N_{2e}
E10.5	480	478	0	2	0.004	0.008	240.0
E11.5	528	519	7	2	0.017	0.077	26.1
E12.5	547	520	23	4	0.049	0.666	6.0
E13.5	620	563	43	14	0.092	2.620	5.3
E14.0	594	553	25	16	0.069	1.415	11.3
E14.5	604	580	16	8	0.040	0.476	16.8

Table 21. Observed and expected frequencies of double-sided telencephalon clones. N_E is the total number of embryos, N_0 is the number of embryos observed to have no labelled telencephalon clone, N_1 is the number observed to have one clone, and N_2 is the number observed to have two clones. X_e is an estimate of the probability of having one clone of the left hand side. $X_e = 1 - N_0 / N_E$. N_{2e} is the predicted number of double-sided clones.

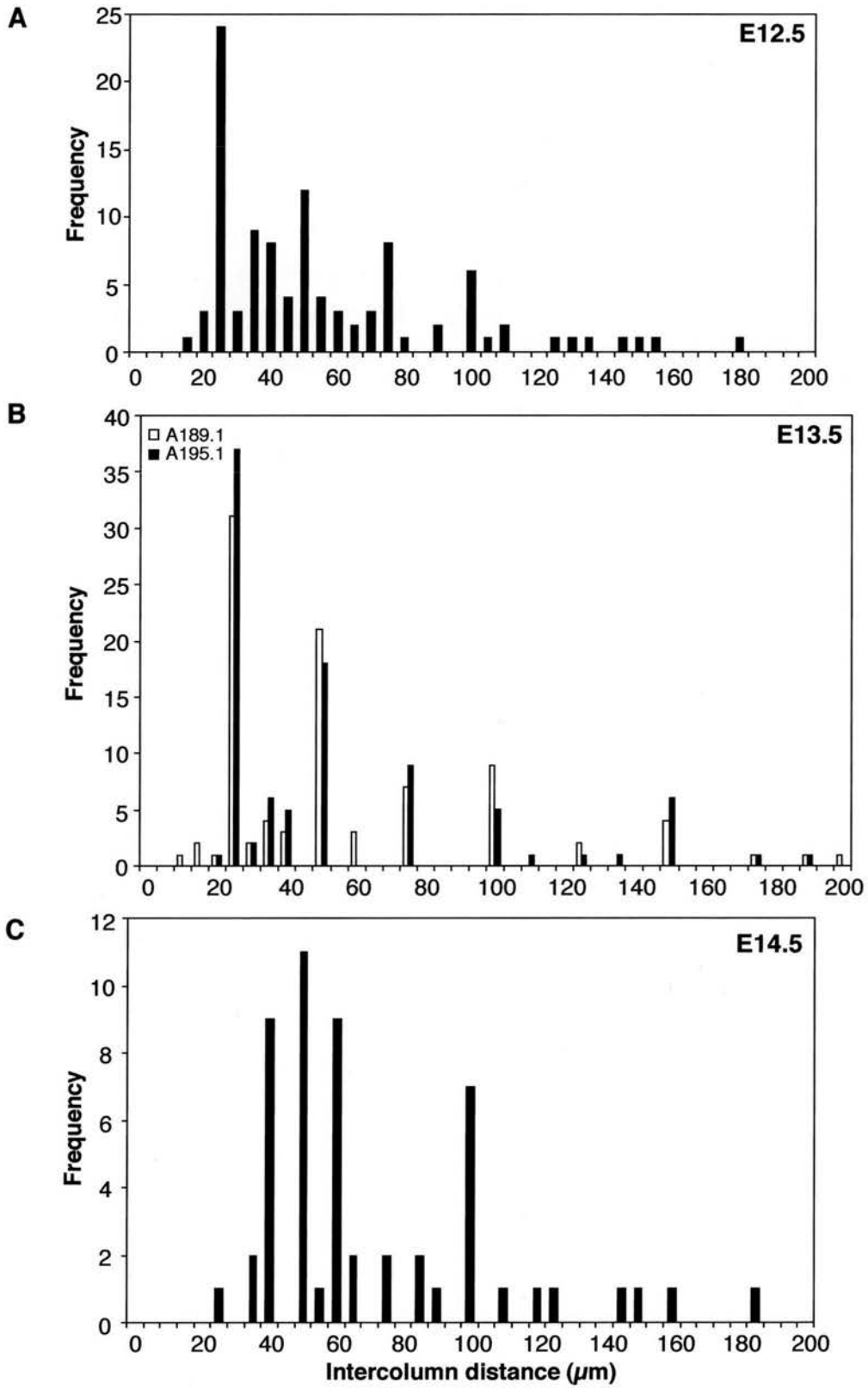

Figure 17. Labelled columns in *Dct-LaacZ* mosaic embryos are periodically spaced in the rostrocaudal axis. a. column spacing in E12.5 A195 clone 207-211.3 (Table 24). (See Plate 11, a.i.) b. column spacing in two E13.5 embryos (from lines A189.1 and A195.1). (See Plate 10, a. and c.) c. column spacing in E14.5 A195 clone 135-136.2 (Table 27). (See Plate 11, a. iii.).

Labelled columns are periodically spaced

Physical sections indicate periodicity in the rostrocaudal axis

Columns appeared to be regularly spaced in wholemount preparations. To test this, embryo heads were processed for paraffin sectioning and 10μm sagittal sections were prepared. The distance between columns at the ventricular surface was measured from photographs. Sections were taken from an E12.5 embryo, two E13.5 embryos, and an E14.5 embryo. Examples of sections from the two E13.5 embryos are presented in Plate . Sections were cut sagittally; therefore, column spacing was measured in the rostrocaudal axis only. Columns in E13.5 embryos showed strong periodicity in the rostrocaudal axis (Figure 17, b.) In E12.5 and E14.5 embryos, most columns did show periodic spacing, but an increased number of intercolumn distances was not consistent with a periodic spacing (Figure 17, a., c.). The average spacing between columns increased between E13.5 and E14.5 from multiples of around 25μm to multiples of around 50μm. This increase may reflect expansion of the telencephalon during this phase of development, however, no such increase was observed from E12.5 to E13.5.

Analysis of paraffin sections also permitted an estimation of the time that clones were labelled. The number of cells in each clone was estimated by directly counting cells from paraffin sections. Blue staining was only considered as a cell if it was intense; weakly stained cell processes, which may belong to a cell spanning two sections, were not counted in order to avoid counting a cell more than once. The number of 10μm sections indicated the mediolateral extent of the clone, and the rostrocaudal extent was determined by direct measurement from photographs. A crude estimate of the cell labelling age was based on a 12 hour cell cycle time with no cell death. Since there is extensive cell death in the telencephalon (see below), the estimated time of labelling represents the latest possible marking day because the clone size will have been underestimated. The results are presented in Table 22.

Embryo	Mediolateral distance	Rostrocaudal distance	Estimated total number of cells	Estimated number of generations	Latest possible marking day
A189.1	500μm	650μm	540	10	E8.5
A195.1	510μm	1.5mm	700	10+	E8.0-E8.5

Table 22. Estimated clone labelling ages for clones A189.1 and A195.1.

3-D reconstructions of clones using Optical Projection Tomography (OPT)

Physical sectioning of clones provided limited information about their overall shape. The periodic spacing of columns observed in paraffin sections should not necessarily be limited to the rostrocaudal axis. Ideally, it would be possible to view clones in three dimensions. Fortunately, it was possible to use a new technique developed by James Sharpe (MRC, Human Genetics Unit) which generates 3-D reconstructions of tissues, with the opportunity to cut virtual sections in multiple planes through the same embryo. This technique is called Optical Projection Tomography (OPT).

Several embryos were processed for OPT. Large widespread clones from different developmental stages were studied in detail. In some reconstructions, the arrangement of labelled columns resembled a wandering path (Plate). (A photograph of clone 268-272.1 is shown in Plate , aiv). In these cases, the pattern was interpreted to record the migratory history of neurogenic stem cells (157). This pattern was not always clear in large clones, but here, any path might be complicated and obscured by branches. Branches would occur if a migrating stem cell underwent a symmetric cell division, generating two new migratory stem cells that would subsequently migrate independently. In these large clones, which are predicted to have been labelled early in cortical development, a history of many early symmetric cell divisions would generate many branches. In clone 268-272.1, labelled cells clearly extended across a large region of the surface of the telencephalon, indicating that labelled cells, if they were to survive, would be positioned in different functional domains in the mature cortex. In clone 160-163.10, which was distributd over a smaller area, labelled cells appeared in a wide but discrete band across the dorsal surface of the lateral ventricle at the midline (Plate). (A wholemount photograph of this clone is shown in Plate , bi.). The

OPT technique was still in development during the analysis of these two clones, accounting for the difference in resolution between them.

These preliminary data will be studied in further detail in the future. For example, by taking virtual sections through these clones, it will be possible to assess periodicity in any given section, for comparison with results from paraffin sections. Currently, only some of the largest, and therefore most complex clones, have been reconstructed. When smaller clones, predicted to produce simpler patterns, are reconstructed, the activities of migratory cells may be more completely analysed. For example, it will be possible to ask whether particular patterns occur more frequently than others do. Further analysis of clones of all sizes will provide information about whether most clones are located in particular regions of the cortex, and excluded from others.

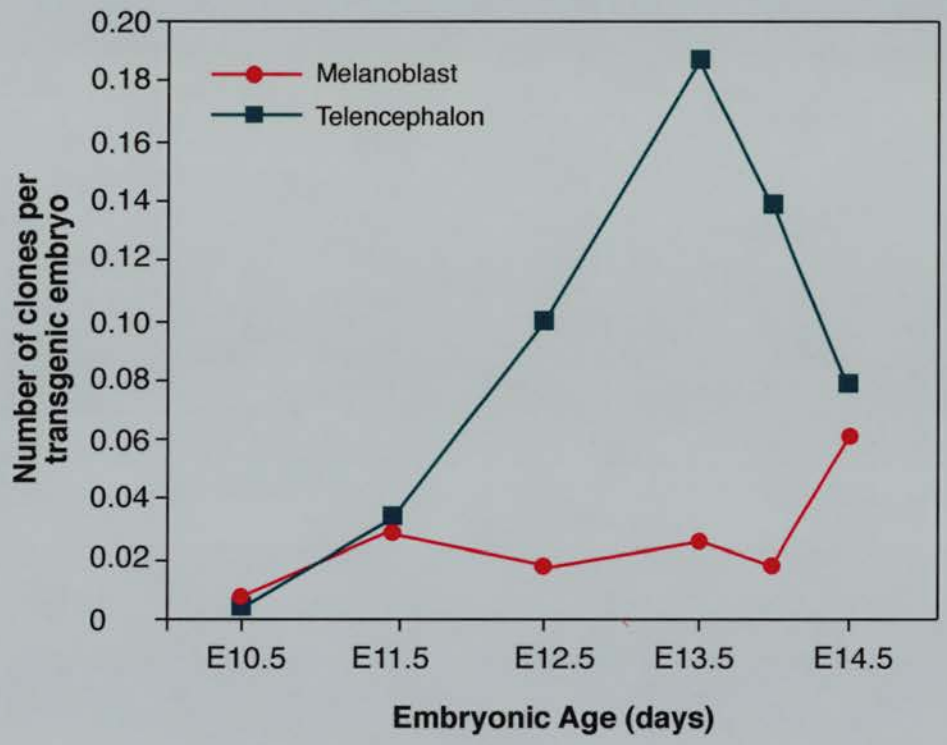

Figure 18. Changes in the clone labelling frequency during cortical development reflect patterns of expansion and decline of the progenitor population. The graph showing variations in the CLF in the melanoblast lineage (Chapter 4) is shown for comparison.

The clone labelling frequency (CLF) varies with embryonic age

In addition to studying how columns are arranged within a clone, it is possible to gain insights into the dynamics of clonally related populations of cells at different stages of development by studying variations in the observed frequency of cell labelling. As described in Chapter 4, the rate of homologous recombination per cell division should remain constant throughout an A195 animal's life. Therefore, any variations in clone labelling frequency during development reflect changes in cell proliferation and death patterns. At each cell division, there is a particular chance that a cell will experience a reversion event. Therefore, as the embryo grows and there are more cell divisions, reversion events should be observed with increasing frequency.

A large number of transgenic embryos were harvested from each age group (Table 24-Table 29) and the observed cell labelling frequency was calculated for each embryonic age (Table 30). There was a dramatic increase in the number of clones recorded in the telencephalon between E10.5 and E13.5, presumably reflecting the massive increase in the size of the progenitor population during this time (Figure 18). Also, the CLF in the telencephalon was much greater than the melanoblast lineage, highlighting the different growth rates of these two tissues. However, between E13.5 and E14.5, the fraction of embryos showing labelled telencephalon clones fell by nearly half. To monitor this drop more closely, embryos were harvested at the intermediate stage of E14.0 (Table 28, Figure 18). *In situ* hybridisation demonstrated the transgene continues to be expressed at high levels in the VZ (Plate), despite reduced clone labelling levels. Even if no new labelling events occurred after E13.5, all of the clones that were labelled prior to E13.5 would still be present, resulting in an unchanged labelling frequency. As there is a decrease, there must be loss of entire clones of cells between E13.5 and E14.5.

To determine whether the drop in clone labelling frequency at E14.0 was statistically significant, the gradients of lines between neighbouring age groups for both the telencephalon and melanoblast lineages were compared by testing the null hypothesis that the slope to the left of each data point was equal to that on the right. The only significant change in gradient occurred on either side of the E13.5 data point ($P= 0.0006$). (The E14.0 time point was ignored in the analysis.) Additionally, the null hypothesis that the difference between successive points was zero was tested against the one-sided alternative that it was negative. In this case, the only significant difference was between E13.5 and E14.5

(P=0.005). These statistical analyses were done by Andrew Carothers (MRC Human Genetics Unit)

If there were an episode of extensive cell death, one would predict existing clones would be trimmed to smaller clones while small clones would be lost altogether, simply by chance. (Cells in large clones that are most likely to contain young postmitotic neurones may not be affected by cell death.) To test this idea, the proportion of clones that are small was assessed from E10.5 to E14.5 (Table 23). This proportion increased from 0.111 at E10.5 to 0.854 at E14.0, reflecting the increase in cell labelling frequency as the progenitor pool expands and there are increasing opportunities for reversion. Over a 12-hour period between E14.0 and E14.5, the proportion of clones that are small indeed decreased markedly by over half from 0.854 to 0.417. A dramatic phase of extensive cell death would remove not only recently formed small clones, but it would also reduce the size of the progenitor pool, making new reversion events less common. That the proportion of small clones actually decreases indicates that the scale of cell death is indeed substantial.

Age	Total no. embryos harvested	Assumed no. TG embryos	Total no. brain clones	Total no. small clones*	Small clones as a proportion of total clones	Total no. single column clones	Single column clones as a proportion of total clones
E10.5	480	240	1	0	0	0	0
E11.5	528	264	9	1	0.111	1	0.111
E12.5	547	273	27	16	0.593	11	0.407
E13.5	620	310	58	36	0.621	26	0.448
E14.0	594	297	41	35	0.854	19	0.463
E14.5	604	302	24	10	0.417	7	0.292
Totals	3373	1686	160	98		64	

Table 23. Frequency of small telencephalon clones in A195 embryos. * Small clones are counted as those clones containing five or fewer columns.

Discussion

In this study, cells in the telencephalon lineage were labelled during the early stages of neurogenesis by reversion of *Dct-LaacZ* to functional wild type *Dct-LacZ* with low frequency and at random. Many labelled clones consisted of multiple radially oriented columns, projecting from the ventricular surface towards superficial layers of the developing cortex. Columns tended to be spaced periodically, and they could be widely distributed. The largest clones appeared to be distributed across multiple functional domains. Reconstructed clones recorded the history of progenitor cell movements in the VZ. Finally, the dramatic decline in the clone labelling frequency between E13.5 and E14.5 suggested a high incidence of cell death in the proliferating population at around E14.0 removes large numbers of proliferating cells.

Progenitor cells are distributed tangentially over large areas early in cortical development

The lineage analyses presented here agree well with the findings from other studies using both chimaeras and retrovirally-labelled clones. Chimaera work showed there is a high degree of cell mixing within the progenitor population (148;152;162). This was supported by retroviral analyses demonstrating multiple widespread clusters belong to the same clone (157), and by direct visualisation of progenitor cell movement within the VZ (161). The results presented here also indicate extensive tangential cell dispersion early in neurogenesis and within the VZ.

In early retroviral work, multiple labelled clones were usually distinguished by the distance separating labelled clusters. However, it is clear from this and previous studies (161;163) that cells disperse tangentially over large distances. Therefore, labelled clusters previously considered only distantly related (i.e., prior to the cell labelling event) and labelled by multiple independent infections may, in fact, share a more common progenitor (i.e., after the cell labelling event). In studies using retroviral libraries, which satisfied the need to identify distantly located cells sharing a recent progenitor and resulting from a single infection event (156;157;163), clone sizes were systematically underestimated due to technical difficulties with PCR. In this study, the low cell labelling frequencies suggest labelled cells do belong to one clone and result from a single reversion event. Even in cases where labelled cells are located in different hemispheres, they are most likely to be part of a single clone. In these

cases, clonally related cells were dispersed exceptionally widely, indicating they must have crossed the ventral midline during the formation of the neural plate.

By generating 3-D reconstructions of several labelled clones, it has been possible to visualise the position of clonally related columns. Reconstructions strongly suggest that the patterns represent the migratory history of progenitor cells within the VZ. In large, early labelled clones, the presence of multiple branches of the migratory route demonstrate that a migrating progenitor cell experiences symmetric divisions, producing multiple independently migrating progenitors, in addition to the asymmetric divisions proposed to generate periodically spaced columns (157). The periodicity reported previously occurred most frequently in the rostrocaudal axis. It is not immediately clear why this should be the case, although rostrocaudal periodicity in column spacing was also seen here in paraffin sections. The radial orientation of labelled columns indicates that, while there is extensive tangential dispersion, radial migration continues to be a fundamental mechanism of postmitotic cell dispersion.

A wave of cell death reduces the size of the progenitor population at E14.0

A rapid and dramatic reduction in the CLF was observed between E13.5 and E14.5. This suggested entire clones were being cleared. Even if no new reversion events occurred after E13.5, one would anticipate seeing all of the clones that were labelled prior to E13.5, resulting in an unchanged labelling frequency. The proportion of clones that were small (five columns or fewer) increased between E10.5 and E13.5, with the increase in clone labelling frequency. At E14.0, the proportion of clones that were small fell by more than half, with a concomitant reduction in the CLF. It has been assumed most small clones represent young, recently labelled clones, and between E10.5 and E13.5 they increase in frequency, presumably due to the growing progenitor population. Their dramatic reduction results from massive cell death, which not only clears recently labelled clones, but also affects the progenitor population generally, therefore reducing the opportunity for further reversion.

Other possible explanations for the reduction in labelling frequency are less satisfactory. Since the transgene continues to be expressed between E13.5 and E14.5, reversion events should remain visible. Given the remarkable potential for tangential migration, it is possible that revertant cells migrate out of the *Dct*-expressing region and into another brain region.

However, progenitor cells within the dorsal telecephalon are thought to be confined there, at least during these early stages of neurogenesis (161). In addition, there is no reason to suspect that β-galactosidase is toxic or confers reduced viability to cells.

Cell death at this stage is assumed to be non-specific, but this may not be the case. Most cells born early in corticogenesis contribute to the subplate and marginal zone, and they are fated to die; however, this death was observed early in postnatal development (173), rather than during neurogenesis. Cell phenotypes were not studied here, so it is unclear whether particular subsets of progenitors (if such subsets exist at this early stage) should be more sensitive to clearance than others. It is strongly temporally controlled, however, and stem cells in the VZ show temporal variation in the types of cells they generate, apparently inherently (164). Late-labelled clones may be more sensitive to death than early-labelled clones. Progenitor cells born at E14 are more likely to die than those born earlier (169), however it is not immediately clear how this might occur.

Nevertheless, cell death has important consequences for cortical development. While the phenotypes of clonally related cells have not determined here, other studies have shown that cells within a cluster share a similar phenotype. Although neuronal clusters usually comprised a single subtype, some contained, for example, a non-pyramidal interneurone and a pyramidal neurone, suggesting different subtypes can share a recent common progenitor. In such cases, cells were considered to be siblings and result from the terminal symmetrical division of a bipotential progenitor (159). If these cells survived to postnatal life in the presence of high cell death levels, it is likely that they were 'cousins' rather than siblings.

Cai *et al* reported that retrovirally-labelled clones were smaller than predicted by the number of cell cycles known to occur between labelling and analysis (E11 to E14). They proposed missing cells were removed, either by tangential dispersion or cell death, or by migration out of the VZ. Mione *et al* also reported 'missing' clonal relatives. In some clones, BrdU levels were too low to account for the small number of observed clone members and they identified clones in which more cells must have been generated.

While early cell lineage analyses largely ignored the potential effects or cell death, Blashke *et al* (169) actually predicted that retroviral cell labelling frequencies should fall following the wave of cell death they proposed to occur at around E14.0:

> If up to 70% of cells are dying during cortical neurogenesis, then it would be likely that a given lineage could be affected by PCD [programmed cell death], resulting in the elimination of entire clones or clone members.

Indeed, cell death, although maximal at around E14, is not limited to this stage. Blashke *et al* showed cell death levels are high and sustained throughout neurogenesis. According their findings, the cell death levels average 50% between E12 and E18, with a peak of almost 75% at E14. Reversion events used to label clones in this study occur concomitantly with this high level of background cell death. However, changes in cell labelling frequencies can only reflect changes in cell death levels; therefore, this constant high background death level would go unnoticed. At E12, reported cell death levels were just under 50% and they increased to over 70% at E14. This reported 50% increase in cell death is crudely consistent with the observed decrease in clone labelling frequency of 50% in *Dct-LaacZ* mosaic embryos presented here. While the probability of losing entire large clones is low, the probability increases as clone sizes become smaller. The most recently labelled clones are smaller and they are most likely to be lost by elevated levels of cell death. It would be highly informative to accurately model cell death levels in an effort predict the consequences that particular death levels would have on progenitor populations.

The *LaacZ* to *LacZ* reversion can occur at any time and in any cell during development. Therefore, clones were labelled at various undetermined times. Large clones were estimated to be labelled earlier than in previous retroviral lineage analyses. Smaller clones occurred with increasing frequency in older embryos up to E13.5. The progressive increase in small clone labelling does not represent the terminal lineage branches because neurogenesis is still in its early to middle stages. Rather, it reflects the increasing progenitor pool size (in an apparently elevated though steady cell death environment) and the accompanying increases in reversion opportunities this affords.

It is attractive to speculate that such extensive cell death has a role during development. Neurogenesis proceeds over an extended time during mammalian development, probably in order to generate such large numbers of cells. Some have suggested that the high cell death levels observed in proliferative regions act as some type of selection mechanism. Before cell death was discovered in the VZ, it was known to occur in the developing laminae where it was thought to be selective as cells form their connections. In this case, neurones are thought to be selected by limited survival factor availability. However, the mechanisms and any potential roles of cell death in the VZ are unknown.

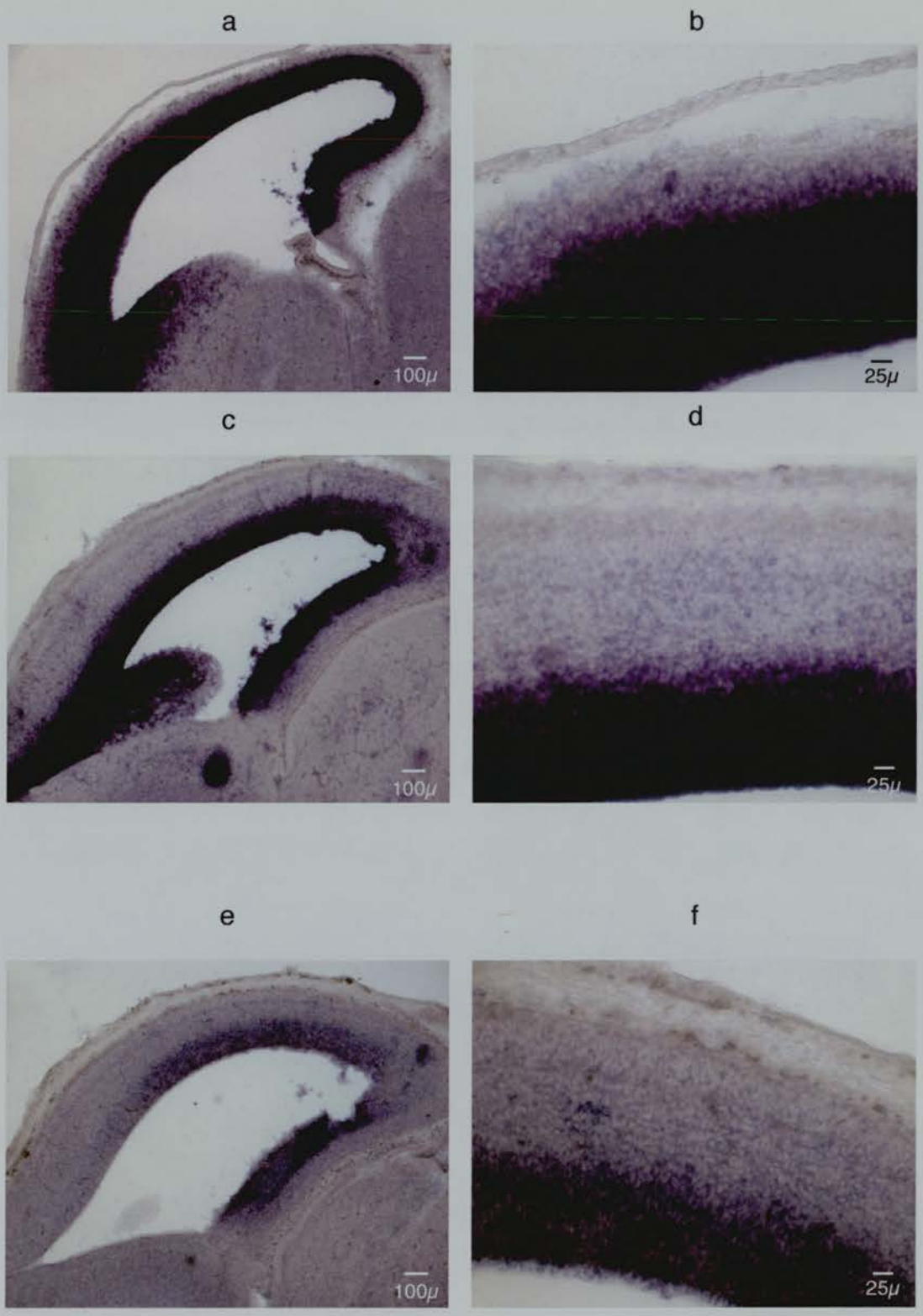

Plate 11. *LaacZ* RNA is expressed at high levels in the telencephalon of A195 embryos at E13.5 and E14.5. a., b. *In situ* hybridisation on E13.5 10mm cryostat sections using a *LacZ* riboprobe. c., d. at E14.5 with a *LacZ* riboprobe. e., f. at E14.5 using a *Dct* riboprobe.

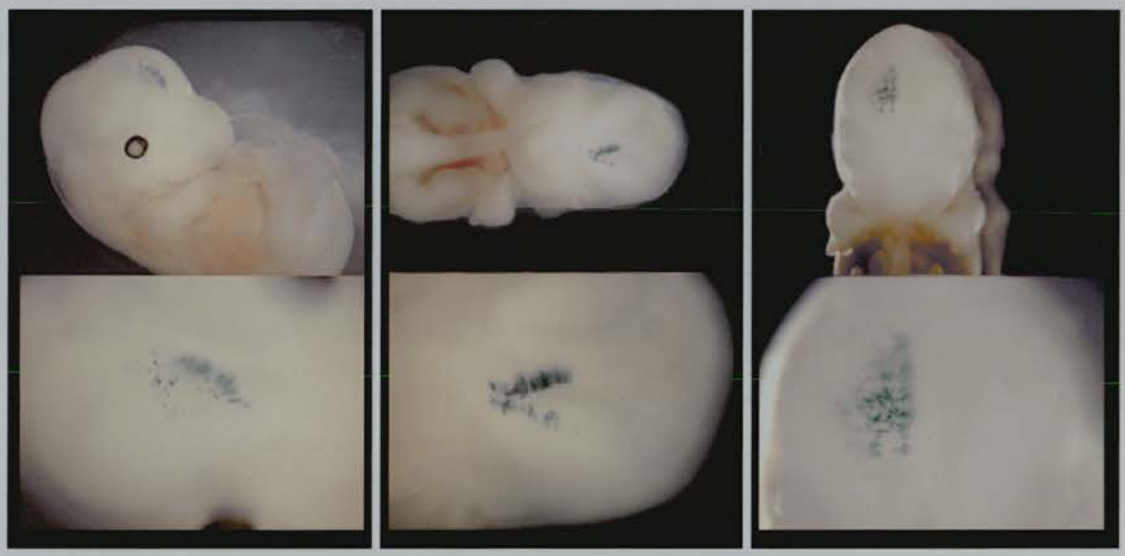

a b c

d

Plate 12. Examples of telencephalon clones labelled in *Dct-LaacZ* mosaic embryos during preliminary studies of the different transgenic lines.
a. E13.5 clone from line A189.1. b. E13.5 clone from line A195 (clone no. 3.1) (recorded in Table 25). c. E13.5 clone from line A195.1. d. E13.5 A12 (*Dct-LacZ*) control embryo.

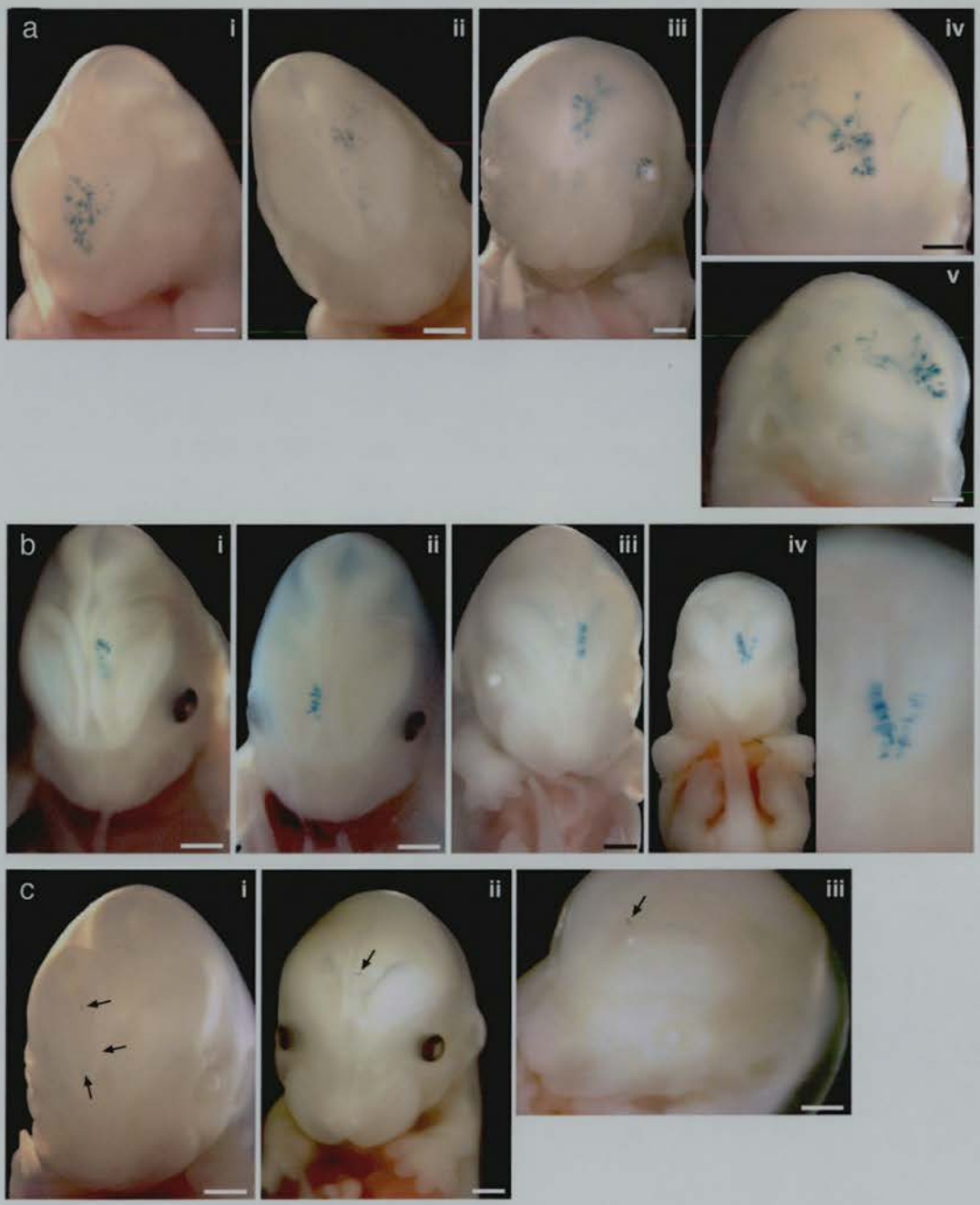

Plate 13. Examples of telencephalon clones labelled in A195 *Dct-LaacZ* mosaic embryos. a., Large clones: i. clone 207-211.3 (E12.5), ii. clone 64-67.2 (E13.5), iii. clone 135-136.2. (E14.0), iv. and v. two views of clone 268-272.1 (E14.5). b. Large clones: i. clone 160-163.10 and ii. clone 120-127.7 (both E12.5), iii. clone 179.2 and iv. clone 3.1 (both E13.5). c. Small clones containing five or fewer columns: i. clone 95-97.1 containing three widespread columns (E13.5), ii. clone 265.3 containing a single column (E14.0), and iii. clone 247-249.2 containing two adjacent columns (E14.0). Clone numbers are listed in the appendix (Table 22-Table 27).

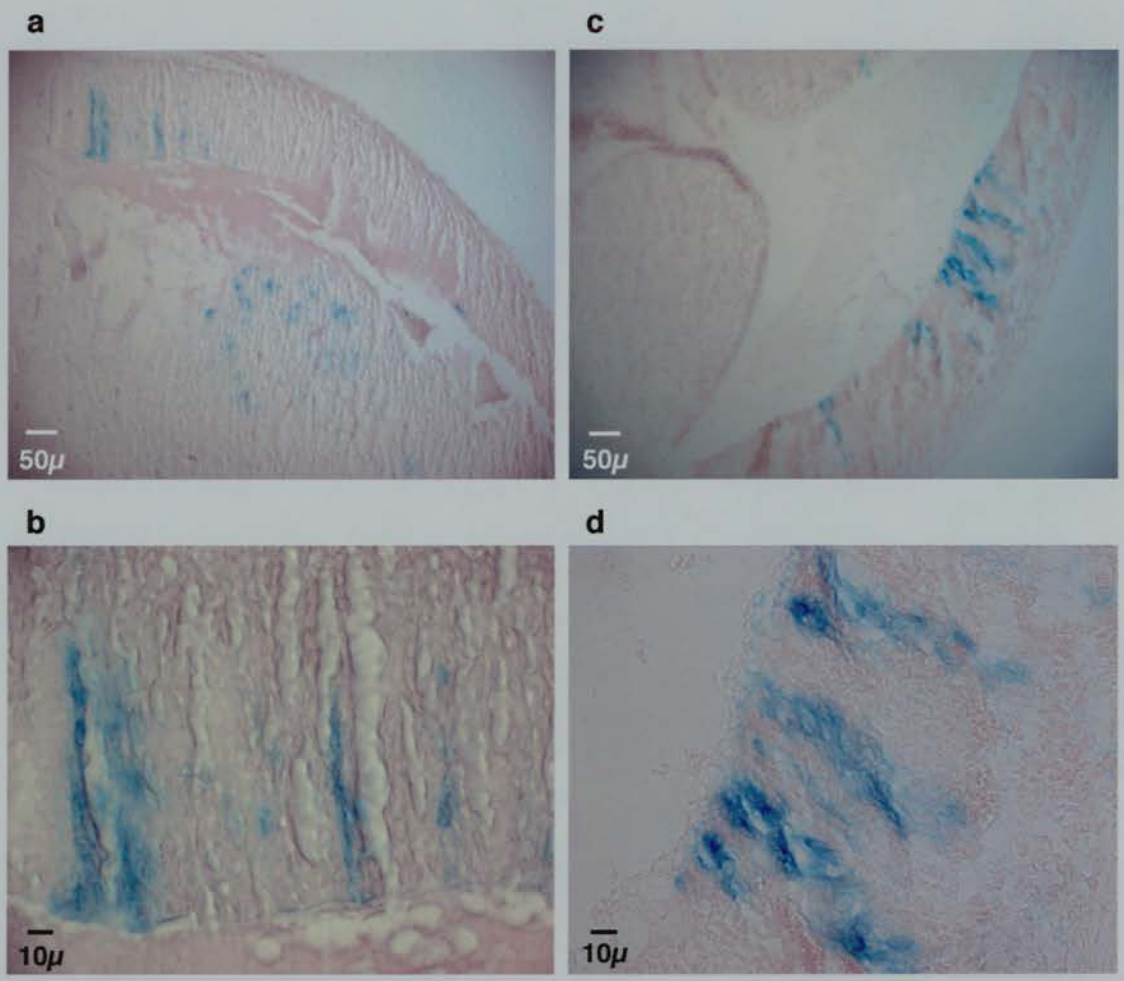

Plate 14. Labelled columns in paraffin sections.
a., b. Sagittal section through embryo A189 (see Plate 10). c., d. Section through embryo A195.1 (see Plate 10).

Plate 15. 3-D reconstruction of embryo 268-272.1. a. Lateral view of entire head, b. Anterior view, c. and d. dorsal views. The lateral ventricle is shaded in grey, and β-gal + cells are coloured blue. Brightfield images of the embryo are shown in Plate 13, a iv and v. The pattern of labelled cells appears to record a path across the surface of the ventricle.

a

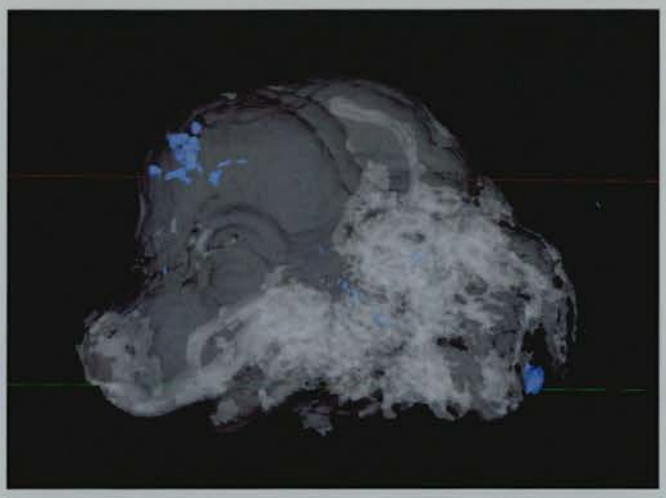

b

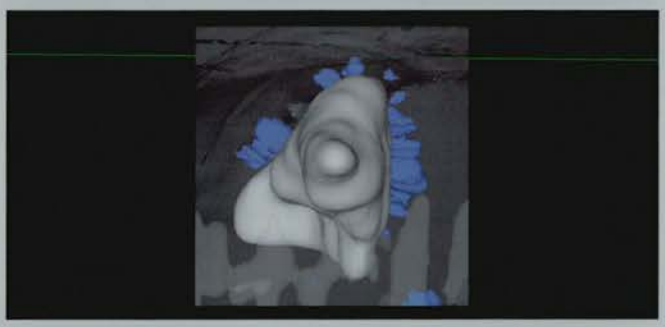

c

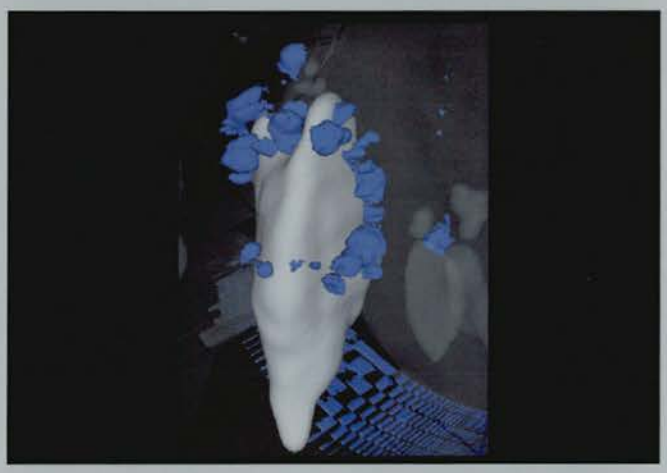

d

Plate 16. 3-D reconstruction of embryo 160-163.10. a-c. posterior views, d. anterior view, e. high resolution posterior view, f. lateral view. The lateral ventricle is shaded in grey, and β-gal + cells are coloured blue. A brightfield image of the embryo is shown in Plate 13, bi.

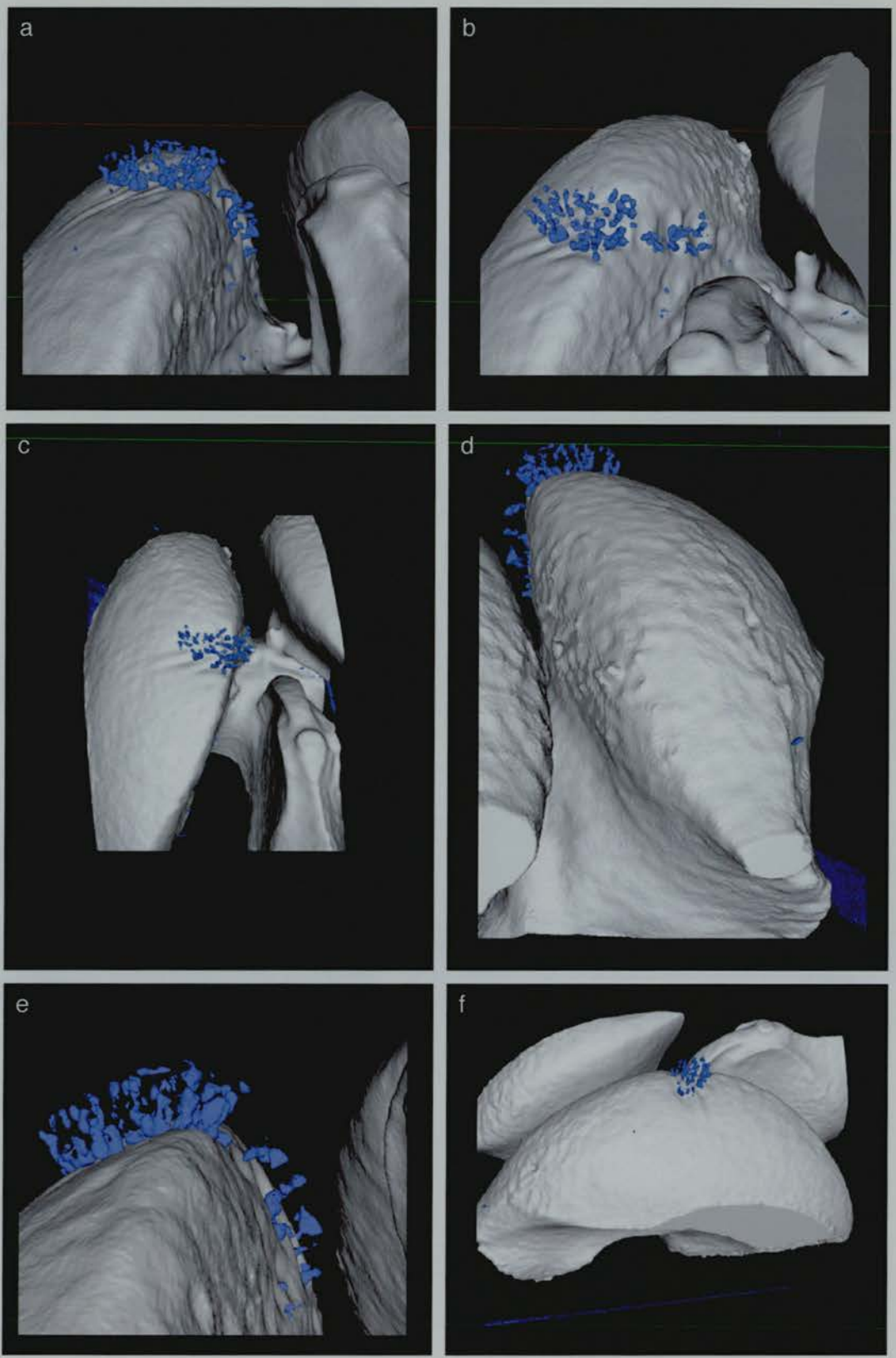
a
b
c
d
e
f

Concluding remarks

In this thesis, genetic and molecular approaches have been used to address long-standing questions regarding melanoblast development and pigmentation patterning. The extrinsic factors affecting melanoblast development were studied using an *in vitro* culturing approach, and the intrinsic factors were addressed by cell lineage analysis. During this process, the expression of the transgene in another tissue, the telencephalon, serendipitously permitted a lineage analysis during the early phases of neurogenesis. In both tissues, clonally related cells became broadly dispersed, a result perhaps not unexpected given the speed at which the embryo increases in size during midgestation, however, this also reflected the migratory behaviour of the progenitor cells. Although the exact number of melanoblast precursors was not determined, the well-established technique of producing chimaeras by aggregation, and the more recent development in cell lineage analysis of genetically marking cells with the *LacZ* gene, continue to prove useful in revealing the behaviour of different populations of cells during embryogenesis. In the melanoblast population, there are more precursors than predicted by Mintz's interpretations of adult coat colours, and they migrate long distances, in both an axial and lateral direction. In the telencephalon, precursor cells may produce a cortex with a mosaic pattern, but any pattern is probably quickly disrupted by the dispersal and mixing of clones, suggesting the functional domains of the cortex are not mapped out in the VZ. Further analyses will reveal to what extent clonally related cells are excluded from particular areas of the developing cortex, but it appears that, at least at early stages, clones can occupy multiple functional domains.

Appendix

Lists of A195 litters, embryos, and clones for all Dct*-expressing lineages*

The data in Table 24-Table 29 is presented as follows: Under melanoblast, eye, and telencephalon headings, data is listed as: the number of clones counted, the hemisphere in which the clone was found (where LHS means left hand side, RHS means right hand side, and DS means double-sided), followed by the number of cells (or columns, if in the telencephalon lineage), if there were five or fewer.

Table 24. Record of embryos analysed at E10.5.

Litter No.	Litter size	Tot. no. embryos stained	Embryo ID	Tot. no clones	Melanoblast	Eye	Telencephalon
37	12	0					
38	19	0					
39	12	0					
40	11	0					
41	11	0					
42	12	0					
43	16	0					
44	11	0					
45	12	0					
77	12	0					
78	14	0					
79	15	0					
80	4	0					
171	11	1	171-173.1	1	1, LHS		
172	10						
173	14						
186	12	2	186-190.1	1		1, LHS	
187	12		186-190.2	1		1, RHS, 1 cell	
188	14						
189	14						
190	14						
192	11	1	192-198.1	1	1, DS	1, DS	1, DS
193	12						
194	12						
195	12						
196	11						
197	11						
198	14						
229	12	0					
230	16	0					
231	13	0					
232	12	0					
238	10	0					

239	13	0					
240	17	0					
241	11	0					
242	17	0					
243	14	0					

Table 25. Record of embryos analysed at E11.5.

Litter No.	Litter size	Tot. no. embryos stained	Embryo ID	Tot. no clones	Melanoblast	Eye	Telencephalon
31	12	1	31.1	3	1, LHS		2, DS
35	12	2	35.1	2	1, DS		1, RHS
			35.2	2	1, RHS		1, RHS
47	11	0					
48	18	0					
51	12	1	46-52.1	2	1 RHS		1, RHS
53	12	2	53-60.1	1		1, LHS, 1 cell	
54	13		53-60.4	1			1, LHS, 1 column
55	11						
56	13						
57	7						
58	11						
59	12						
60	11						
84	14	2	84-92.1	1		1, LHS, 1 cell	
85	9		84-92.2	1		1, LHS, 1 cell	
86	11						
87	14						
88	12						
89	13						
90	10						
91	14						
92	12						
114	17	1	114.1	1		1, RHS, 1 cell	
115	16	0					
165	15	4	165-169.1	1	1, tail, RHS		
166	15		165-169.2	1		1, RHS 1 cell	
167	14		165-169.3	1	1, RHS, 1 cell		
168	16		165-169.4	2		1, LHS, 1 cell	1, RHS
169	13						
219	7	5	219-228.1	1		1, DS	
220	12		219-228.2	3	1, RHS	1, LHS	1, RHS
221	11		219-228.3	1		1, LHS	
222	12		219-228.4	1		1, RHS	
223	12		219-228.5	2	1, LHS		1, LHS
224	12						
225	11						
226	14						
227	15						
228	10						
273	15	0					
274	13	0					
275	14	0					

Table 26. Record of embryos analysed at E12.5.

Litter No.	Litter size	Tot. no. embryos stained	Embryo ID	Tot. no clones	Melanoblast	Eye	Telencephalon
30	17	0					
32	14	1	32.1	2			2, DS, 1 column LHS, 5 columns RHS
33	14	1	33.1	2		1, LHS	1, LHS l
34	11	2	34.1	1			1, RHS, 1 column
			34.2	1		1, LHS	
36	15	1	36.1	1			1, LHS, 1 column
46	19	0					
49	8	0					
50	10	1	46-52.2	1		1, RHS	
52	12	2	53-60.2	1		1, LHS, 1 cell	
			53-60.3	1		1, LHS, 1 cell	
81	11	1	81-83.1	1			1, RHS, 2 columns
82	9						
83	9						
112	9	1	112.1	1		1, RHS, 1cell	
120	10	7	120-127.1	1			1, LHS, 3 columns
121	8		120-127.2	1			1, RHS, 1 column
122	12		120-127.3	1		1, RHS	
123	9		120-127.4	1			1, LHS
124	12		120-127.5	1			1, LHS, 1 column
125	10		120-127.6	1			1, LHS, 4 columns
126	13		120-127.7	1			1, RHS
127	17						
154	12	4	154-159.1	1			1, LHS
155	13		154-159.2	1		1, LHS, 1 cell	
156	12		154-159.3	1		1, DS	
157	17		154-159.4	2		1, RHS, 1 cell	1, LHS
158	12						
159	11						
160	14	11	160-163.1	1			1, RHS, 1 column
161	14		160-163.2	1			1, LHS, 1 column
162	15		160-163.3	1	1, RHS		
163	12		160-163.4	1		1, LHS, 1 cell	
			160-163.5	1		1, RHS, 1 cell	
			160-163.6	1			1, RHS, 1 column
			160-163.7	1			1, RHS, 2 columns
			160-163.8	1			1, RHS, 1 column
			160-163.9	1		1, RHS, 1	

						cell	
			160-163.10	1			1, LHS,
			160-163.11	1		1, DS, 1 cell each	
170	10	1	170.1	1		1, DS, 1 cell each	
191	12	2	191.1	1			1, LHS
			191.2	3	1, LHS	1, DS	1, LHS
207	11	7	207-211.1	1	1, RHS		
207	14		207-211.2	1		1, RHS, 1 cell	
209	12		207-211.3	1			1, RHS
210	12		207-211.4	1	1, DS		
211	11		207-211.5	4	1, RHS	1, LHS	2, DS
			207-211.6	1			1, RHS, 1 column
			207-211.7	1			1, LHS, 1 column
214	16	1	214-218.1	1		1, LHS, 1 cell	
215	14						
216	10						
217	14						
218	15						
276	2	0					
277	13	0					

Table 27. Record of embryos analysed at E13.5.

Litter No.	Litter size	Tot. no. embryos stained	Embryo ID	Tot. no clones	Melanoblast	Eye	Telencephalon
1	12	0					
2	12	1	2.1	3	1, RHS		2, DS
3	8	1	3.1	1			1, LHS
4	12	3	4.1	1			1, LHS
			4.2	1			1, LHS
			4.3	2		1, LHS	1, LHS
5	12	0					
6	11	2	6.1	1			1, RHS
			6.2	2		1, LHS	1, LHS
7	5	0					
8	12	1	8.1	1			1, LHS, <5 col
17	15	4	17.1	1			1, LHS
			17.2	1			1, RHS
			17.3	1			1, LHS
			17.4	1	1, RHS, 1 cell		
20	11	0					
21	8	1	21.1	1	1, RHS		
22	16	0					
64	13	7	64-67.1	1			1, LHS
			64-67.2	2		1, LHS	1, LHS
			64-67.3	1		1, RHS, 1 cell	
			64-67.4	1		1, LHS, 2 cell	
			64-67.5	1			1, RHS, 3 columns
			64-67.6	1			1, LHS, 1 column
			64-67.7	1		1, LHS, 1 cell	
65	10						
66	9						
67	2						
68	14	3	68-70.1	1			1, LHS, 1 column
			68-70.2	1		1, DS, 1 cell LHS	
			68-70.3	1			1, LHS, 2 columns
69	9						
70	9						
71	15	18	71-76.1	1		1, RHS, 1 cell	
72	18		71-76.2	1		1, LHS, 1 cell	
73	11		71-76.3	1		1, LHS	
74	12		71-76.4	1		1, LHS, 3 cells	
75	14		71-76.5	1		1, RHS, 1 cell	
76	15		71-76.6	1			1, RHS, 2 columns widespread
			71-76.7	1			1, LHS
			71-76.8	1			1, LHS, 1 column

			71-76.9	1			1, RHS, 1 columns
			71-76.10	1			1, RHS, 3 columns widespread
			71-76.11	1		1, LHS, 1 cell	
			71-76.12	2	1, LHS		1, RHS
			71-76.13	3		1, RHS, 1 cell	2, DS, 1 column each
			71-76.14	1			1, RHS, 1 column
			71-76.15	2			2, DS, 1 column each
			71-76.16	1			1, RHS, 2 column widespread
			71-76.17	1			1, RHS, 1 column
			71-76.18	1			1, RHS, 1 column
93	13	3	93-95.1	1		1, LHS, 1 cell	
94	16		93-95.2	2		1, RHS, 1 cell	1, LHS, 1 column
95	13		93-95.3	3	1, RHS	1, LHS, 1 cell	1, LHS
96	13	7	95-97.1	1			1, RHS 4 columns
97	13		95-97.2	2			2, DS, 1 + 2 columns
			95-97.3	1			1, LHS, 1 column
			95-97.4	1			1, LHS, 1 column
			95-97.5	1		1, RHS, 1 cell	
			95-97.6	1	1, LHS		
			95-97.7	1			1, LHS
98	13	4	98-100.1	1			1, LHS, 4 columns
99	14		98-100.2	1	1, LHS		
100	13		98-100.3	1			1, LHS, 1 column
			98-100.4	2		1, LHS, 2 cells	1, LHS
101	14	1	101-102.1	1		1, RHS, 1 cell	
102	14						
103	12	4	103-105.1	1			1, LHS, 1 col
104	11		103-105.2	2			2, DS, 2 + 1 column
105	10		103-105.3	1			1, LHS, 1 column
			103-105.4	1		1, RHS, 2 cells	
106	14	4	106-108.1	1		1, LHS	
107	13		106-108.2	1	1, RHS		
108	14		106-108.3	1		1, RHS	
			106-108.4	1		1, RHS, 1 cell	
109	13	7	109-111.1	1		1, LHS, 1 cell	
110	15		109-111.2	1		1, LHS, 1 cell	
111	11		109-111.3	1		1, RHS, 1 cell	

			109-111.4	1		1, RHS, 1 cell	
			109-111.5	2			2, DS, 1 column each
			109-111.6	2		1, RHS, 2 cells	1, RHS, 1 column
			109-111.7	1			1, RHS, 1 column
164	12	0					
177	13	2	177.1	1			1, RHS
			177.2	1			1, RHS
178	13	0					
179	10	2	179.1	1			1, RHS, 1 column
			179.2	3		1, LHS	2, DS, 1 column RHS
246	16	1	246.1	1			1, RHS
278	11	1	278-279.1	1			1, LHS, 1 column
279	11						

Table 28. Record of embryos analysed at E14.0.

Litter No.	Litter size	Tot. no. embryos stained	Embryo ID	Tot. no clones	Melanoblast	Eye	Telencephalon
174	14	5	174-176.1	1		1, RHS, 1 cell	
175	13		174-176.2	1		1, DS, 1 cell each side	
176	14		174-176.3	2		1, RHS, 1 cell	1, LHS
			174-176.4	1		1, LHS, 3 cells	
			174-176.5	1	1, LHS, 4 cells		
205	6	2	205-206.1	1			1, LHS
206	8		205-206.2	1		1, RHS, 1 cell	
244	16	2	244.1	1			1, RHS, 1 column
			244.2	1			1, LHS 1 column
245	32	1	245.1	1	Early reversion		
247	20	8	247-249.1	1			1, RHS, 1 column
248	13		247-249.2	1			1, LHS, 2 column
249	16		247-249.3	1		1, LHS, 1 cell	
			247-249.4	2			2, DS, 1 column RHS
			247-249.5	2			2, DS, 1 column RHS
			247-249.6	1		1, LHS	
			247-249.7	1		1, LHS, 1 cell	
			247-249.8	2			2, DS, 3 column RHS, 2 column LHS
250	16	2	250-252.1	2		1, RHS	1, LHS 4 column
251	15		250-252.2	2			2, DS, 3 columns each
252	19						
253	11	3	253-256.1	1		1, LHS, 1 cell	
254	10		253-256.2	2		1, RHS	1, RHS, 1 column
255	13		253-256.3	1		1, RHS, 2 cells	
256	17						
257	16	4	257-260.1	2			2, DS, 1 + 3 columns
258	15		257-260.2	1			1, LHS, 2 columns
259	6		257-260.3	2			2, DS, 3 columns RHS, 2 columns LHS
260	13		257-260.4	2		1, LHS	1, LHS, 1 column
261	16	6	261-264.1	2			2, DS, 3 + 2 columns

262	10		261-264.2	1	1, RHS		
263	14		261-264.3	1			1, RHS, 1 column
264	16		261-264.4	1	1, RHS, 1 cell		
			261-264.5	1			1, RHS, 1 column
			261-264.6	1	1, RHS, 3 cells		
265	15	4	265.1	1			1, LHS, 2 columns
			265.2	1			1, LHS, 1 column
			265.3	1			1, LHS, 1 column
			265.4	1			1, RHS, 1 column
266	17	3	266-267.1	2			2, DS, 4 columns each
267	13		266-267.2	1			1, RHS, 1 column
			266-267.3	2		1, RHS	1, RHS, 1 column
268	13	3	268-272.1	1			1, RHS
269	4		268-272.2	1			1, RHS, 1 column
270	13		267-272.3	1		1, RHS, 1 cell	
271	10						
272	15						
280	11	1	280-283.1	1			1, LHS
281	11						
282	13						
283	10						
284	13	0					
285	16						
286	16						
287	13	6	287-289.1	1			1, LHS, 1 column
288	16		287-289.2	1			1, RHS, 3 column
289	16		287-289.3	1			1, LHS, 1 column
			287-289.4	1			1, RHS, 1 column
			287-289.5	1		1, RHS, 1 cell	
			287-289.6	1		1, RHS, 1 cell	

Table 29. Record of embryos analysed at E14.5.

Litter No.	Litter size	Tot. No. Embryos Stained	Embryo ID	Tot. no clones	Melanoblast	Eye	Telencephalon
13	8	2	13.1	1	1, LHS		
			13.2	4	1, RHS	1, DS	2, DS
18	12	1	18.1	1			1, LHS, 2, columns
19	7	0					
23	8	1	23.1	1	1, LHS		
24	9	1	24.1	1			1, LHS, 1 column
25	13	0					
26	13	1	26.1	1			1, RHS
27	12	1	27.1	1		1, RHS	
28	18	1	28.1	1		1, RHS, 2 cells	
29	16	0					
61	14	2	61-63.1	1		1, DS	
62	16		61-63.2	1		1, LHS, 1 cell	
63	15						
116	14	3	116.1	1		1, LHS	
			116.2	1		1, LHS	
			116.3	1		1, LHS, 2 cells	
117	13	2	117-118.1	1			1, RHS, 1 column
118	13		117-118.2	1		1, RHS, 1 cell	
119	11	0					
132	12	7	132-134.1	1	1, LHS, 4 cells		
133	11		132-134.2	1	1, LHS, 2 cells		
134	10		132-134.3	1	1, LHS, 1 cell		
			132-134.4	1		1, RHS, 1 cell	
			132-134.5	1		1, RHS, 1 cell	
			132-134.6	2		1, RHS, 1 cell	1, LHS
			132-134.7	3		1, LHS	2, DS
135	12	2	135-136.1	2		1, RHS, 1 cell	1, RHS
136	11		135-136.2	2		1, LHS	1, LHS
137	15	5	137-138.1	1		1, RHS, 1 cell	
138	12		137-138.2	1			1, RHS, 1 column
			137-138.3	2	1, RHS, 1 cell		1, LHS, 1 column
			137-138.4	1	1, LHS, 2 cells		
			137-138.5	1		1, RHS, 1 cell	
139	11	1	139-141.1	1		1, RHS, 1	

						cell	
140	5						
141	13						
142	11	4	142-143.1	1			1, LHS, 1 column
143	13		142-143.2	1			1, RHS
			142-143.3	1	1, LHS		
			142-143.4	1		1, RHS, 1 cell	
144	13	1	144-145.1	1	1, RHS, 2 cells		
145	13						
146	12	6	146-148.1	1		1, LHS, 1 cell	
147	7		146-148.2	1	1, RHS		
148	14		146-148.3	1	1, RHS		
			146-148.4	2	1, RHS	1, RHS, 1 cell	
			146-148.5	2	2, DS		
			146-148.6	1	1, LHS, 5 cells		
149	13	2	149-151.1	1		1, RHS, 3 cells	
150	11		149-151.2	1			1, LHS
151	5						
152	8		0				
153	14		0				
181	13	1	181-182.1	1		1, LHS, 1 cell	
182	13						
183	17	3	183.1	1		1, LHS, 2 cells	
			183.2	2		1, LHS, 2 cells	1, RHS, 2 columns
			183.3	1		1, RHS, 1 cell	
184	14	4	184-185.1	3	1, LHS		2, DS, 1 column, RHS
185	11		184-185.2	1			1, RHS, 4 columns
			184-185.3	1			1, LHS
			184-185.4	2	1, LHS, 2 cells		1, LHS, 1 column
212	11	0					
213	14	0					
233	23	1	233-234.1	3		1, LHS, 1 cell	2, DS
235	30	1	235-237.1	1		1, RHS, 1 cell	
236							
237							

Summary data for all A195 embryos harvested

Table 30. Cell labelling frequencies (CLF) at different stages of development. The total number of embryos screened includes non-transgenic embryos; half of these were assumed to be transgenic. The CLF is expressed as the number of labelled clones per transgenic embryo.

Embryonic Age	Total no. embryos screened	Estimated no. transgenic embryos	Total stained embryos		Total no. clones	Melanoblast clones	Eye clones	Telencephalon clones
E10.5	480	240	4		4	2	2	1
				CLF:	0.017	0.008	0.008	0.004
E11.5	528	264	18		27	8	10	9
				CLF:	0.102	0.03	0.038	0.034
E12.5	547	273	43		51	5	19	27
				CLF:	0.186	0.018	0.069	0.099
E13.5	620	310	77		96	8	30	58
				CLF:	0.31	0.026	0.097	0.187
E14.0	594	297	50		63	5	17	41
				CLF:	0.212	0.017	0.057	0.138
E14.5	604	302	53		70	18	28	24
				CLF:	0.232	0.06	0.093	0.079

		Melanoblast					Telencephalon					Eye				
Age	**No. embryos with clones**	**Total no. clones**	**No. of 1 cell clones**	**LHS**	**RHS**	**DS**	**Total no. clones**	**No. of 1 cell clones**	**LHS**	**RHS**	**DS***	**Total no. clones**	**No. of 1 cell clones**	**LHS**	**RHS**	**DS**
E10.5	4	2	0	2	1	1	1	0	1	1	1	3	1	1	1	2
E11.5	18	8	1	3	6	1	9	1	3	6	1	10	6	6	5	1
E12.5	43	5	0	2	4	1	27	11	16	11	2	19	14	12	11	4
E13.5	77	8	1	3	5	0	57	26	32	25	7	30	17	7	11	1
E14.0	50	5	1	2	4	1	41	19	21	20	8	17	9	7	11	1
E14.5	53	18	2	11	7	1	24	7	13	11	4	28	16	13	17	2
Totals	245	46	5	23	27	5	160	64	86	74	23	107	63	46	56	11

Table 31. Distribution of clones on the left and rights sides of the body. LHS: left hand sided clones, RHS: right hand sided clones, DS: double sided clones. *DS clones in the telencephalon are calculated as resulting from more than one recombination event.

Assessment of double-sided telencephalon clones

The data presented in Table 21 was calculated by Andrew Carothers and based on the following suppositions:

The probability that there is at least one clone on the left hand side is x. Therefore, the probability of there being none is $1-x$. Assuming the labelling events occur independently on the two sides and with equal probability, and the probability that an embryo is transgenic is $^1/_2$,

Pr(no clones on LHS or RHS) $= 1-x+{}^1/_2 x^2$
Pr(no clones on LHS, at least one clone RHS) $= {}^1/_2 x(1-x)$
Pr(no clones on RHS, at least one clone LHS) $= {}^1/_2 x(1-x)$
Pr(at least one clone LHS, at least one clone RHS) $= {}^1/_2 x^2$

Let N_E denote the total number of embryos (transgenic and non-transgenic), and N_I, the number with i clones, so that $N_E = N_0 + N_1 + N_2$. The log-liklihood is then

$$N_0 \log\{1-x+{}^1/_2 x^2\} + N_1 \log\{x(1-x)\} N_2 \log\{{}^1/_2 x^2\}$$

This equation could be used to obtain a maximum liklihood of x, however, it would be tedious and require a customised program to solve. A simpler but less efficient way is to note that if x is small so that the second order terms can be ignored, it can be estimated by $x_e = 1 - N_o/N_E$. If clones do occur independently on the left and right sides, N_2 can be predicted by $N_{2E} = N_E \times {}^1/_2 x^2$. This gives the results presented in Table 21.

Reference List

1. **Mayer TC.** The migratory pathway of neural crest cells into the skin of mouse embryos . *Dev.Biol.* 1973; 34: 39-46.

2. **Jackson IJ.** Homologous pigmentation mutations in human, mouse and other model organisms. *Hum.Mol.Genet.* 1997; 6: 1613-24.

3. **Baker CV, Bronner-Fraser M.** The origins of the neural crest. Part I: embryonic induction. *Mech Dev* 1997; 69: 3-11.

4. **Erickson CA, Reedy MV.** Neural crest development: the interplay between morphogenesis and cell differentiation. *Curr Top Dev Biol* 1998; 40: 177-209.

5. **Groves AK, Bronner-Fraser M.** Neural crest diversification. *Curr.Top.Dev.Biol.* 1999; 43: 221-58.

6. **Bronner-Fraser M, Fraser SE.** Cell lineage analysis reveals multipotency of some avian neural crest cells. *Nature* 1988; 335: 161-4.

7. **Serbedzija GN, Bronner-Fraser M, Fraser SE.** Developmental potential of trunk neural crest cells in the mouse . *Development* 1994; 120: 1709-18.

8. **Ruffins S, Artinger KB, Bronner-Fraser M.** Early migrating neural crest cells can form ventral neural tube derivatives when challenged by transplantation. *Dev Biol* 1998; 203: 295-304.

9. **Marchant L, Linker C, Ruiz P, Guerrero N, Mayor R.** The inductive properties of mesoderm suggest that the neural crest cells are specified by a BMP gradient. *Dev Biol* 1998; 198: 319-29.

10. **LaBonne C, Bronner-Fraser M.** Neural crest induction in Xenopus: evidence for a two-signal model. *Development* 1998; 125: 2403-14.

11. **Carl TF, Dufton C, Hanken J, Klymkowsky MW.** Inhibition of neural crest migration in Xenopus using antisense slug RNA. *Dev.Biol.* 1999; 213: 101-15.

12. **Jiang R, Lan Y, Norton CR, Sundberg JP, Gridley T.** The Slug gene is not essential for mesoderm or neural crest development in mice. *Dev Biol* 1998; 198: 277-85.

13. **Nieto MA, Sargent MG, Wilkinson DG, Cooke J.** Control of cell behavior during vertebrate development by Slug, a zinc finger gene. *Science* 1994; 264: 835-9.

14. **LaBonne C, Bronner-Fraser M.** Snail-related transcriptional repressors are required in Xenopus for both the induction of the neural crest and its subsequent migration. *Dev.Biol.* 2000; 221: 195-205.

15. **Barembaum M, Moreno TA, LaBonne C, Sechrist J, Bronner-Fraser M.** Noelin-1 is a secreted glycoprotein involved in generation of the neural crest. *Nat.Cell Biol.* 2000; 2: 219-25.

16. **Liu JP, Jessell TM.** A role for rhoB in the delamination of neural crest cells from the dorsal neural tube. *Development* 1998; 125: 5055-67.

17. **Sela-Donenfeld D, Kalcheim C.** Regulation of the onset of neural crest migration by coordinated activity of BMP4 and Noggin in the dorsal neural tube. *Development* 1999; 126 : 4749-62.

18. **Bronner-Fraser M, Fraser SE.** Differentiation of the vertebrate neural tube. *Curr Opin Cell Biol* 1997; 9: 885-91.

19. **Le Douarin NM, Ziller C, Couly GF.** Patterning of neural crest derivatives in the avian embryo: in vivo and in vitro studies. *Dev Biol* 1993; 159: 24-49.

20. **Baker CV, Bronner-Fraser M, Le Douarin NM, Teillet MA.** Early- and late-migrating cranial neural crest cell populations have equivalent developmental potential in vivo. *Development* 1997; 124: 3077-87.

21. **Bronner-Fraser M.** Mechanisms of neural crest cell migration. *Bioessays* 1993; 15: 221-30.

22. **Selleck MA, Garcia-Castro MI, Artinger KB, Bronner-Fraser M.** Effects of Shh and Noggin on neural crest formation demonstrate that BMP is required in the neural tube but not ectoderm. *Development* 1998; 125: 4919-30.

23. **Eisen JS, Weston JA.** Development of the neural crest in the zebrafish. *Dev Biol* 1993; 159: 50-9.

24. **Serbedzija GN, Fraser SE, Bronner-Fraser M.** Pathways of trunk neural crest cell migration in the mouse embryo as revealed by vital dye labelling. *Development* 1990; 108: 605-12.

25. **Wehrle-Haller B, Weston JA.** Soluble and cell-bound forms of steel factor activity play distinct roles in melanocyte precursor dispersal and survival on the lateral neural crest migration pathway. *Development* 1995; 121: 731-42.

26. **Erickson CA, Duong TD, Tosney KW.** Descriptive and experimental analysis of the dispersion of neural crest cells along the dorsolateral path and their entry into ectoderm in the chick embryo. *Dev Biol* 1992; 151: 251-72.

27. **Erickson CA, Goins TL.** Avian neural crest cells can migrate in the dorsolateral path only if they are specified as melanocytes. *Development* 1995; 121: 915-24.

28. **Reedy MV, Faraco CD, Erickson CA.** The delayed entry of thoracic neural crest cells into the dorsolateral path is a consequence of the late emigration of melanogenic neural crest cells from the neural tube. *Dev Biol* 1998; 200 : 234-46.

29. **Wakamatsu Y, Mochii M, Vogel KS, Weston JA.** Avian neural crest-derived neurogenic precursors undergo apoptosis on the lateral migration pathway. *Development* 1998; 125: 4205-13.

30. **Cable J, Jackson IJ, Steel KP.** Mutations at the W locus affect survival of neural crest-derived melanocytes in the mouse. *Mech Dev* 1995; 50: 139-50.

31. **Henion PD, Weston JA.** Timing and pattern of cell fate restrictions in the neural crest lineage. *Development* 1997; 124: 4351-9.

32. **Collazo A, Bronner-Fraser M, Fraser SE.** Vital dye labelling of Xenopus laevis trunk neural crest reveals multipotency and novel pathways of migration. *Development* 1993; 118: 363-76.

33. **Mayor R, Young R, Vargas A.** Development of neural crest in Xenopus. *Curr.Top.Dev.Biol.* 1999; 43: 85-113.

34. **Henderson DJ, Copp AJ.** Role of the extracellular matrix in neural crest cell migration. *J Anat* 1997; 191 (Pt 4): 507-15.

35. **Zagris N, Chung AE, Stavridis V.** Differential expression of laminin genes in early chick embryo. *Int.J.Dev.Biol.* 2000; 44: 815-8.

36. **Hynes RO.** The dynamic dialogue between cells and matrices: implications of fibronectin's elasticity. *Proc Natl Acad Sci U S A* 1999; 96: 2588-90.

37. **Rovasio RA, Delouvee A, Yamada KM, Timpl R, Thiery JP.** Neural crest cell migration: requirements for exogenous fibronectin and high cell density. *J.Cell Biol.* 1983; 96: 462-73.

38. **Paglini MG, Rovasio RA.** Fibronectin substrate induces shortening of in vitro neural crest cell mitotic cycle. *Biocell* 1999; 23: 119-24.

39. **Beauvais-Jouneau A, Thiery JP.** Multiple roles for integrins during development. *Biol Cell* 1997; 89: 5-11.

40. **Beauvais A, Erickson CA, Goins T et al.** Changes in the fibronectin-specific integrin expression pattern modify the migratory behavior of sarcoma S180 cells in vitro and in the embryonic environment. *J Cell Biol* 1995; 128: 699-713.

41. **Kil SH, Krull CE, Cann G, Clegg D, Bronner-Fraser M.** The alpha4 subunit of integrin is important for neural crest cell migration. *Dev Biol* 1998; 202: 29-42.

42. **Horwitz AR, Parsons JT.** Cell migration--movin' on. *Science* 1999; 286: 1102-3.

43. **Sheetz MP, Felsenfeld DP, Galbraith CG.** Cell migration: regulation of force on extracellular-matrix-integrin complexes. *Trends Cell Biol.* 1998; 8: 51-4.

44. **Kerr RSE, Newgreen DF.** Isolation and characterization of chondroitin sulfate proteoglycans from embryonic quail that influence neural crest cell behavior. *Dev Biol* 1997; 192: 108-24.

45. **Kubota Y, Morita T, Kusakabe M, Sakakura T, Ito K.** Spatial and temporal changes in chondroitin sulfate distribution in the sclerotome play an essential role in the formation of migration patterns of mouse neural crest cells. *Dev Dyn* 1999; 214: 55-65.

46. **Henderson DJ, Ybot-Gonzalez P, Copp AJ.** Over-expression of the chondroitin sulphate proteoglycan versican is associated with defective neural crest migration in the Pax3 mutant mouse (splotch). *Mech Dev* 1997; 69: 39-51.

47. **Jackson IJ.** Molecular and developmental genetics of mouse coat color. *Annu Rev Genet* 1994; 28: 189-217.

48. **Eickholt BJ, Mackenzie SL, Graham A, Walsh FS, Doherty P.** Evidence for collapsin-1 functioning in the control of neural crest migration in both trunk and hindbrain regions. *Development* 1999; 126: 2181-9.

49. **Erickson CA.** From the crest to the periphery: control of pigment cell migration and lineage segregation. *Pigment Cell Res.* 1993; 6: 336-47.

50. **Fraser SE, Bronner-Fraser M.** Migrating neural crest cells in the trunk of the avian embryo are multipotent. *Development* 1991; 112: 913-20.

51. **Baroffio A, Dupin E, Le Douarin NM.** Common precursors for neural and mesectodermal derivatives in the cephalic neural crest. *Development* 1991; 112: 301-5.

52. **Sieber-Blum M, Cohen AM.** Clonal analysis of quail neural crest cells: they are pluripotent and differentiate in vitro in the absence of noncrest cells. *Dev Biol* 1980; 80: 96-106.

53. **Sharma K, Korade Z, Frank E.** Late-migrating neuroepithelial cells from the spinal cord differentiate into sensory ganglion cells and melanocytes. *Neuron* 1995; 14: 143-52.

54. **Ito K, Morita T, Sieber-Blum M.** In vitro clonal analysis of mouse neural crest development. *Dev.Biol.* 1993; 157: 517-25.

55. **Mintz B.** Clonal basis of mammalian differentiation. *Symp Soc Exp Biol* 1971; 25: 345-70.

56. **Mintz B.** Gene control of mammalian pigmentary differentiation. I. Clonal origin of melanocytes. *Proc Natl Acad Sci U S A* 1967; 58: 344-51.

57. **LaBonne C, Bronner-Fraser M.** Induction and patterning of the neural crest, a stem cell-like precursor population. *J Neurobiol* 1998; 36: 175-89.

58. **Huszar D, Sharpe A, Jaenisch R.** Migration and proliferation of cultured neural crest cells in W mutant neural crest chimeras. *Development* 1991; 112: 131-41.

59. **Stemple DL, Anderson DJ.** Isolation of a stem cell for neurons and glia from the mammalian neural crest. *Cell* 1992; 71: 973-85.

60. **Nishikawa S, Kusakabe M, Yoshinaga K et al.** In utero manipulation of coat color formation by a monoclonal anti-c- kit antibody: two distinct waves of c-kit-dependency during melanocyte development. *EMBO J* 1991; 10: 2111-8.

61. **Erickson CA.** From the crest to the periphery: control of pigment cell migration and lineage segregation. *Pigment Cell Res.* 1993; 6: 336-47.

62. **Kelsh RN, Schmid B, Eisen JS.** Genetic analysis of melanophore development in zebrafish embryos. *Dev.Biol.* 2000; 225: 277-93.

63. **Johnson SL, Africa D, Walker C, Weston JA.** Genetic control of adult pigment stripe development in zebrafish. *Dev Biol* 1995; 167: 27-33.

64. **Mason KA, Mason SK.** Evolution and development of pigment cells: at the crossroads of the discipline. *Pigment Cell Res.* 2000; 13 Suppl 8: 150-5.

65. **Parichy DM, Rawls JF, Pratt SJ, Whitfield TT, Johnson SL.** Zebrafish sparse corresponds to an orthologue of c-kit and is required for the morphogenesis of a subpopulation of melanocytes, but is not essential for hematopoiesis or primordial germ cell development [In Process Citation]. *Development* 1999; 126: 3425-36.

66. **Kelsh RN, Eisen JS.** The zebrafish colourless gene regulates development of non-ectomesenchymal neural crest derivatives. *Development* 2000; 127: 515-25.

67. **Boissy RE, Nordlund JJ.** Molecular basis of congenital hypopigmentary disorders in humans: a review. *Pigment Cell Res.* 1997; 10: 12-24.

68. **Bondurand N, Pingault V, Goerich DE et al.** Interaction among SOX10, PAX3 and MITF, three genes altered in Waardenburg syndrome. *Hum.Mol.Genet.* 2000; 9: 1907-17.

69. **Steel KP, Davidson DR, Jackson IJ.** TRP-2/DT, a new early melanoblast marker, shows that steel growth factor (c-kit ligand) is a survival factor. *Development* 1992; 115: 1111-9.

70. **Mackenzie MA, Jordan SA, Budd PS, Jackson IJ.** Activation of the receptor tyrosine kinase Kit is required for the proliferation of melanoblasts in the mouse embryo. *Dev Biol* 1997; 192: 99-107.

71. **Zhao S, Overbeek PA.** Tyrosinase-related protein 2 promoter targets transgene expression to ocular and neural crest-derived tissues. *Dev.Biol.* 1999; 216: 154-63.

72. **Opdecamp K, Nakayama A, Nguyen MT, Hodgkinson CA, Pavan WJ, Arnheiter H.** Melanocyte development in vivo and in neural crest cell cultures: crucial dependence on the Mitf basic-helix-loop-helix-zipper transcription factor. *Development* 1997; 124: 2377-86.

73. **Bedell MA, Cleveland LS, O'Sullivan TN, Copeland NG, Jenkins NA.** Deletion and interallelic complementation analysis of Steel mutant mice. *Genetics* 1996; 142: 935-44.

74. **Copeland NG, Gilbert DJ, Cho BC et al.** Mast cell growth factor maps near the steel locus on mouse chromosome 10 and is deleted in a number of steel alleles. *Cell* 1990; 63: 175-83.

75. **Geissler EN, Ryan MA, Housman DE.** The dominant-white spotting (W) locus of the mouse encodes the c-kit proto-oncogene. *Cell* 1988; 55: 185-92.

76. **Huang E, Nocka K, Beier DR et al.** The hematopoietic growth factor KL is encoded by the Sl locus and is the ligand of the c-kit receptor, the gene product of the W locus. *Cell* 1990; 63: 225-33.

77. **Williams DE, Eisenman J, Baird A et al.** Identification of a ligand for the c-kit proto-oncogene. *Cell* 1990; 63: 167-74.

78. **Zsebo KM, Williams DA, Geissler EN et al.** Stem cell factor is encoded at the Sl locus of the mouse and is the ligand for the c-kit tyrosine kinase receptor. *Cell* 1990; 63: 213-24.

79. **Tajima Y, Moore MA, Soares V, Ono M, Kissel H, Besmer P.** Consequences of exclusive expression in vivo of Kit-ligand lacking the major proteolytic cleavage site. *Proc Natl Acad Sci U S A* 1998; 95: 11903-8.

80. **Wehrle-Haller B, Weston JA.** Altered cell-surface targeting of stem cell factor causes loss of melanocyte precursors in Steel17H mutant mice. *Dev Biol* 1999; 210: 71-86.

81. **Ashman LK.** The biology of stem cell factor and its receptor C-kit. *Int.J.Biochem.Cell Biol.* 1999; 31: 1037-51.

82. **Besmer P, Manova K, Duttlinger R et al.** The kit-ligand (steel factor) and its receptor c-kit/W: pleiotropic roles in gametogenesis and melanogenesis. *Dev Suppl* 1993; 125-37.

83. **Philo JS, Wen J, Wypych J, Schwartz MG, Mendiaz EA, Langley KE.** Human stem cell factor dimer forms a complex with two molecules of the extracellular domain of its receptor, Kit. *J Biol Chem* 1996; 271: 6895-902.

84. **Blume-Jensen P, Claesson-Welsh L, Siegbahn A, Zsebo KM, Westermark B, Heldin CH.** Activation of the human c-kit product by ligand-induced dimerization mediates circular actin reorganization and chemotaxis. *EMBO J.* 1991; 10: 4121-8.

85. **Lemmon MA, Pinchasi D, Zhou M, Lax I, Schlessinger J.** Kit receptor dimerization is driven by bivalent binding of stem cell factor. *J.Biol.Chem.* 1997; 272: 6311-7.

86. **Morrison-Graham K, Takahashi Y.** Steel factor and c-kit receptor: from mutants to a growth factor system. *Bioessays* 1993; 15: 77-83.

87. **Keshet E, Lyman SD, Williams DE et al.** Embryonic RNA expression patterns of the c-kit receptor and its cognate ligand suggest multiple functional roles in mouse development. *EMBO J.* 1991; 10: 2425-35.

88. **Kunisada T, Yoshida H, Yamazaki H et al.** Transgene expression of steel factor in the basal layer of epidermis promotes survival, proliferation, differentiation and migration of melanocyte precursors. *Development* 1998; 125: 2915-23.

89. **Hirata T, Morii E, Morimoto M et al.** Stem cell factor induces outgrowth of c-kit-positive neurites and supports the survival of c-kit-positive neurons in dorsal root ganglia of mouse embryos. *Development* 1993; 119: 49-56.

90. **Motro B, van der KD, Rossant J, Reith A, Bernstein A.** Contiguous patterns of c-kit and steel expression: analysis of mutations at the W and Sl loci. *Development* 1991; 113: 1207-21.

91. **Guo CS, Wehrle-Haller B, Rossi J, Ciment G.** Autocrine regulation of neural crest cell development by steel factor. *Dev Biol* 1997; 184: 61-9.

92. **Brannan CI, Lyman SD, Williams DE et al.** Steel-Dickie mutation encodes a c-kit ligand lacking transmembrane and cytoplasmic domains. *Proc Natl Acad Sci U S A* 1991; 88: 4671-4.

93. **Brannan CI, Bedell MA, Resnick JL et al.** Developmental abnormalities in Steel17H mice result from a splicing defect in the steel factor cytoplasmic tail. *Genes Dev.* 1992; 6: 1832-42.

94. **Pesce M, Di Carlo A, De Felici M.** The c-kit receptor is involved in the adhesion of mouse primordial germ cells to somatic cells in culture. *Mech Dev* 1997; 68: 37-44.

95. **Wehrle-Haller B, Morrison-Graham K, Weston JA.** Ectopic c-kit expression affects the fate of melanocyte precursors in Patch mutant embryos. *Dev Biol* 1996; 177: 463-74.

96. **Robbins JR, McGuire PG, Wehrle-Haller B, Rogers SL.** Diminished matrix metalloproteinase 2 (MMP-2) in ectomesenchyme-derived tissues of the Patch mutant mouse: regulation of MMP-2 by PDGF and effects on mesenchymal cell migration. *Dev.Biol.* 1999; 212: 255-63.

97. **Bernex F, De Sepulveda P, Kress C, Elbaz C, Delouis C, Panthier JJ.** Spatial and temporal patterns of c-kit-expressing cells in WlacZ/+ and WlacZ/WlacZ mouse embryos. *Development* 1996; 122: 3023-33.

98. **Jordan SA, Jackson IJ.** A late wave of melanoblast differentiation and rostrocaudal migration revealed in patch and rump-white embryos. *Mech Dev* 2000; 92: 135-43.

99. **Jordan SA, Jackson IJ.** MGF (KIT ligand) is a chemokinetic factor for melanoblast migration into hair follicles. *Dev Biol* 2000; 225: 424-36.

100. **Hosoda K, Hammer RE, Richardson JA et al.** Targeted and natural (piebald-lethal) mutations of endothelin-B receptor gene produce megacolon associated with spotted coat color in mice. *Cell* 1994; 79: 1267-76.

101. **Baynash AG, Hosoda K, Giaid A et al.** Interaction of endothelin-3 with endothelin-B receptor is essential for development of epidermal melanocytes and enteric neurons. *Cell* 1994; 79: 1277-85.

102. **Kurihara H, Kurihara Y, Nagai R, Yazaki Y.** Endothelin and neural crest development. *Cell Mol.Biol.(Noisy.-le-grand)* 1999; 45: 639-51.

103. **Yanagisawa H, Yanagisawa M, Kapur RP et al.** Dual genetic pathways of endothelin-mediated intercellular signaling revealed by targeted disruption of endothelin converting enzyme-1 gene. *Development* 1998; 125: 825-36.

104. **Clouthier DE, Hosoda K, Richardson JA et al.** Cranial and cardiac neural crest defects in endothelin-A receptor- deficient mice. *Development* 1998; 125: 813-24.

105. **Nataf V, Lecoin L, Eichmann A, Le Douarin NM.** Endothelin-B receptor is expressed by neural crest cells in the avian embryo. *Proc.Natl.Acad.Sci.U.S.A* 1996; 93: 9645-50.

106. **Lahav R, Dupin E, Lecoin L et al.** Endothelin 3 selectively promotes survival and proliferation of neural crest-derived glial and melanocytic precursors in vitro. *Proc.Natl.Acad.Sci.U.S.A* 1998; 95: 14214-9.

107. **Reid K, Turnley AM, Maxwell GD et al.** Multiple roles for endothelin in melanocyte development: regulation of progenitor number and stimulation of differentiation. *Development* 1996; 122: 3911-9.

108. **Pavan WJ, Tilghman SM.** Piebald lethal (sl) acts early to disrupt the development of neural crest-derived melanocytes. *Proc Natl Acad Sci U S A* 1994; 91: 7159-63.

109. **Shin MK, Levorse JM, Ingram RS, Tilghman SM.** The temporal requirement for endothelin receptor-B signalling during neural crest development. *Nature* 1999; 402: 496-501.

110. **Matsumoto K, Nakamura T.** Hepatocyte growth factor (HGF) as a tissue organizer for organogenesis and regeneration. *Biochem Biophys Res Commun* 1997; 239: 639-44.

111. **Birchmeier C, Gherardi E.** Developmental roles of HGF/SF and its receptor, the c-Met tyrosine kinase. *Trends Cell Biol* 1998; 8: 404-10.

112. **Kos L, Aronzon A, Takayama H et al.** Hepatocyte growth factor/scatter factor-MET signaling in neural crest- derived melanocyte development. *Pigment Cell Res* 1999; 12: 13-21.

113. **Takayama H, La Rochelle WJ, Anver M, Bockman DE, Merlin G.** Scatter factor/hepatocyte growth factor as a regulator of skeletal muscle and neural crest development. *Proc Natl Acad Sci U S A* 1996; 93: 5866-71.

114. **Sieber-Blum M, Zhang JM.** Growth factor action in neural crest cell diversification. *J Anat* 1997; 191 (Pt 4): 493-9.

115. **Smith A, Ramos-Morales F, Ashworth A, Collins M.** A role for JNK/SAPK in proliferation, but not apoptosis, of IL-3- dependent cells. *Curr Biol* 1997; 7: 893-6.

116. **Blume-Jensen P, Janknecht R, Hunter T.** The kit receptor promotes cell survival via activation of PI 3-kinase and subsequent Akt-mediated phosphorylation of Bad on Ser136. *Curr Biol* 1998; 8: 779-82.

117. **Timokhina I, Kissel H, Stella G, Besmer P.** Kit signaling through PI 3-kinase and Src kinase pathways: an essential role for Rac1 and JNK activation in mast cell proliferation. *EMBO J* 1998; 17: 6250-62.

118. **Ito K, Takeuchi T.** The differentiation in vitro of the neural crest cells of the mouse embryo. *J Embryol Exp Morphol* 1984; 84: 49-62.

119. **Ono H, Kawa Y, Asano M et al.** Development of melanocyte progenitors in murine Steel mutant neural crest explants cultured with stem cell factor, endothelin-3, or TPA. *Pigment Cell Res* 1998; 11: 291-8.

120. **Reid K, Nishikawa S, Bartlett PF, Murphy M.** Steel factor directs melanocyte development in vitro through selective regulation of the number of c-kit+ progenitors. *Dev Biol* 1995; 169: 568-79.

121. **Murphy M, Reid K, Williams DE, Lyman SD, Bartlett PF.** Steel factor is required for maintenance, but not differentiation, of melanocyte precursors in the neural crest. *Dev Biol* 1992; 153: 396-401.

122. **Ito M, Kawa Y, Ono H et al.** Removal of stem cell factor or addition of monoclonal anti-c-KIT antibody induces apoptosis in murine melanocyte precursors. *J Invest Dermatol* 1999; 112: 796-801.

123. **Scott G, Ewing J, Ryan D, Abboud C.** Stem cell factor regulates human melanocyte-matrix interactions. *Pigment Cell Res* 1994; 7: 44-51.

124. **Nataf V, Le Douarin NM.** Induction of melanogenesis by tetradecanoylphorbol-13 acetate and endothelin 3 in embryonic avian peripheral nerve cultures. *Pigment Cell Res.* 2000; 13: 172-8.

125. **Stone JG, Spirling LI, Richardson MK.** The neural crest population responding to endothelin-3 in vitro includes multipotent cells. *J.Cell Sci.* 1997; 110 (Pt 14): 1673-82.

126. **Dupin E, Glavieux C, Vaigot P, Le Douarin NM.** Endothelin 3 induces the reversion of melanocytes to glia through a neural crest-derived glial-melanocytic progenitor. *Proc Natl Acad Sci U S A* 2000; 97 : 7882-7.

127. **Imokawa G, Kobayasi T, Miyagishi M.** Intracellular signaling mechanisms leading to synergistic effects of endothelin-1 and stem cell factor on proliferation of cultured human melanocytes. Cross-talk via trans-activation of the tyrosine kinase c- kit receptor. *J.Biol.Chem.* 2000; 275: 33321-8.

128. **Blume-Jensen P, Siegbahn A, Stabel S, Heldin CH, Ronnstrand L.** Increased Kit/SCF receptor induced mitogenicity but abolished cell motility after inhibition of protein kinase C. *EMBO J.* 1993; 12: 4199-209.

129. **West JD.** Insights into development and genetics from mouse chimeras. *Curr Top Dev Biol* 1999; 44: 21-66.

130. **Mintz B, Bradl M.** Mosaic expression of a tyrosinase fusion gene in albino mice yields a heritable striped coat color pattern in transgenic homozygotes. *Proc Natl Acad Sci U S A* 1991; 88: 9643-7.

131. **McLaren A, Bowman P.** Mouse chimaeras derived from fusion of embryos differing by nine genetic factors. *Nature* 1969; 224: 238-40.

132. **McLaren A.** *Mammalian Chimaeras*. Cambridge University Press ; 1976.

133. **West JD, McLaren A.** The distribution of melanocytes in the dorsal coats of a series of chimaeric mice. *J.Embryol.Exp.Morphol.* 1976; 35: 87-93.

134. **Bonnerot C, Nicolas JF.** Clonal analysis in the intact mouse embryo by intragenic homologous recombination. *C R Acad Sci III* 1993; 316: 1207-17.

135. **Sanes JR.** Lineage tracing. The laatest in lineaage. *Curr Biol* 1994; 4: 1162-4.

136. **Mathis L, Bonnerot C, Puelles L, Nicolas JF.** Retrospective clonal analysis of the cerebellum using genetic laacZ/lacZ mouse mosaics. *Development* 1997; 124: 4089-104.

137. **Mathis L, Sieur J, Voiculescu O, Charnay P, Nicolas JF.** Successive patterns of clonal cell dispersion in relation to neuromeric subdivision in the mouse neuroepithelium. *Development* 1999; 126: 4095-106.

138. **Nicolas JF, Mathis L, Bonnerot C, Saurin W.** Evidence in the mouse for self-renewing stem cells in the formation of a segmented longitudinal structure, the myotome . *Development* 1996; 122: 2933-46.

139. **Porter S, Larue L, Mintz B.** Mosaicism of tyrosinase-locus transcription and chromatin structure in dark vs. light melanocyte clones of homozygous chinchilla-mottled mice. *Dev Genet* 1991; 12: 393-402.

140. **Gondo Y, Gardner JM, Nakatsu Y et al.** High-frequency genetic reversion mediated by a DNA duplication: the mouse pink-eyed unstable mutation. *Proc.Natl.Acad.Sci.U.S.A* 1993; 90: 297-301.

141. **Price D, Willshaw D.** *Mechanisms of cortical devcelopment*. Oxford, Oxford University Press; 2000.

142. **Lillien L.** Progenitor cells: what do they know and when do they know it? *Curr.Biol.* 1998; 8: R872-R874.

143. **Williams BP.** Precursor cell types in the germinal zone of the cerebral cortex. *Bioessays* 1995; 17: 391-3.

144. **Walsh C.** Cell lineage and regional specification in the mammalian neocortex. *Perspect.Dev.Neurobiol.* 1993; 1: 75-80.

145. **McConnell SK.** Constructing the cerebral cortex: neurogenesis and fate determination. *Neuron* 1995; 15: 761-8.

146. **Blakemore C.** Mysteries in the making of the cerebral cortex. *Ciba Found.Symp.* 1995; 193: 1-20.

147. **Reid CB, Walsh CA.** Early development of the cerebral cortex. *Prog.Brain Res.* 1996; 108: 17-30.

148. **Herrup K, Silver J.** Cortical development and topographic maps: patterns of cell dispersion in developing cerebral cortex. *Curr.Opin.Neurobiol.* 1994; 4: 108-11.

149. **Gillies K, Price DJ.** The fates of cells in the developing cerebral cortex of normal and methylazoxymethanol acetate-lesioned mice. *Eur.J.Neurosci.* 1993; 5: 73-84.

150. **Rakic P.** Specification of cerebral cortical areas. *Science* 1988; 241: 170-6.

151. **Cai L, Hayes NL, Nowakowski RS.** Synchrony of clonal cell proliferation and contiguity of clonally related cells: production of mosaicism in the ventricular zone of developing mouse neocortex. *J.Neurosci.* 1997; 17: 2088-100.

152. **Tan SS, Faulkner-Jones B, Breen SJ, Walsh M, Bertram JF, Reese BE.** Cell dispersion patterns in different cortical regions studied with an X-inactivated transgenic marker. *Development* 1995; 121: 1029-39.

153. **Noctor SC, Flint AC, Weissman TA, Dammerman RS, Kriegstein AR.** Neurons derived from radial glial cells establish radial units in neocortex. *Nature* 2001; 409: 714-20.

154. **Altaba A, Gitton Y, Dahmane N.** Embryonic regionalization of the neocortex. *Mech.Dev.* 2001; 107: 3-11.

155. **Tan SS, Kalloniatis M, Sturm K, Tam PP, Reese BE, Faulkner-Jones B.** Separate progenitors for radial and tangential cell dispersion during development of the cerebral neocortex. *Neuron* 1998; 21: 295-304.

156. **Walsh C, Cepko CL.** Clonal dispersion in proliferative layers of developing cerebral cortex. *Nature* 1993; 362: 632-5.

157. **Reid CB, Liang I, Walsh C.** Systematic widespread clonal organization in cerebral cortex. *Neuron* 1995; 15: 299-310.

158. **Price J, Thurlow L.** Cell lineage in the rat cerebral cortex: a study using retroviral-mediated gene transfer. *Development* 1988; 104: 473-82.

159. **Mione MC, Cavanagh JF, Harris B, Parnavelas JG.** Cell fate specification and symmetrical/asymmetrical divisions in the developing cerebral cortex. *J.Neurosci.* 1997; 17: 2018-29.

160. **Grove EA, Williams BP, Li DQ, Hajihosseini M, Friedrich A, Price J.** Multiple restricted lineages in the embryonic rat cerebral cortex. *Development* 1993; 117: 553-61.

161. **Fishell G, Mason CA, Hatten ME.** Dispersion of neural progenitors within the germinal zones of the forebrain. *Nature* 1993; 362: 636-8.

162. **Tan SS, Breen S.** Radial mosaicism and tangential cell dispersion both contribute to mouse neocortical development. *Nature* 1993; 362: 638-40.

163. **Walsh C, Cepko CL.** Widespread dispersion of neuronal clones across functional regions of the cerebral cortex. *Science* 1992; 255: 434-40.

164. **Qian X, Shen Q, Goderie SK et al.** Timing of CNS cell generation: a programmed sequence of neuron and glial cell production from isolated murine cortical stem cells. *Neuron* 2000; 28: 69-80.

165. **Walsh C, Reid C.** Cell lineage and patterns of migration in the developing cortex. *Ciba Found.Symp.* 1995; 193: 21-40.

166. **Ferrer I, Soriano E, Del Rio JA, Alcantara S, Auladell C.** Cell death and removal in the cerebral cortex during development. *Prog.Neurobiol.* 1992; 39: 1-43.

167. **Heumann D, Leuba G.** Neuronal death in the development and aging of the cerebral cortex of the mouse. *Neuropathol.Appl.Neurobiol.* 1983; 9: 297-311.

168. **Voyvodic JT.** Cell death in cortical development: How much? Why? So what? *Neuron* 1996; 16: 693-6.

169. **Blaschke AJ, Staley K, Chun J.** Widespread programmed cell death in proliferative and postmitotic regions of the fetal cerebral cortex. *Development* 1996; 122: 1165-74.

170. **Blaschke AJ, Weiner JA, Chun J.** Programmed cell death is a universal feature of embryonic and postnatal neuroproliferative regions throughout the central nervous system. *J.Comp Neurol.* 1998; 396: 39-50.

171. **Spreafico R, Frassoni C, Arcelli P, Selvaggio M, De Biasi S.** In situ labeling of apoptotic cell death in the cerebral cortex and thalamus of rats during development. *J.Comp Neurol.* 1995; 363: 281-95.

172. **Thomaidou D, Mione MC, Cavanagh JF, Parnavelas JG.** Apoptosis and its relation to the cell cycle in the developing cerebral cortex. *J.Neurosci.* 1997; 17: 1075-85.

173. **Price DJ, Aslam S, Tasker L, Gillies K.** Fates of the earliest generated cells in the developing murine neocortex. *J.Comp Neurol.* 1997; 377: 414-22.